Hybridization of MIMO Radar with Phased and Frequency Diverse Array Radar

By

Wasim Khan

Reg. No. 36-FET/PHDEE/S10

A dissertation submitted to I.I.U. in partial fulfillment of the requirements for the degree of

DOCTOR OF PHILOSOPHY

Department of Electronic Engineering
Faculty of Engineering and Technology
INTERNATIONAL ISLAMIC UNIVERSITY
ISLAMABAD

2016

DEDICATED TO

My Teachers,

Parents,

Wife, Kids,

Sister and Brothers

CERTIFICATE OF APPROVAL

Title of Thesis: Hybridization of MIMO Radar with Phased and Frequency Diverse Array Radar

Name of Student: Wasim Khan

Registration No: 36-FET/PHDEE/S10

Accepted by the Department of Electronic Engineering, Faculty of Engineering and Technology, International Islamic University, Islamabad, in partial fulfillment of the requirements for the Doctor of Philosophy degree in Electronic Engineering.

Viva voce committee:

Prof. Dr. Aqdas Naveed Malik
Dean Faculty of Engineering and Technology
International Islamic University, Islamabad.

Prof. Dr. Muhammad Amir (Internal Examiner)
Chairman Department of Electronic Engineering
International Islamic University, Islamabad.

Prof. Dr. Tanveer Ahmed Cheema (External Examiner - I)
School of Engineering & Applied Sciences
Isra University, Islamabad.

Dr. M. M. Talha (External Examiner -II)
Principle Scientist
KRL, Islamabad.

Prof. Dr. Ijaz Mansoor Qureshi (Supervisor)
Department of Electrical Engineering
Air University, Islamabad

August 3, 2016

ABSTRACT

Motivated by recent research in modern radar systems, this dissertation presents new schemes for hybrid design of MIMO radar with phased array radar (PAR) and frequency diverse array (FDA) radar. Hybrid radars have exploited the benefits of conventional radars by merging their prominent features into a single radar system. Hybrid of MIMO with PAR i.e. Phased-MIMO radar, has enjoyed coherent processing gain of PAR and waveform diversity of MIMO radar. Likewise, a hybrid of MIMO radar with FDA radar i.e. MIMO-FDA radar has exploited the range dependent nature of FDA radar beampattern to provide target localization in range as well as in angle dimension.

The contributions of this work have explored transmit array partitioning schemes and the selection of effective configuration parameters such as frequency offset for hybrid radars. In case of hybrid Phased-MIMO radar, we propose two new schemes of unequal subarrays for transmit array partitioning. Idea is to illuminate the target with more focused beam of variable width to strengthen the reflections from target. Moreover, the interference cancellation capability is enhanced by maximizing the waveform diversity of hybrid radar. Results of proposed designs have achieved significant improvement in terms of transmit / received beampatterns, SINR and interference cancellation.

In case of MIMO-FDA radar, we have categorized the proposed systems on the basis of uniform and non-uniform frequency offset. For uniform frequency offset based systems, we propose two new schemes. First scheme uses the unequal subarray based partitioning for FDA radar to enhance localization in range as well as angle dimension. In the second scheme, we present a double pulse MIMO-FDA radar, which removes the range-angle coupling of FDA beampattern. In MIMO-FDA with non-uniform frequency offset, we explore the logarithmic frequency offset in our proposed schemes. Range bins based system has been proposed which allows us to place one maxima each for targets present at different ranges. Moreover, a design with variable logarithmic offset is also investigated to analyze the impact of variable configuring parameter on the localization of MIMO-FDA radar. Proposed designs have achieved better SINR, detection probability and improved Cramer Rao lower bound (CRLB) as compared to existing FDA and MIMO-FDA radars. The Proposed schemes of this work can indeed contribute in building an efficient hybrid radar system capable of providing all the features of modern radar system.

LIST OF PUBLICATIONS AND SUBMISSIONS

[1]. **Wasim Khan**, I.M. Qureshi, Abdul Basit, Muhammad Zubair, "Hybrid phased MIMO radar with Unequal Subarrays," *IEEE Antenna and Wireless Propagation Letters (AWPL)*, pp. 1702 - 1705, Vol. 14 , 2015 **(IF 1.75)**

[2]. **Wasim Khan**, I.M. Qureshi, Abdul Basit, Muhammad Zubair, "Transmit/ Receive Beamforming and Interference Cancellation using Phased MIMO Radar with Full Waveform Diversity," *World Applied Sciences Journal,* Vol. 27: pp.392-399, 2013.

[3]. **Wasim Khan**, I.M. Qureshi, Abdul Basit. Muhammad Zubair, "A Double Pulse MIMO Frequency Diverse Array Radar for Improved Range-Angle Localization of Target", *Wireless Personal Communications*, Vol. 82:pp.2199–2213, 2015 **(IF 0.7)**

[4]. **Wasim Khan**, I.M. Qureshi, Abdul Basit, Waseem Khan, "Range Bins Based MIMO-Frequency Diverse Array with logarithmic offset," *IEEE Antenna and Wireless Propagation Letters (AWPL)* VOL. 15, pp. 885-888, 2016 **(IF 1.75)**

[5]. **Wasim Khan**, I.M. Qureshi, Abdul Basit, Bilal Shoaib , "Transmit/Received beamforming for MIMO-Log-Frequency Diverse Array radar" , *IEEE 13th International Bhurban Conference on Applied Sciences and Technology (IBCAST)*, January 2016.

[6]. **Wasim Khan**, I.M. Qureshi, Abdul Basit, Aqdas Naveed Malik, Adnan Umar , "Performance Analysis of MIMO-Frequency diverse array radar with variable logarithmic offset", *Progress in electromagnetic research (PIER) C,* Vol. 62, pp. 23-34 2016.

[7]. Abdul Basit, I.M. Qureshi, **Wasim Khan** and A. N. Malik, "Range–Angle-Dependent Beamforming for Cognitive Antenna Array Radar with Frequency Diversity", *Cognitive Computation*, pp. 1-13, 2015. **(IF 1.9)**

[8]. Abdul Basit, I.M. Qureshi, **Wasim Khan**, Ihsan ul Haq and Shafqat Ullah Khan, "Hybridization of Cognitive Radar and Phased Array Radar Having Low Probability of Intercept Transmit Beamforming" *International Journal of Antennas and Propagation, 2014.* Article ID 129172. **(IF 0.8)**

[9]. Abdul Basit, I.M. Qureshi, **Wasim Khan** and A. N. Malik, "Cognitive Frequency Diverse Array Radar with Symmetric Non-uniform Frequency Offset," *Science china information sciences* (Accepted) 2016. **(IF 0.8)**

[10]. Abdul Basit, I.M. Qureshi, Ihsan ul Haq, A.N. Malik and **Wasim Khan**, "Evolutionary Computing Based Antenna Array Beamforming with Low Probability of Intercept Property," *World Applied Sciences Journal,* 23 (11): 1570-1575, 2013.

[11]. Abdul Basit, I.M. Qureshi, **Wasim Khan**, Ihsan ul Haq and Shafqat Ullah Khan, "Cognitive frequency offset calculation for frequency diverse array radar," *IEEE 12th IBCAST conference, 2015* , vol., no., pp.641,645, 13-17 Jan. 2015

[12]. Abdul Basit, I.M. Qureshi, **Wasim Khan** and Bilal Shoaib, " Beam Sharpening of a Range-angle-dependent pattern using Non-uniform Symmetric but integer Frequency Offset," *IEEE* International conference on intelligent system engineering (ICISE) Jan 2016.

[13]. Abdul Basit, I.M. Qureshi, **Wasim Khan** and Bilal Shoaib, " Beam Pattern Synthesis for a Cognitive Frequency Diverse Array Radar to Localize Multiple Targets With Same Direction But Different Ranges," *IEEE International Bhurban Conference on Applied Sciences and Technology (IBCAST), 2016 13th*, Jan. 2016.

[14]. Shafqat Ullah Khan, I.M. Qureshi, Fawad Zaman and **Wasim Khan**, " Detection of faulty sensor in array using symmetrical structure and cultural algorithm hybridized with differential evolution" , *Frontiers of Information Technology & Electronic Engineering*, 2016 **(IF 0.39)**

[15]. Shafqat Ullah Khan, I.M. Qureshi, Fawad Zaman, Abdul Basit and **Wasim Khan**, "Application of Firefly Algorithm to Fault Finding in Linear Arrays Antenna," *World Applied Sciences Journal,* 26 (2): 232-238, 2013.

[16]. B Shoaib, I.M. Qureshi , Sharjeel Abid Butt, S.U. khan and **Wasim khan**, "An adaptive step size kernel least mean square algorithm for Lorenz time series prediction," IEEE 12th *International Bhurban Conference on Applied Sciences and Technology (IBCAST), 2015* (Accepted)

SUBMITTED PAPERS

[1]. **Wasim Khan**, I.M. Qureshi, Abdul Basit, Shafqat Ullah Khan , "MIMO-FDA radar with unequal subarrays for improved Range-angle beamforming" , *Wireless Personal Communications* (submitted) 2016.

[2]. Abdul Basit, I.M. Qureshi, **Wasim Khan** and A. N. Malik, "An Improved Transmit Beam Pattern Synthesis for a Symmetric Frequency Diverse Array Radar," *IEEE Antennas and Wireless Propagation Letters* (submitted) 2015.

[3]. Waseem Khan, I.M. Qureshi, Sara Saeed, Abdul Basit and **Wasim Khan** "Receiver for FDA Radar with Time-Dependent Frequency Offset", *Remote Sensing Letters*, 2016.

[4]. Shuja Ur Rehman, Hafiz Abdul Wajid, I.M. Qureshi, Aqdas Naveed Malik, Abdul Basit and **Wasim Khan** "Explicit Beam Spoiling Phase Shifts for Phased Array Radar with Improved LPI Property" , *IEEE Antennas and Wireless Propagation Letters* (submitted) 2016.

The research work presented in this dissertation is based on the accepted publications 1 to 6 and the submitted publication 1.

ACKNOWLEDGEMENTS

In the name of Allah (Subhanahu Wa Ta'ala), who is the most gracious and the merciful. I would like to thank Allah for giving me strength and patience to complete this research work. Peace and blessings of Allah be upon His last Prophet Muhammad (Sallulah-o-Alaihihe-Wassalam) and all his Sahaba (Razi-Allah-o-Anhu) who dedicated their lives for Dawah and spread of Knowledge.

I am truly grateful to my supervisor Prof. Dr. Ijaz Mansoor Quershi, whose inspiration, ideas and efforts make it possible for me to complete my higher studies. He has been a role model for me and many others in teaching, research and other aspects of life. I would also like to thank Dr. Muhammad Zubair for his support during my research work. I owe my special thanks to my external examiners Prof. Dr. Tanveer Ahmed Cheema and Dr. M. M. Talha for their critical review of the thesis and useful inputs and suggestions.

I offer my sincere thanks to my colleagues Dr. Jawad Ali Shah, Dr. Abdul Basit, Hafiz Muhammad Zaheer, Dr. Shafqatullah Khan and Engr. Sharjeel Abid Butt for their never ending support during last few years. I also thank Bilal Shoaib, Atif Ellahi and other PhD scholars for their useful discussions. I would like to acknowledge the support of International Islamic University Islamabad Pakistan for providing me full fee waiver during the PhD studies. I am thankful to administration at department as well as university level for their kind support.

I am really grateful to my father, mother, sister and brothers for their love and support throughout my life. I am also very thankful to my wife for her patience, encouragement and prayers during every stage of my PhD degree. Finally, I am thankful to my kids, whose innocent gestures were source of inspiration for me.

(Wasim Khan)

TABLE OF CONTENTS

LIST OF FIGURES

LIST OF ABBREVIATIONS

AI	Aircraft Interception
ATC	Air Traffic Controller
AWGN	Additive White Gaussian Noise
CW	Continuous Wave
CR	Cognitive radar
CRLB	Cramer Rao lower bound
DOA	Direction of arrival
DP	Double Pulse
EKF	Extended Kalman Filter
EM	Electo_Magnetic
ESPRIT	Estimation of signal parameters by rotational invariance techniques
EW	Electronic warfare
FDA	Frequency diverse array
FDTD	Finite difference time domain
FWD	Full Waveform Diverse
GMTI	Ground moving target indication
HPMR-ES	Hybrid Phased MIMO radar with equal subarrays
HPMR-US	Hybrid Phased MIMO radar with unequal subarrays
KF	Kalman filter
LCMV	Linear constrained minimum variance
LFM	Linear frequency modulated
LPI	Low probability of intercept
MIMO	Multiple input multiple output

MIMO-FDA	Multiple input multiple output- frequency diverse array
MSE	Mean square error
MUSIC	Multiple signal classification
MVDR	Minimum variance distortion less response
PAR	Phased array radar
RCS	Radar cross section
SAR	Synthetic aperture radar
SINR	Signal to interference and noise ratio
SLL	Side lobe levels
SNR	Signal to noise ratio
STAP	Space-time adaptive processing
ULA	Uniform linear array

LIST OF SYMBOLS

A list of commonly used symbols in this dissertation are given below.

P	Number of antenna elements in a transmit-array
R	Number of antenna elements in a receive-array
d	Inter-element distance in an array of antennas
N	Number of subarrays
L	Number of antenna elements in a sub-array
$\mathbf{w}$	Weight vector of a subarray
θ	All angle w.r.t. bore sight of a radar
θ_t	Angle of a target
c	Speed of light
λ	Wavelength
t	Time
k	Discrete time instant
τ	Time delay
k'	Wave number
r	All range values
r_t	Range of a target
α	Reflections coefficient from target
B	Beam pattern
AF	Array factor
f_0	Fundamental frequency
Δf	Frequency offset

s	Waveform transmitted from a subarray
γ	Waveform transmitted by each antenna element
$\mathbf{u}$	Transmit steering vector of an array
$\mathbf{v}$	Receive steering vector of an array
ρ	Power given to a subarray
$\mathbf{z}$	Virtual steering vector
$\mathbf{y}$	Output of the receiving array after match filtering
$\mathbf{C}_{i+n}$	Interference plus noise covariance matrix
H_0	Hypothesis when target is not present in the surveillance region
H_1	Hypothesis when target is present in the surveillance region
p_d	Probability of detection
p_{fa}	Probability of false alarm
δ	Configuring parameter for frequency offset
(θ_t, r_t)	Target position in terms of range-angle
$\mathbf{J}$	Fisher information matrix (FIM)

Chapter 1

Introduction

Radar has been commonly used for detecting and localizing the objects in terms of direction, range and velocity. An electro-magnetic (EM) signal is transmitted into region of interest and the reflected signal is processed to get some useful information about targets of interest. Initially, radar was developed to fulfill military requirements to detect aircraft or ships, however, now it has also been used for various civilian applications such as ocean surface waves measurements, air traffic control (ATC), over speeding detection by traffic police on highways, geographical surveys and preventing car collisions.

1.1 Background

In order to meet the increasing demands of modern era, a lot of research is being carried out for advancement in radar technology. As a result, different types of radar systems have been developed over the years including Phased array radar (PAR), MIMO radar and Frequency diverse array (FDA) radar. All these radars used array of antenna elements and electronic scanning as a replacement of conventional single antenna with mechanical scanning in early radar systems. PAR is an electronic scanning radar in which the whole input array transmits phased shifted versions of same signal to form a directional

beam towards the target. This high gain beam, a prominent feature of PAR, is very useful in detecting weak targets.

Another variant called FDA radar uses small frequency increments across antenna elements to form a joint range and angle dependent beampattern, in contrast to angle dependent beampattern of PAR. FDA radar can effectively cancel range dependent interferences to significantly improve the received signal to noise ratio (SNR). On the other hand, beampattern of FDA radar is periodic in time and range dimension i.e. the maxima of beampattern repeats in range dimension at a particular time. Moreover, the beampattern of FDA radar has a strong coupling in range and angle dimension which can affect the localization performance.

In order to overcome some deficiencies of PAR, MIMO radar has also been proposed in last decade after a rigorous research on MIMO wireless communications. Idea has gained much attention of radar researchers due to similarity between radar and communication systems in terms of using antennas for transmitting and receiving EM signals. MIMO radar sends out unique waveform from each antenna element of an array in contrast to single waveform in PAR and FDA radar. MIMO radars can be divided into two broad categories. First category uses collocated or closely spaced antennas for providing waveform diversity, while the second category uses widely separated antenna to provide spatial diversity. Some of the benefits gained from MIMO radar are interference cancellation and resolution enhancement, which resulted in better target detection and parameter estimation.

Hybrid of MIMO radar with phased array radar has also been investigated in recent research. Resultant system called Phased-MIMO radar exploits the advantages of both

PAR and MIMO radar in terms of coherent processing gain and waveform diversity respectively. The idea is to divide the input array of antennas into sub-arrays which may be overlapping or non-overlapping. The signal within a particular sub array is same but the signals among the sub-arrays are different. Each sub-array transmits a unique waveform to form a beam towards the target by adjusting weights across the subarray. As a result, we have multiple PAR steering their beam towards the desired direction. Since all the beams are formed by using independent signals in each subarray, so there is a flavor of MIMO radar in it.

Likewise, MIMO radar has also been combined with FDA radar called MIMO-FDA radar, which enjoys the advantages of both radars. Two different types have been utilized by researchers. One of them uses subarray structure and apply different waveform as well as frequency increment in each subarray. Second scheme apply unique waveform as well as frequency increment at each antenna element. Like an FDA radar, MIMO-FDA radar can effectively locate the target in range as well as angle dimension due to frequency diversity in each subarray.

1.2 Motivation of Hybrid Radars

With the advancement in Electronic Warfare (EW), the demand of an efficient radar system is highly desirable for detecting, localizing and tracking the target. Modern radar system must be able to perform multiple tasks simultaneously i.e. it should have good gain, as well as, waveform diversity to detect target and avoid jammers at a particular frequency. It should be able to detect targets present in different ranges. Likewise, suppressing range dependent interferences to maintain good SNR is another necessary feature. Keeping these features in view, the combination of different radar systems to exploit their benefits and

mitigate their weaknesses can be a very reasonable choice. Consequently, the following research in hybrid radar systems has been conducted.

1.3 Research Problem

Hybrid radars are relatively new in research, therefore, they have open issues to be addressed. First of all, the hybrid radars demand efficient schemes for partitioning of an array into subarrays, so that the radar system can offer some extra benefits in addition to existing features. Secondly, the frequency offset selection can be considered as a very important feature to improve the localization of target in terms of range and angle. Consequently, new techniques are required to build up an effective and intelligent radar system having multiple capabilities associated with a radar system. In this work, we are focusing on these parameters by presenting new array partitioning techniques as well as effective configuring parameter that leads to the effective localization and better parameter estimation of target.

1.4 Contributions of the dissertation

In this work, the main objective is to introduce new partitioning schemes and frequency offset selection for hybrid radar systems. Using these schemes, we gain some extra features in two hybrid radar systems. First one is the hybrid of MIMO radar with phased array radar, while the second is hybridization of MIMO radar with frequency diverse array radar. Both type of hybrid radar models have been analyzed in terms of transmit and received beampatterns as well as various performance parameters such as Signal to interference plus noise ratio (SINR), Probability of Detection and Cramer Rao Lower bound (CRLB). Contributions of this dissertation can be summarized as follows

1. Hybrid Phased MIMO radar with unequal subarrays (HPMR-US) has been proposed to show its superiority over PAR, MIMO and existing phased MIMO radar. We have introduced a different formation of subarrays in a sense that they have variable sizes as well as overlapping. The extension in aperture of subarrays offers an extra beam focusing that leads to better returns from the target. HPMR-US radar has shown improvement in terms of transmit/received beampattern as well as output SINR.
2. Another variant of Phased-MIMO radar called full waveform diverse Phased MIMO radar (FWD-PMIMO) has been presented. It uses a slightly different kind of subarray partitioning such that the number of transmitted waveforms are equal to waveforms transmitted by MIMO radar. The major contribution of this proposed model is effective cancellation of interferences compared to PAR and phased MIMO radar. Moreover, it also exhibits improvement in received beampattern as well as SINR.
3. In this next contribution, we have applied the concept of unequal subarray to the MIMO-FDA radar. Objective is to improve beamforming and detection performance of the radar system in range dimension as well as angle dimension. Proposed radar has outperformed the FDA radar and existing MIMO-FDA radar in terms of transmit/received beampatterns and probability of detection.
4. The concept of double pulse has been applied to the subarrays of MIMO-FDA radar. A pulse with zero frequency offset has localized the target in angle dimension followed by a pulse with suitable frequency increment to localize the target in range. Resulting radar, called double pulse MIMO-FDA (DP-MIMO-FDA), combines the result of both pulses to localize target in angle and range. In this way, the coupling of FDA beampattern is removed, resulting in better localization of target. Performance

analysis of proposed radar has also been done in terms of CRLB and compared with the existing radar system.

5. In the next contribution, Range bins based MIMO-FDA with logarithmic frequency offset (MIMO-Log-FDA) is proposed to remove the periodicity in MIMO-FDA beampattern. The transmit array is divided into number of non-overlapped subarrays. Each subarray is used to produce single maxima for the target present in a particular range bin. Proposed design also allows us to overcome the inability of log-FDA radar to place maxima for multiple targets present at different ranges.
6. Finally, a new design of MIMO-Log-FDA has been proposed, which applied a variable logarithmic offset in each subarray to achieve a sharp beampattern. Since, the increase in logarithmic offset has increased the sharpness of beampattern, so each subarray has been assigned a different logarithmic offset, resulting in improved received beampattern. It is worth mentioning that overlapped subarrays has been used in design to get more focused beams. This work has also presented the received signal model for MIMO-Log-FDA radar. Proposed design has achieved low side lobes levels (SLL) and sharper beampattern in range and angle dimension. Performance analysis has also been done in terms of SINR and CRLB

1.5 Organization of the dissertation

This dissertation has been organized as follows

In Chapter 2, a brief history and designs of some modern radar systems i.e., PAR, MIMO radar and FDA radar, have been presented. The latest research work on these modern radar technologies has been highlighted to uncover their achievements and

deficiencies. Moreover, the existing literature on hybrid Phased MIMO radar and hybrid MIMO-FDA radar has also been explored towards the end of chapter.

In chapter 3, two new designs of Phased MIMO radar have been proposed. First the Hybrid Phased MIMO radar with unequal subarrays has been explored followed by a design Full waveform diverse-Phased MIMO radar in the second section of chapter. Results of both radar have also been shown at the end of each design.

In chapter 4, new schemes for Hybrid MIMO-frequency diverse array radar with uniform frequency offset have been presented. It includes a MIMO-FDA with unequal subarrays for better focusing of target and a double pulse MIMO-FDA radar for improved range-angle localization of target. Furthermore, the simulation results have also been illustrated along with useful discussions on results.

In chapter 5, MIMO-FDA with logarithmic frequency offset has been presented. First a range bins based MIMO-Log-FDA radar is presented. This is followed by a design a MIMO-FDA with variable logarithmic offset. Results in terms of transmit/received beampatterns, SINR and CRLB have also been presented.

In chapter 6, concluding remarks have been made about the current research followed by some future directions of research.

Chapter 2

Literature Review

This chapter presents necessary details about existing literature before entering into presentation of proposed work in the next chapters. It starts with a brief history of radar followed by some important details and latest research on PAR, FDA radar and MIMO radar. Moreover, existing research on Hybrid radar like Phased MIMO radar and MIMO-FDA radar has been explored. Some of the challenges faced by existing hybrid radars have also been highlighted towards the end of chapter.

2.1 History of Radar

Radar is an abbreviation for *RAdio Detection And Ranging*, however, its worldwide use makes it a common English word. History of Radar extended way back to 1886, when Heinrich Hertz showed that the radio waves can be reflected by a metallic object [1]. In 1903, Hiilsmeyer successfully performed an experiment for detection of ships using reflected radio waves at a range of just over one mile. After a slow progress in next three decades, aircraft detection at a distance of 50 miles was achieved in 1932. This was followed by a patent on aircrafts detection in 1934 awarded to Taylor, Young, and Hyland [2],[3].

In an anticipation of World War II, all important countries especially Britain worked for development of radars that could detect from large distances. A pulsed radar with full

capability of detection and ranging was presented by Robert Watson-Watt in 1935 [3]. Building on it, they developed an Aircraft-Interception (AI) radar in 1939, for the detection and interception of hostile aircraft. The system was mounted on an aircraft and had the capability to detect ships from air [4].

Radar systems, designed in earlier years, were huge mechanical bodies involving a lot of mechanical movement for detecting an aircraft. Therefore, a great urge was there to develop a radar system with the capability of electronic steering instead of mechanical steering. Dedicated research to produce a radar system with electronic steering resulted in development of most popular radar system in 1960 by the name of phased array radar (PAR) [5]–[7]. Antenna arrays using electronic beam steering techniques were explored and employed in military and civilian radars in the late 1970s. e.g., the PAVE PAWS radar [8]. This was followed by multimode programmable radar in 1980's and air borne electronically scanned antenna radar in 1990's [9].

2.2 Classifications of Radar

Radar systems can be classified in terms of the distance between transmitter and receiver, duration of signal, number of antennas used for transmission and structure of transmit array. Based on distance between transmitter and receiver ,there are monostatic, bistatic and multistatic radar systems [1]. In mono-static radar, the transmitter and receiver antenna elements are closely placed and only one antenna element performs both transmitting and receiving tasks by time multiplexing. Bistatic system, on the other hand, uses one transmitter and one receiver antenna that are separated by a significant distance [2]. Multi-static radar uses two or more transmitting or receiving antennas, where all antennas are separated by large distances [10] .

In terms of signal duration, a radar system can be continuous waveform (CW) radar or pulse radar. CW radar transmits a steady frequency in continuous fashion and processes the received signal for Doppler shift in the received frequency followed by estimating speed of target. These radars, also called Doppler radars, have the inability to measure the range of target, however, applying a linear frequency modulation (LFM) to CW radar allows us to measure range as well as speed of target. Pulse radar on the other hand transmits a train of RF pulses with a low duty cycle. Direction of the target can be acquired from the angle of arrival and range can be measured from propagation time of the reflected signal. These radars, also known as pulse-Doppler radars, can also estimate the speed of target by using Doppler frequency [2].

In terms of number of antennas used, radar can be categorized as single-antenna and multiple-antenna radar. For single-antenna based radar, a directional antenna is rotated on a mechanical pedestal to scan the whole region of interest, as in synthetic aperture radar (SAR). Multiple antennas radar uses an array of antenna to steer a beam towards target, as in PAR and FDA radar. Moreover, the electronic beam steering also eliminates the need of mechanical steering.

Finally, array radars use three different kinds of basic array structures. First is linear array in which antennas are placed close to each other in a straight line. In case of equal distance between antennas, it is called Uniform Linear array (ULA) [11]. Second array structure is planar array, which arranges the antenna elements as a grid of antenna in two dimensions [12]. Third type of array structure is circular array, in which antenna elements are placed in a circle [13]. In this work, we have focused on pulsed radar using linear arrays for all proposed schemes.

2.3 Phased Array radar

Phased array radar (PAR) has been widely used around the world after its first realistic and effective design in 1960's [14], [15]. It is a multiple antenna radar, which exploits the variation of phase between antenna elements to send a directional beam in the direction of target and nulls in the direction of interferences [16]. The most important feature of PAR is its high gain beam towards a target that allows better detection at the receiver. Some other features of PAR are low side lobes, interference cancellation, narrow beam width and variable scan rates[17].

2.3.1 Signal Model and beampattern of PAR

Signal model of PAR is presented for an array of P elements with uniform inter-element spacing. PAR uses phase shifted version of single waveform for the whole array. The phase shifters are attached to each antenna element, as shown in Fig. 2.1. The array factor of this uniform linear PAR is given as [18]

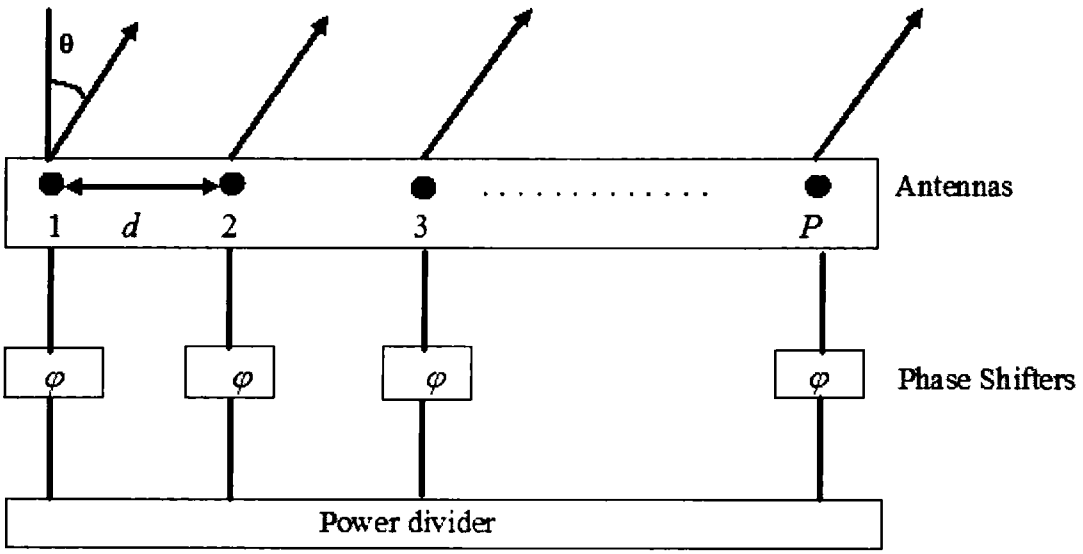

Fig. 2.1 Phased array with P elements of uniform spacing

$$AF(\theta)=\sum_{p=0}^{P-1} w_n^* e^{jn(k' d\sin\theta)} \tag{2.1}$$

where $k' = 2\pi / \lambda$ is wave number, λ is the wavelength and θ is desired direction. This array factor of PAR can be expressed in a vector form as

$$AF(\theta)=\mathbf{w}^H \mathbf{u}(\theta) \tag{2.2}$$

where $\mathbf{w}=[w_0, w_1, ..., w_{P-1}]^T$ is the weight vector associated with transmit array, $(.)^H$ represents conjugate transpose of vector and $\mathbf{u}(\theta)$ is the transmit array steering vector given as

$$\mathbf{u}(\theta)=\left[1 \; e^{jk'd\sin\theta} \; e^{j2k'd\sin\theta} \; . \; . \; . \; e^{j(P-1)k'd\sin\theta}\right]^T \tag{2.3}$$

$[.]^T$ represents transpose of a vector. This design of PAR assumes a uniform inter-element spacing, however, the spacing between elements can also be non-uniform according to scenario and applications [19],[20]. Moreover, the antennas can be placed as a rectangular grid of antennas according to requirement. In any case, the elements of array are fed with same frequency and waveform [21]–[23]. Furthermore, the overall electric field radiated by an array towards any point target in space is obtained by multiplying electric field of a single antenna with array factor [24]. A beam can be formed by adjusting the phase shift across each antenna elements. Steering of beam can be achieved by changing the inter-element phased offset, while the shape of radiation patterns can be controlled by adjusting amplitude associated with each phase shifter [25].

Beampattern is commonly used to represent the radiation pattern of a radiating array. It actually shows the distribution of transmitted power in space and can be obtained by magnitude square of array factor given in (2.2). The beam pattern for PAR can be given as

$$B_{PAR}(\theta)=\left|\mathrm{AF}(\theta)\right|^2=\left|\mathbf{w}^H\mathbf{u}(\theta)\right|^2 \tag{2.4}$$

It can be observed from (2.4) that a beampattern towards a target can be formed and adjusted by setting a suitable weight vector. The weight vector is also called a beam former, which can be either non-adaptive for maximum gain in a particular direction or adaptive to provide optimal performance in terms of coherent processing gain and interference cancellation. Non-adaptive beamformer uses uniform weight distributions and also known as conventional beamformer. Adaptive beamformer calculates the weights by using some adaptive processing methods like linear constrained minimum variance (LCMV) and minimum variance distortion less response (MVDR) beam formers [26]–[28]. These two beamformers will be used in the performance analysis of our proposed systems.

In order to place a maxima in desired direction θ_t, the beam pattern of a PAR using conventional beam former can be expressed as

$$B_{PAR}(\theta)=\left|\mathbf{w}^H\mathbf{u}(\theta)\right|^2=\left|\sum_{n=0}^{N-1}e^{jn\left(k'd\left(\sin\theta-\sin\theta_t\right)\right)}\right|^2 \tag{2.5}$$

This beam pattern in (2.5) will give a maxima in direction θ_t provided the inter-element distance does not exceeds $\lambda/2$. In case of $d > \lambda/2$, the beampattern also exhibits maxima at other angles, thus resulting in grating lobes [29]. It is important to mention that inter-element distance for PAR is always less than or equal to $\lambda/2$. Figure 2.2 shows a PAR beampattern steered to angle $\theta_t = 10^o$ by using 15 antenna elements and an interelement spacing of $\lambda/2$.

Some common areas of research in PAR are angle estimation of multiple targets, moving target detection in clutter, tracking of target and interference cancellation. Angle

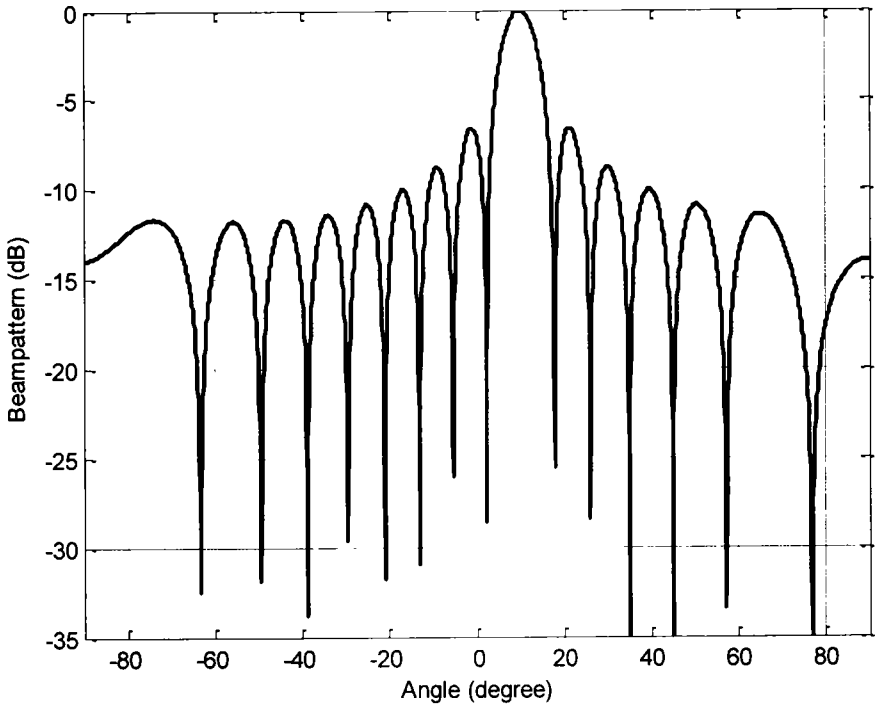

Fig. 2.2 PAR beampattern by using a non-adaptive Beamformer

$$\left(P=15,\theta_t=10^{\circ},d=\lambda/2\right)$$

estimation of multiple targets has been effectively done by Multiple Signal Classification (MUSIC) algorithm [30] and Estimation of Signal Parameters by Rotational Invariance Techniques (ESPRIT) algorithm [31]. For moving targets detection, the space-time adaptive processing (STAP) has suppressed the real time clutter by exploiting the space-Doppler properties of clutter. [32]. For tracking of target, the famous Kalman filter (KF) [33] and Extended Kalman Filter (EKF) [34] have been widely applied in PAR to improve the tracking of target. Finally, Low side lobes levels and interference cancellation have been thoroughly investigated by researchers over the year with an aim to improve performance of PAR [35]–[39].

In the end, it is important to mention that PAR has some limitations along with its advantages. Most important of these limitations is to give maxima only in angle dimension and keep it same for all ranges. i.e. range dependent targets and interferences cannot be handled effectively by a PAR. Another important limitation is lacking the waveform diversity i.e. it uses same waveform from each antenna element. Although gain provided by PAR is very important, some scenarios demands diversity of waveform instead of high transmit gain. To overcome these limitations, FDA radar and MIMO radar has been introduced in recent years. FDA radar has contributed in terms of range dependent detection and suppression, while MIMO radar has provided useful waveform diversity.

2.4 Frequency Diverse Array Radar

PAR, despite its better performance in different scenarios, is unable to scan in range dimension. Beam steering in range dimension can be very useful in localizing a target in range dimension as well as rejecting the range dependent clutter. To overcome this inability of PAR in range dimension, a new type of radar has been proposed in [40], which uses frequency increment across each antenna element to produce a range-angle dependent beampattern .i.e. it has the ability to scan both in angle and range. In rest of this section, we present an overview of research in FDA radar followed by brief data model and beampattern of FDA radar.

In a conventional FDA radar, same waveform and uniform frequency offset are used across the antenna elements of a transmit array. Initially, FDA was investigated by Antonik [40]–[43]. In [40], it is shown that the apparent angle of a FDA beam can be outside of real beam space, which can be exploited by a system designer to achieve a better performance and additional capability. According to [41], FDA radar can be used for multiple mission

simultaneously by utilizing the additional degree of freedom in terms of time, space, frequency and modulation. Two patents [42][43] have also been issued to show the independent modulation of frequency, amplitude and phase in an FDA radar.

The periodicity of FDA beampattern in terms of time, angle and range was explored by the authors of [44] .This periodicity can play a very important role in affecting the overall SINR at the receiver, thus it will also be further explored in the proposed designs of this research. Since FDA scans without phase shifters, the radiation characteristics of FDA has been simulated in [45] to show beam scanning feature of an FDA radar. It has been presented in [46] that FDA radar can be very effective in detecting slow moving targets and can also improve performance in terms of detection. The enhancement in target detection of a multistatic radar through an FDA has been shown in [47]. Moreover, a mathematical design and analysis of linear frequency modulated continuous waveform for FDA radar has also been presented in [48].

Another important research area is the application of FDA to synthetic aperture radar (SAR) [49], [50]. It has been shown that application of FDA to SAR has improved the high resolution imaging. In addition to uniform linear array, FDA has also been investigated for planar arrays [51] and circular arrays[52]. Receiver architectures for different types of FDA arrays have been proposed in [53]. The features of an FDA beam pattern by changing inter-element spacing and frequency offset have been investigated in [54] using finite difference time domain (FDTD) method. Furthermore, FDA is quite different from frequency scanned arrays which uses same frequency for each element at a particular time [55][56].

Range-angle dependent beampatterns of FDA radar have been studied in literature to show its worth compared to angle only beampattern [57]–[59]. A detailed analysis of

range-angle dependence of FDA radar has also been explored by Aytun in his MS thesis [60]. Higgins and Blunt [61] have used chirp signal with frequency diversity to explore the range and angle coupled beamforming. A double pulse FDA radar has been presented to compute range and angle maxima directly from beampatterns [62]. The precise steering of FDA beam in desired range-angle pair is another very important issue due to range-angle coupled beampattern. Since FDA apparent scanning angle is not equal to nominal scanning angle, a precise beam steering depends on both range and angle parameters [63].

Literature has also shown that frequency offset plays a very important role in improving overall performance of an FDA radar in terms of controlling range-angle dependency and spatial distribution of generated beam pattern [64]–[68]. Therefore, researchers have shown great interest to investigate proper selection of frequency offset between the adjacent elements of a linear FDA, so that an improved performance can be attained. Recently, an FDA radar with adaptive frequency offset has been proposed in [65] that select the frequency offset on the basis of maximizing output SINR. Likewise, an FDA radar with a time dependent frequency offset has been proposed in [66] to produce a time dependent beampattern for a given range-angle of target.

A new dimension of FDA research has applied non-uniform offsets between antenna elements to uncover some new interesting features of FDA radar. In [67], the inter-element spacing of FDA proportional to the wavelength has been studied for improved range-angle localization of targets. An FDA radar with logarithmically increasing inter-element frequency offset on antenna elements has been presented in [68], which generated a beampattern with single maxima for a particular frequency offset. Finally, the author of [69] has uncovered some new research opportunities in FDA radar.

2.4.1 Signal Model and Beampattern of FDA radar

In this subsection, the basic signal model for FDA radar is presented. Consider an FDA radar with fundamental frequency f_0 and a small frequency increment Δf at the input of array elements [70]. Fig. 2.3 shows an FDA of P antenna elements, where frequency at the input of p^{th} element can be given as [45],

$$f_p = f_0 + p\ .\Delta f\ ; \qquad p=0,1,\ldots,(P-1) \tag{2.6}$$

The signal $s_p(t)$ transmitted by p^{th} transmits antenna is

$$s_p(t)=\exp(-j2\pi f_p t); \qquad p=0,1,\ldots,(P-1) \tag{2.7}$$

The array factor of an FDA radar, derived in [44], has been rewritten to make it compatible with notation of this dissertation. Modified array factor is

$$AF(t,\Delta f,r,\theta)=\sum_{p=0}^{P-1} w_p^* \times \frac{1}{r_p} \exp\left\{-j2\pi\left(f_p t-\frac{r_p}{\lambda_p}\right)\right\} \tag{2.8}$$

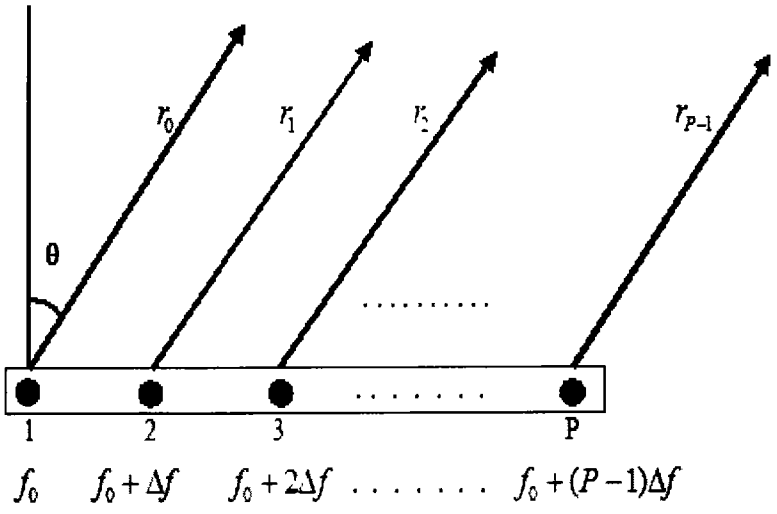

Fig. 2.3 Frequency diverse array

where, r_p is the range of target from P_{th} antenna element and λ is the wavelength. Assuming a point target in space, the FDA beam pattern B_{FDA} with uniform weights i.e., $w_p = 1$, can be written as

$$B_{FDA}(t,\Delta f,r,\theta)=\left|\sum_{p=0}^{P-1}\frac{1}{r_p}\exp\left\{-j2\pi f_p\left(t-\frac{r_p}{c}\right)\right\}\right|^2 \tag{2.9}$$

By using the value of f_p from (2.6) and taking the path difference as $r_p = r_0 - p.d\sin\theta$, the beampattern can further written as

$$B_{FDA}(t,\Delta f,r,\theta)=\left|\sum_{p=0}^{P-1}\frac{1}{r_p}\exp\left\{-j2\pi\left(f_0+p.\Delta_f\right)\left(t-\frac{r_0}{c}+\frac{pd\sin\theta}{c}\right)\right\}\right|^2 \tag{2.10}$$

Using the far field assumption i.e., $r_n \approx r_0$ and considering $f_0 \gg \Delta f$, the beampattern in (2.10) can be approximated as

$$B_{FDA}(t,\Delta f,r,\theta)\approx\left|\frac{\exp(j\gamma)}{r_0}\sum_{p=0}^{P-1}\exp\{-jp\eta\}\right|^2 \tag{2.11}$$

where $\gamma=-2\pi f_0\left(t-\frac{r_0}{c}\right)$ and $\eta=\left(2\pi\Delta ft+\frac{2\pi f_0 d\sin\theta}{c}-\frac{2\pi\Delta fr}{c}\right)$

According to [71], the beampattern in (2.11) can be further simplified and expressed as

$$B_{FDA}(t,\Delta f,r,\theta)=\left|\frac{\sin\left(\frac{P}{2}\left(2\pi\Delta ft+\frac{2\pi f_0 d\sin\theta}{c}-\frac{2\pi\Delta fr}{c}\right)\right)}{\sin\left(\frac{1}{2}\left(2\pi\Delta ft+\frac{2\pi f_0 d\sin\theta}{c}-\frac{2\pi\Delta fr}{c}\right)\right)}\right|^2=\left|\frac{\sin\left(\frac{P}{2}\eta\right)}{\sin\left(\frac{1}{2}\eta\right)}\right|^2 \tag{2.12}$$

The FDA pattern in (2.12) is a function of angle(θ) as well as time(t), frequency offset (Δf) and range(r). By using any two fixed parameters, the beampattern will vary

as function of other two parameters i.e. for a given frequency offset, if we fix range, the beampattern will vary in time and angle. Since we are interested in range-angle analysis in this work, therefore, for a fixed frequency offset and time, FDA beampattern will vary in both angle and range dimension, as shown in Fig 2.4. It can be observed that the beampattern has more than one maxima at different ranges due to periodicity property of FDA. The color bar in the Fig. 2.4 showed the values of beampattern in dBs at the entire range and angle dimension for radar scene. Furthermore, for $\Delta f = 0$, (2.12) reduces to the beampattern for conventional uniform linear array. The beampattern isin angle dimension only and constant for all ranges i.e. the beampattern of a PAR, as shown in Fig. 2.5.

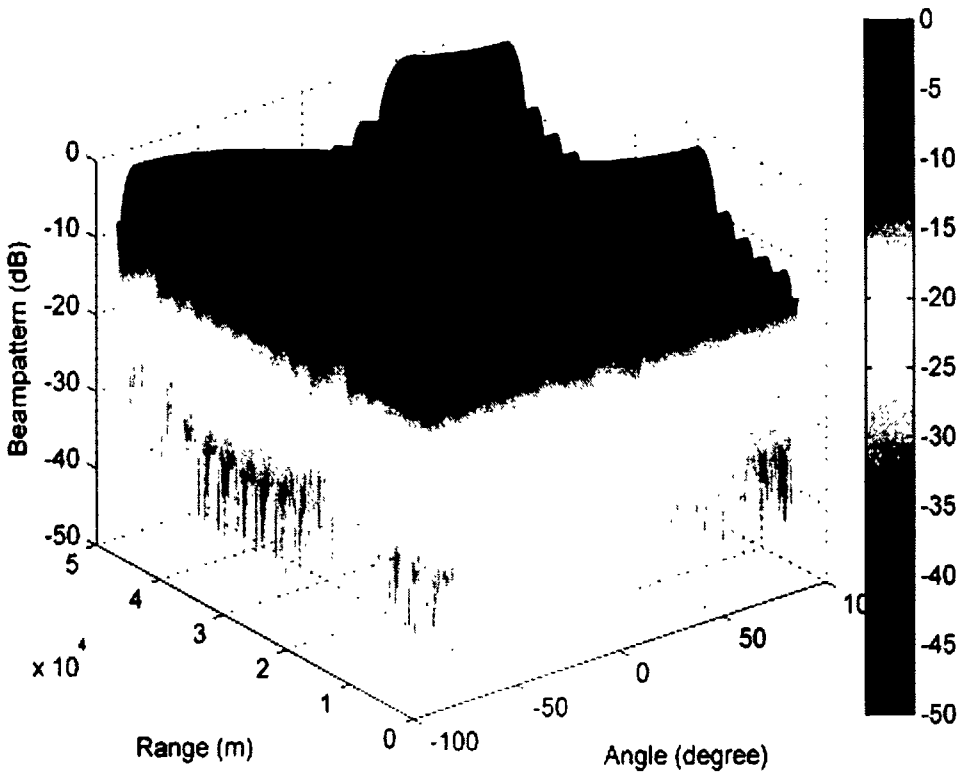

Fig. 2.4 FDA beam pattern $(P = 10,\ f_0 = 10GHz,\ \Delta f = 10KHz, d = \lambda/2)$

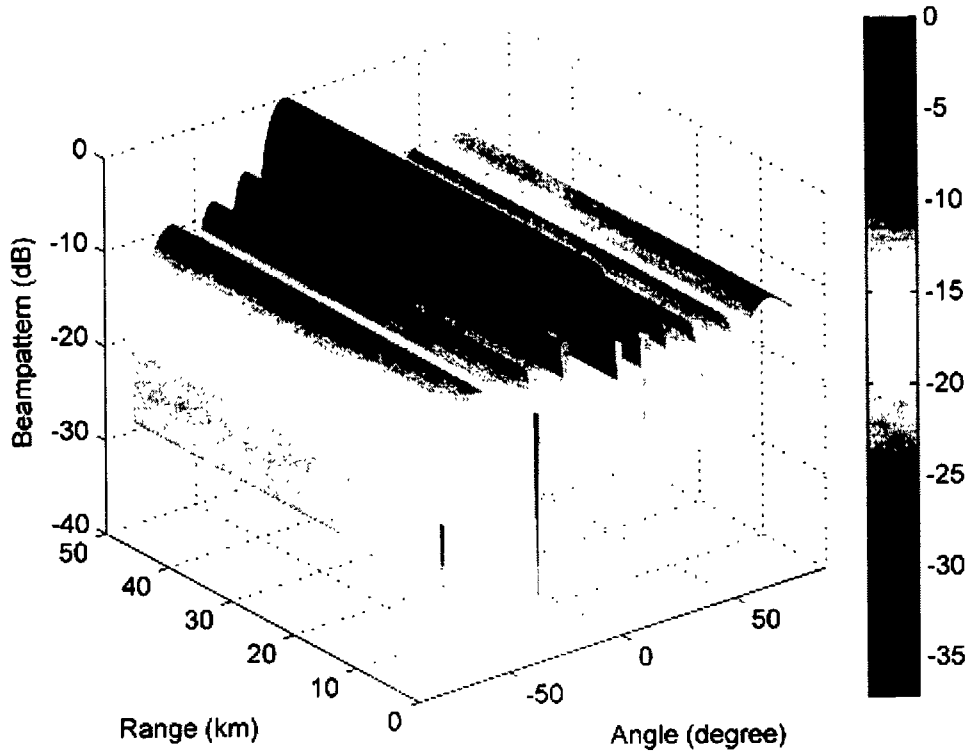

Fig. 2.5 PAR beam pattern $\left(P=10,\ f_0=10GHz,\ \Delta f=0KHz, d=\lambda/2\right)$

In order to clearly highlight this multiple maxima property, another view of normalized FDA beampattern has been presented in Fig. 2.6, which shows the behavior of range and angle dimension in 2-D graph. Beampattern has been colored coded on the third axis, where bar on the right side of beampattern showed the normalized values according to color. It can also observed that FDA radar produces multiple periodic maxima in range dimension. Moreover, it can be seen that number of maxima increases due to larger frequency offset (Δf). Multiple maxima property is not desirable due to its effects on target returns from a particular range-angle pair, resulting in low overall SINR. Reduction in SINR directly impact the probability of detection and parameter estimation performance.

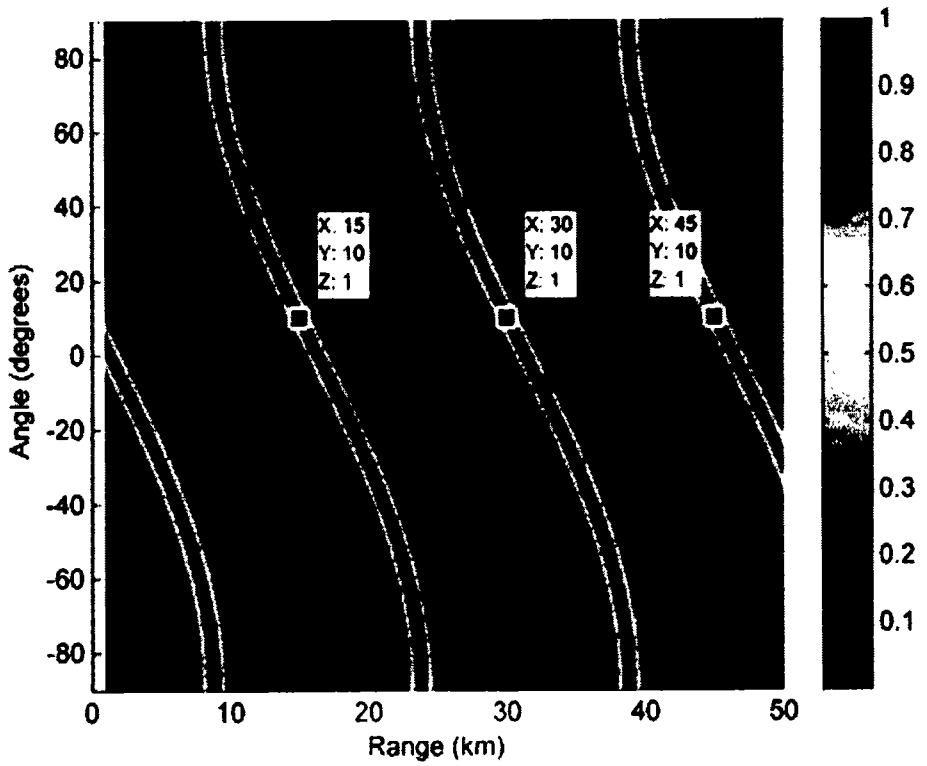

Fig. 2.6 FDA Normalized beam pattern $\left(P=15,\ f_0=10GHz,\ \Delta f=20KHz, d=\lambda/2\right)$

2.5 MIMO radar

The idea of MIMO was first introduced in wireless communications to achieve reasonably high data rate with some added reliability [72][73]. MIMO system transmits same or different signal from multiple transmitters, which can see channel independently to avoid the problem of fading. Due to path independence, different transmitted signals experience different level of fading, resulting in more or less constant average signal-to-noise ratio (SNR) levels. This was contrary to existing system at that time which transmit all of their energy over a single path, resulting in considerable variation in SNR level [74]. After a substantial progress in MIMO communication theory, MIMO radar was introduced and explored in [75]. A basic MIMO radar transmits multiple unique probing signals or

waveforms from its antennas as shown in Fig 2.7. It can transmit orthogonal waveforms [76], [77] as well as partially correlated waveforms [78], [79]. Orthogonality among the waveforms can be achieved by using frequency spread waveforms[80], spread spectrum coding [81] and phase coding [82], [83]. Waveform design is one of the important area of research in which the objective is to produce robust waveforms for best possible performance of MIMO radar in different scenarios [84]–[88]. Additionally, the research of MIMO radar also showed contribution in terms of improving detection performance, localization [89], [90] and parameter estimation of target [91], [92].

MIMO radar improves detection and estimation capability by exploiting independence among signals from each element and target radar cross section (RCS) scintillation. Since the received signal is a mixture of independently faded signals, so the average SNR of this overall signal remains constant, regardless of rapid variation in SNR of individual signal.

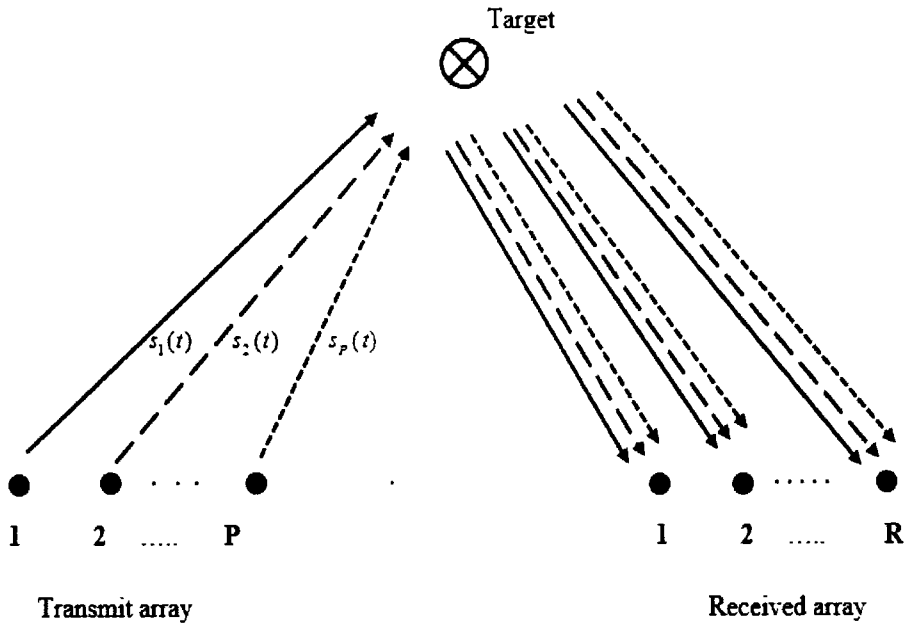

Fig. 2.7 Basic concept of MIMO radar

PAR, on the other hand, exploits maximum correlation among the signals transmitted by each antenna element and its performance degrades due to any scintillations in target RCS. In addition, under classical Swerling models [1], PAR suffers from large variations in the received signal power. MIMO radar also contributes in providing waveform diversity, which can be considered as one of the great advantage over PAR. This waveform diversity will be discussed in next subsection and its effectiveness will also be exploited in various proposed schemes of this work.

2.5.1 Classifications of MIMO Radar

In terms of distance between antenna elements, MIMO radar can be classified as MIMO radar with widely separated antennas and MIMO radar with colocated antennas.

2.5.1.1 MIMO radar with widely separated antennas

PAR uses its coherent processing gain to form a beam toward the target direction in an attempt to overcome scintillation problem. Although maximizing energy on target is helpful, however, reflected energy is considerably reduced due to same fading coefficient for all transmit-receive antenna pairs. In order to overcome this inability of PAR, antenna elements for MIMO radar are placed far from each other to see different views of a target. As a result, in addition to waveform diversity due to orthogonal waveform, it also gives spatial diversity by observing the target from different angels [93], [94]. This type of MIMO radar, also called statistical MIMO radar, can be bistatic or multistatic radar depending upon the number of widely separated transmit/receive antennas.

Spatial diversity gain, also called geometry gain, is the main essence of widely separated MIMO radar, since it prevents the radar from being blind to any type of target. This scheme loses the processing gain offered by PAR but it can synthesize the output of

multiple radars observing the target from a different aspect. Statistical MIMO radar will only be effected by deep fade in a very unlikely scenario, in which all the independent paths experience severe fading. Some important contribution of widely spaced antenna array are in improving the target detection capabilities [90], [95]and its ability to accurately measure the Angle of arrival [96]. Moreover, it can also provide a good range resolution in terms of resolving closely located targets present in same range cell [97]. Although statistical MIMO radar provides spatial diversity, however, it also demands a lot of synchronization and processing to combine the signals from different directions. This leads the research of MIMO radar towards closely located antennas.

2.5.1.2 MIMO radar with colocated antennas

In this scheme of MIMO radar, antenna elements are placed close to each other in such a way that each element observe same aspect of the target. A lot of research has been done in this scheme of MIMO radar, investigating its benefits over existing conventional radar system [98]–[111]. Although antenna placement is very similar to PAR, the colocated MIMO transmits a different waveform from each antenna element. This diversity in waveform is key to provide the extra advantages over the existing radar systems. It is worth mentioning that the effect of MIMO can be best realized on the receiver, where transmitted waveform are matched filtered and processed by suitable algorithms to get desired information about the target.

Another important benefit of waveform diversity is the formation of virtual array at the receiver [98], [99]. This virtual array or virtual extension in array can be understood as convolution of actual locations of transmitter and receiver antennas. It can improve the parameter identifiability, enhance target detection capability and achieve accurate

parameter estimation [91], [112], [113]. The optimized sparse arrays can also significantly improve the parameters estimation of MIMO radar [114]. Moreover, the receiver steering vector of MIMO radar is simply the kronecker product of transmit and receive steering vectors and can be written as

$$\mathbf{z}_{mimo}(\theta) = \mathbf{u}(\theta) \otimes \mathbf{v}(\theta) \tag{2.13}$$

Where $\mathbf{z}_{mimo}(\theta)$ is MIMO virtual steering vector with dimension $PR \times 1$. $\mathbf{u}(\theta)$ is $P \times 1$ transmit steering vector and $\mathbf{v}(\theta)$ is $R \times 1$ received steering vector given as

$$\mathbf{u}(\theta) = \left[1 \; e^{jk'd_t \sin\theta} \; e^{j2k'd_t \sin\theta} \; \ldots \; e^{j(P-1)k'd_t \sin\theta}\right]^T \tag{2.14}$$

$$\mathbf{v}(\theta) = \left[1 \; e^{jk'd_r \sin\theta} \; e^{j2k'd_r \sin\theta} \; \ldots \; e^{j(R-1)k'd_r \sin\theta}\right]^T \tag{2.15}$$

Where d_t and d_r are the distance between antenna elements of transmitter array and receiver array respectively.

2.5.2 Signal Model

In signal Model, MIMO radar with colocated antenna has been presented due to the fact that this work only focus on MIMO radar with closely placed antennas. A MIMO radar transmit multiple orthogonal signal from the transmit array in an omnidirectional fashion. Keeping this in view, let us consider a MIMO radar with P transmit antennas and R received antennas, where each transmit antenna element transmit an orthogonal waveform $\mathbf{s}_p(t), p = 1, 2, \ldots\ldots, P$. This MIMO configuration is shown in Fig. 2.7 at the start of this section. The orthogonality of signal is ensured through following condition

$$\int_T \mathbf{s}(t)\mathbf{s}(t)^H dt = \mathbf{I}_P \tag{2.16}$$

Where T is the pulse width of radar, t is the time within that pulse. $\mathrm{I_p}$ is the $P \times P$ identity matrix and $(.)^H$ is the hermitian transpose. The signal received at the receiver array can be expressed as

$$\mathbf{m}_r(t) = \mathbf{m}_s(t) + \mathbf{m}_i(t) + \mathbf{n}(t) \tag{2.17}$$

Where $\mathbf{m}_s(t)$, $\mathbf{m}_i(t)$ and $\mathbf{n}(t)$ are components of target signal, interference signal and noise respectively. Using assumption of point target, the signal from target can be

$$\mathbf{m}_s(t) = \alpha(\tau)\left[\mathbf{u}^T(\theta_t)\mathbf{s}(t)\right]\mathbf{v}(\theta_t) \tag{2.18}$$

$\alpha(\tau)$ is the complex reflection coefficient from the targets, θ_t is the angle of target and $\mathbf{s}(t)$ is the waveform. Each waveform can be filtered by using the matched filter given as

$$\mathbf{y}_p(\tau) = \frac{\int_T \mathbf{m}_r(t,\tau)s_p^*(t)dt}{\int_T \left|s_p^*(t)\right|^2 dt} \tag{2.19}$$

Where $(.)^*$ is the conjugate operator. Since we have used different waveform for each antenna element, so after matched filtering for P waveform, the $PR \times 1$ virtual data vector can be given as

$$\mathbf{y}(t) \triangleq \left[\mathbf{y}_1^T(t) \quad \mathbf{y}_2^T(t) \ldots\ldots \mathbf{y}_N^T(t)\right]^T \tag{2.20}$$

$$\mathbf{y}(t) = \alpha(\tau)\left(\mathbf{u}^T(\theta_t) \otimes \mathbf{v}(\theta_t)\right) \tag{2.21}$$

where $\otimes$ is the kronker product. The virtual steering vector is same as in (2.13) and resulted from waveform diversity provided by coherent MIMO radar. It plays a very important role

in various improvements provided by MIMO radar such as improved detection performance, angular resolution and interference cancellation.

2.6 Hybrid Radar systems

In order to exploit the advantages of more than one radar systems presented in previous sections, hybrid radars have also been explored in literature. These radars have been built with the philosophy that no radar system alone can provide every feature desired by a modern radar system. However, disadvantages of one radar system can be mitigated by other radar system, if used intelligently. Therefore, radars have been combined to overcome various inabilities of existing radars, e.g. PAR has a high transmit gain but it doesn't have any waveform diversity, MIMO radar has waveform diversity but no transmit gain. By combining them, we can have radar system with both transmit gain and waveform diversity. In next two subsection we will discuss two hybrid radar systems involving PAR, MIMO radar and FDA radar.

2.6.1 Phased MIMO Radar

Phased MIMO radar [115], [116] has been introduced in last decade to combine superior features of both PAR and MIMO radar in a single radar system. This radar has colocated antenna elements at the transmitter and receiver side just like PAR and Coherent MIMO radar. Transmit array can be divided into a number of subarrays with non-overlapped or fully overlapped structure. Each subarray transmits a unique waveform and steers a beam of reasonable gain towards a target in the region of interest by designing proper weight vector. Furthermore, the waveforms transmitted by different subarray are orthogonal to give a flavor of MIMO radar.

2.6.1.1. Signal Model of Phased MIMO Radar

For signal model of Phased MIMO radar, a transmit array of P antenna elements and a received array of R antenna elements has been considered. Antenna elements are placed in the vicinity of each other to make it a colocated radar. This phased MIMO radar divides the whole transmit array into subarrays which have full overlapping, as shown in Figure 2.8. In order to steer a beam in desired region, the antenna elements of N^{th} subarray will transmit waveform $s_n(k)$, where $k = 1,2,.....,K$ is the number of samples of each pulse. At the output of N^{th}subarray, transmitted signal can be expressed as

$$f_n(k) = \rho \mathbf{w}_n{}^H \mathbf{u}(\theta) s_n(k) \qquad n = 1,2,.....,N \qquad (2.22)$$

where $(.)^H$ is the hermition operator, s_n is the signal send by N^{th} subarray, $\mathbf{u}(\theta)$ is steering vector associated with transmit array and $\mathbf{w}_n$ is the weight vector consisting of complex weights for N^{th} subarray . This weight vector contains P_n beamforming weights for active elements and $P - P_n$ zeros for inactive elements. ρ represents the energy share of each subarray and can be given as

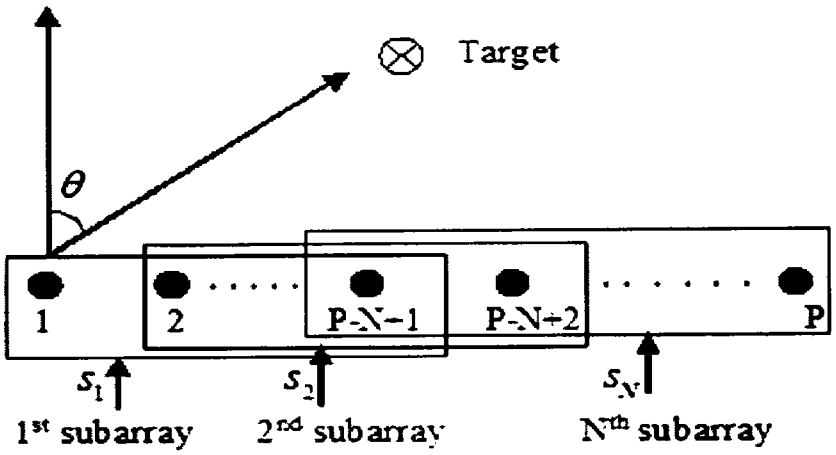

Fig. 2.8 Hybrid Phased MIMO radar

$$\rho = \frac{P}{N} \tag{2.23}$$

Sum of beams from all the subarrays pointing towards angle θ can be expressed as

$$f(k) = \rho \sum_{n=1}^{N} \mathbf{w}_n{}^H \mathbf{u}(\theta) s_n(k) \tag{2.24}$$

$$= \rho \left[\mathbf{W}^H \mathbf{u}(\theta) \right] \mathbf{s}_N(k) \tag{2.25}$$

$\mathbf{W} = [\mathbf{w}_1, \mathbf{w}_2 ..... \mathbf{w}_N]$ is $P \times N$ weight matrix and $\mathbf{s}_N(\mathbf{k}) = [\mathrm{s}_1(k), \mathrm{s}_2(k) ..... \mathrm{s}_N(k)]$ is the waveform vector of length $N \times 1$. Each entry of weight matrix will represent the association of an antenna element to a particular subarray. If a weight $w_{n,p}$ is zero, it means that p^{th} element doesn't belong to n^{th} subarray. On the other hand, a non-zero weight simply showed the association of p^{th} element to the n^{th} subarray. Moreover, all non-zero weights in a subarray scale same waveform to steer a beam towards region of interest. Transmitted signal by each antenna element can be represented as

$$\gamma(k) = \rho \mathbf{W}^* \mathbf{s}_N(k) \tag{2.26}$$

It can be seen that each antenna element will transmit a linear combination of different waveforms at a particular time. Moreover, the signals $s_n(k)$, $n = 1, 2, ..., N$ are orthogonal to each other, however, the signals $\gamma_i(k)$, $i = 1, 2, ..., P$ are not orthogonal to each other. The normalized beampattern produced by n^{th} subarray of a Phased MIMO radar towards a target in direction θ_t can be obtained as

$$B_n(\theta) = \frac{\left| \mathbf{w}_n^H \mathbf{u}(\theta) \right|^2}{\left| \mathbf{w}_n^H \mathbf{u}(\theta) \right|^2} \tag{2.28}$$

The effectiveness of this Phased-MIMO radar lies in gain provided by multiple beams and diversity provided by multiple waveforms. Moreover, it gives a tradeoff between beam shape loss and angular resolution by efficiently selecting the number of subarrays. Phased MIMO radar discussed here will be termed as Hybrid Phased MIMO radar with equal subarrays (HPMR-ES) in coming chapter due to same number of elements in each subarray, which can be given by following relation

$$L = P - N + 1 \tag{2.29}$$

In literature, the phased MIMO radar has been presented in two different types of subarray arrangements i.e. overlapped subarrays [116]–[118] and disjoint subarrays [119]–[125]. The disjoint subarrays have further applied to two different array architectures. One of them has used ULA as a transmitting array and divide it into disjoint subarrays [119]–[122]. The other architecture has simply divided a planar array into disjoint subarrays and used partially correlated waveforms in different subrrays [123]–[125].

It is worth mentioning that Phased-MIMO radar is a tradeoff between PAR and MIMO radar in terms of robustness against beam shape loss and angular resolution. Its robustness against beamshape loss is not as good as a PAR and its angular resolution is also less than MIMO radar but it has both the features, making it more effective than PAR and MIMO radar alone [116]. Thus, it is important to adjust the number of subarrays for a robust and effective design for Phased MIMO radar. Beampattern and SINR of Phased MIMO radar has also been analyzed and compared with existing radar systems to show its superior performance [117][118].

An important work has optimized the covariance matrix of subarrayed-MIMO radar array or Phased MIMO radar, to show the improvement on target parameter estimation in

terms of Cramér-Rao bound (CRB) [121]. MIMO-Phased array radar using waveforms with different correlation and different signaling strategies have been explored in [123]–[125]. In particular, the authors of [124] have proposed a scheme to produce correlated signals for a grid of rectangular arrays. The proposed signals provide two dimensional rectangular beampatterns that maintain desired temporal properties. Such rectangular array architecture are very effective in concurrent searching, tracking and detection of targets.

Moreover, the results for different number of partitions in Phased MIMO radar have presented in terms of beampattern and SINR [126]. Lastly, the frequency diversity has been applied to a Phased MIMO radar by Wang [127], where each subarray gives range dependent beampattern as well as angle dependent beampattern. This has provided a foundation for an entirely new type of hybrid radar discussed in next subsection. In all Phased MIMO radars discussed so far, the subarrays have equal size and thus they steer beams of same width towards any type of target, resulting in same focusing of a target by each subarray. Since the beams of variable width can add extra degree of freedom in terms of controlling the reflections from a particular target, so their effectiveness will be explored in next chapters of this work.

2.6.2 MIMO-FDA Radar

In this section, MIMO-FDA radar signal model has been presented followed by existing literature on MIMO-FDA radar.

2.6.2.1. Signal Model of MIMO-FDA Radar

The signal model of MIMO-FDA will be presented after giving the steering vector for FDA radar. For a conventional FDA radar, at a particular time t, the steering vector can be

expressed in terms of range and angle as [59]

$$\mathbf{u}(\theta,r)=\left[1 \quad e^{-j\left(\frac{2\pi f_0 d\sin\theta}{c_0}+\frac{2\pi \Delta f d\sin\theta}{c_0}-\frac{2\pi \Delta f\, r}{c_0}\right)} \ldots\ldots\ldots e^{-j\left(\frac{2\pi f_0 (p-1)d\sin\theta}{c_0}+\frac{2\pi (p-1)\Delta f d\sin\theta}{c_0}-\frac{2\pi (p-1)\Delta f\, r}{c_0}\right)}\right] \tag{2.30}$$

Since $f_1 >> \Delta f$, so $\frac{2\pi.\Delta f.d\sin\theta}{c_0}$ has negligible impact. Thus equation (2.30) will be

$$\mathbf{u}(\theta,r)=\left[1 \quad e^{-j\left(\frac{2\pi f_0 d\sin\theta}{c_0}-\frac{2\pi.\Delta f\, r}{c_0}\right)} \ldots\ldots\ldots e^{-j\left(\frac{2\pi f_0 (p-1)d\sin\theta}{c_0}-\frac{2\pi (p-1)\Delta f.r}{c_0}\right)}\right] \tag{2.31}$$

This steering vector has been used in signal model of MIMO-FDA by all subarray based designs and it can also be represented or can be divided into two parts as

$$\mathbf{u}(\theta,r)=\mathbf{u}(\theta)\odot\mathbf{u}(r) \tag{2.32}$$

where,

$$\mathbf{u}(\theta)=\left[1 \quad e^{-j\left(\frac{2\pi f_0 d\sin\theta}{c_0}\right)} \ldots\ldots\ldots e^{-j\left(\frac{2\pi f_0 (p-1)d\sin\theta}{c_0}\right)}\right] \tag{2.33}$$

$$\mathbf{u}(r)=\left[1 \quad e^{-j\left(\frac{2\pi \Delta f\, r}{c_0}\right)} \ldots\ldots\ldots e^{-j\left(\frac{2\pi (p-1)\Delta f\, r}{c_0}\right)}\right] \tag{2.34}$$

(2.31) and (2.32) show that angle dimension in an FDA and MIMO-FDA radar is independent of frequency offset. Frequency offset only affects the range dimension. The steering vector in (2.30) is multiplied with weight vector to determine the size of subarray in MIMO-FDA radar.

MIMO-FDA radar is a hybrid radar, in which frequency diverse array is divided into number of overlapping subarrays and each subarray is modulated by a distinct waveform

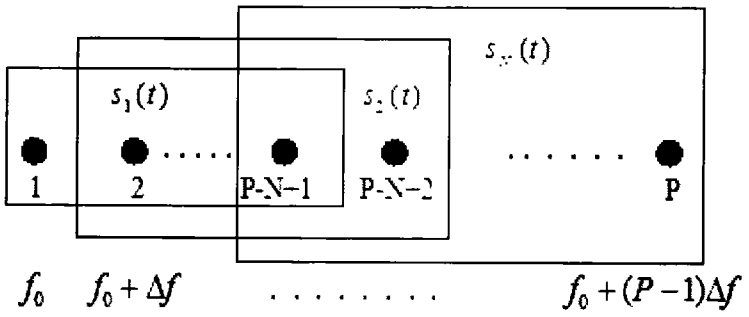

Fig. 2.9 Conventional MIMO-frequency diverse array radar

as shown in Fig. 2.9. Using an array of P elements and N subarrays, the signal radiated by N^{th} subarray can be expressed as

$$m_n(k,\theta,r)=\left[\mathbf{w}_n{}^H\mathbf{u}(\theta,r)\right]s_n(k) \tag{2.35}$$

Where $\mathbf{W}_n$ is the weight vector containing only the weights for active antennas in N^{th} subarray, $\mathbf{u}(\theta,r)$ is steering vector and $s_N(k)$ is the baseband waveform transmitted by N^{th} subarray with k being the current sample in time. The weight vector can be adjusted to get maximum coherent gain in a particular direction and at a particular range. The signal radiated by all the beams towards a target at (θ,r) can be written as

$$m(k,\theta,r)=\sum_{n=1}^{N}\left[\mathbf{w}_n{}^H\mathbf{u}(\theta,r)\right]s_n(k) \tag{2.36}$$

It is important to mention that the all the subarrays are of the same size in the conventional MIMO-FDA radar i.e. each subarray contains $P-N+1$ elements.

Inspiration for MIMO-FDA radar is very much similar to Phased MIMO radar i.e. to exploit the benefits of both radars, while mitigating their weaknesses. MIMO-FDA radar has been the focus of most recent research done in hybrid radars. According to the literature of MIMO-FDA radar, MIMO is hybridized with FDA radar in two different arrangements.

One of them transmits different waveform from each antenna element of a frequency diverse array [128]–[131], while the other divides FDA into subarrays and transmits different waveform from each subarray [132]–[134].

The authors of [128], besides some other contributions, present a model that transmits the pseudo noise (PN) codes at slightly different frequencies to show the range dependent behavior of MIMO waveforms. FDA-MIMO radar configuration has also been used for suppressing the deceptive jamming i.e. true and false targets have been be separated more effectively by exploiting the range-angle dependent nature of beampattern [129]. Another recent work has presented an improved joint range-angle estimation method by resolving the range ambiguity using an *a priori* knowledge of target [130]. Moreover, range dependent interference suppression through a FDA-MIMO radar has also been reported, resulting in improved localization and estimation performance [131] .

MIMO-FDA with subarrays has also been considered for hybridization of two radars. In [132], each subarray transmitted a waveform at slightly different frequency from the other subarrays. In other words frequency diversity is among the subarrays instead of antenna elements. A slightly different work has divided the conventional frequency diverse array into number of overlapped subarrays, where each subarray used a distinct waveform to steer a beam in the region of interest [133]. Furthermore, the concept of sub-arrayed FDA in [134] has helped in estimating the target positions by using the beamspace-based MUSIC algorithm. In [135], two subarrays have been used to estimate range and angle by simply using FDA in both subarray. However, the system is not MIMO-FDA due to same waveform in each subarray.

2.7 Summary of Chapter

This chapter presents an overview of exiting radar technologies like PAR, FDA radar, MIMO Radar, Phased MIMO radar and MIMO-FDA radar. Advantages of these radars have been highlighted and some weaknesses have been mentioned to show the motivations towards this research. It can be concluded that hybridization of different radar technologies can definitely build a radar system that can outclass all the existing conventional radar technologies. However, hybridization of radars has also faced some issues that must be resolved in order to attain maximum advantages and to mitigate the limitations of hybrid radars. In particular, the partitioning of arrays needs new schemes for better information about target. Likewise, frequency offset selection and adjustment can be further explored.

Chapter 3

New Schemes in Hybridization of MIMO radar with Phased Array Radar

3.1 Introduction

Hybrid radars is an emerging field with a lot of potential for new research areas. As concluded in last chapter, these hybrid radars can outperform the existing radars by combining their benefits. The hybrid radars, proposed in literature, are still in their early stages and need further investigation to achieve maximum performance. Thus, a lot of research needs to be done on different aspects of hybrid radars. In this regard, we aim to focus on new partitioning schemes for hybrid radars, which allow them to perform better as compared to existing partitioning schemes.

This chapter explores the advantages of unequal subarrays in hybridization of MIMO radar with phased array radar. Unequal subarray based structure allows more focusing of target at the transmit side by steering beams of variable width towards target of interest, thus adding an extra degree of freedom to the radar system. These focused beams along with the waveform diversity provided by MIMO radar gives superior results at the receiver end. Two schemes of unequal subarrays are proposed which show improvements as compared to PAR, MIMO radar and existing phased MIMO radar.

First scheme presents a simple overlapping structure, where each subarray has different number of antenna elements. Waveform diversity is applied by sending different

waveforms from each subarray. The reflections obtained from a single target are matched-filtered to get desired information about the target. Moreover, information from each waveform has been stacked to get an extended data vector, which results in improved beampattern. The second scheme presents a different unequal subarray structure called Full waveform diverse Phased MIMO (FWD-PMIMO) radar. Proposed system not only provide beam focusing but also offer maximum waveform diversity that is equal to the conventional MIMO radar. Results for FWD-PMIMO radar exhibit improvement in terms of transmit/received beampatterns, interference rejection capability and signal to interference plus noise ratio (SINR).

3.2 Phased MIMO Radar with Unequal Subarrays

This section presents a new Phased MIMO radar with variable number of elements in each subarray. Resultant system, called Hybrid Phased MIMO radar with unequal subarrays (HPMR-US), gives same diversity as conventional Phased MIMO radar and the gain of system increases as we move from one subarray to the other. This increase in gain, by properly incrementing number of elements, gives us directed beams of variable width towards a target. Consequently, the small targets in the presence of interfering targets can be effectively tracked and detected by this radar system.

3.2.1 Signal model

In the signal model, we assume a transmit array of P antenna elements divided into N subarrays by applying unequal array partitioning, as shown in Fig. 3.1. It can be observed that most of antennas contribute in more than one subarray. Therefore, if an antenna element contributes in a particular subarray, then it is an active element for that subarray. Likewise, the element with no contribution will be termed as inactive element.

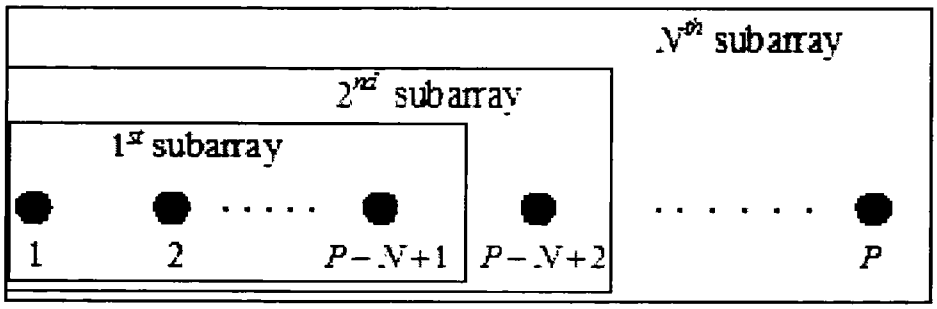

Fig. 3.1 Hybrid Phased MIMO radar with unequal subarrays

for that particular subarray. The antennas of n^{th} subarray will transmit a waveform $s_n(k)$ to steer a beam in the direction of target, where $k = 1,2,.....,K$ are the samples of each pulse. At the output of n^{th} subarray, complex envelop of signals can be expressed as

$$\mathbf{f}_n(k) = \rho s_n(k)\mathbf{w}_n^* \qquad n = 1,2,.....,N \tag{3.1}$$

where $\mathbf{w}_n$ represents weight vector of n^{th} subarray, containing weights belonging to the active elements of this subarray, $(.)^*$ is the conjugate operator and ρ is the energy given to each subarray. It is important to mention that the number of active weights in each $\mathbf{w}$ will be different depending upon the number of element in the subarrays. For first subarray, there are $P-N+1$ active weights, while the last subarray has P active weighs. This variation allows us to steer variable size beams in the direction of target. Moreover, total energy is shared by N subarrays i.e. $\rho = \sqrt{P/N}$. In order to produce beam towards a target in the direction θ , the signal radiated by n^{th} subarray can be given as

$$m_n(k,\theta) = \rho\left[\mathbf{w}_n^H \mathbf{u}_n(\theta)\right] s_n(k) \tag{3.2}$$

where $\mathbf{u}_n(\theta)$ is the steering vector of n^{th} subarray and $(.)^H$ is hermitien operator. Since all the elements in n^{th} subarray transmit same waveform, so a beam will be formed.

The signal reflected by a far field target at angle θ can be given by

$$m_r(k,\theta) = \rho\alpha(\theta)\sum_{n=1}^{N}\mathbf{w}_n^H\mathbf{u}_n\, e^{j\tau_n}(\theta)s_n(k) \tag{3.3}$$

where $\alpha(\theta)$ represents complex valued reflection coefficient from target and τ_n represents the propagation time associated with n^{th} subarray. Although, all the subarrays start at the first element of transmit array, however, due to variable sizes of subarrays, time of propagation for the waveforms across each subarray will be slightly different from each other. Equation (3.3) can be further expressed as

$$m_r(k,\theta) = \rho\alpha(\theta)\left[\mathbf{x}(\theta)\odot\mathbf{d}(\theta)\right]^T\mathbf{s}_N(k) \tag{3.4}$$

where $\odot$ is the Hadamard product. $\mathbf{x}(\theta)$, $\mathbf{d}(\theta)$ and $\mathbf{s}_N(\theta)$ are $N\times 1$ vectors given as

$$\mathbf{x}(\theta) = \left[\mathbf{w}_1\mathbf{u}_1, \mathbf{w}_2\mathbf{u}_2, \ldots\ldots\ldots \mathbf{w}_N\mathbf{u}_N\right]^T \tag{3.5}$$

$$\mathbf{d}(\theta) = \left[e^{j\tau_1}, e^{j\tau_2}, \ldots\ldots\ldots, e^{j\tau_N}\right]^T \tag{3.6}$$

$$\mathbf{s}_N(k) = \left[s_1(k), s_2(k)\ldots\ldots\ldots s_N(k)\right]^T \tag{3.7}$$

If we assume θ_t as the angle of desired target with Q interferences around it, then the received signal at a receiver array of R antennas elements can be given by

$$\mathbf{g}(k) = m_r(k,\theta_t)\mathbf{v}(\theta_t) + \sum_{i=1}^{Q} m_r(k,\theta_i)\mathbf{v}(\theta_i) + \mathbf{n}_g(k) \tag{3.8}$$

where $\mathbf{v}(\theta)$ is $R\times 1$ steering vector of the receiver side. Applying a matched filter for N different waveforms, a virtual data vector with extended dimension of $NR\times 1$ will be formed that can be expressed as

$$\mathbf{y} = \rho\alpha_t\mathbf{z}(\theta_t) + \sum_{i=1}^{Q}\rho\alpha_i\mathbf{z}(\theta_i) + \tilde{\mathbf{n}} \tag{3.9}$$

where $$\mathbf{z}(\theta)=\left[\mathbf{x}(\theta)\odot\mathbf{d}(\theta)\right]\otimes\mathbf{v}(\theta) \tag{3.10}$$

The data vector $\mathbf{y}$ is obtained by stacking the vectors of (3.8). $\otimes$ is the kronecker product, $\tilde{\mathbf{n}}$ is noise vector of length $NR\times 1$ and $\mathbf{z}(\theta)$ is extended steering vector of length $NR\times 1$. For PAR and MIMO radar, this steering vector has length of $R\times 1$ and $PR\times 1$ respectively. In case of PAR, virtual steering vector reduces to normal steering vector given as

$$\mathbf{z}_{PAR}(\theta)=x(\theta).\mathbf{v}(\theta)=\left[\mathbf{w}^{H}\mathbf{u}(\theta)\right].\mathbf{v}(\theta) \tag{3.11}$$

PAR has only one weight vector comprising of all the elements of transmit array and the vector $\mathbf{d}(\theta)$ vanishes due to single waveform. MIMO has same steering vector as (3.10), however, length of waveform diversity vector is $P\times 1$ instead of $N\times 1$ due to P waveforms, resulting in $PR\times 1$ steering vector. This waveform diversity feature of MIMO radar has been inherited by all Phased MIMO radars.

3.2.2 Discussion and Practical considerations

For better detection of target in background of strong interferences, gain as well as interference rejection of radar has a very important role. The radar under discussion will provide the interference rejection through diversity in transmitted waveform. Additionally, it will also enhance the signal to noise ratio by introducing an increase in number of elements for a subarray. The number of elements in a subarray can be calculated by

$$L = P-N+n; \qquad n = 1,2,.....N \tag{3.12}$$

Number of antenna elements are variable in each subarray i.e. for $P=15$ transmit antenna elements and $N=7$ subarrays, the first subarray will have 9 elements, second subarray will have 10 elements and the last subarray will contain all 15 elements.

The next step is to present transmit beamforming weight matrix, baseband signal and combination of signal transmitted by each antenna element. Weight matrix for the proposed radar system can be given as

$$\mathbf{W} = \begin{bmatrix} w_{1,1} & w_{2,1} & \cdot & \cdot & \cdot & \cdot & w_{N,1} \\ w_{1,2} & w_{2,2} & \cdot & \cdot & \cdot & \cdot & w_{N,1} \\ \cdot & \cdot & \cdot & & & & \cdot \\ \cdot & \cdot & & \cdot & & & \cdot \\ \cdot & \cdot & & & \cdot & & \cdot \\ w_{1,P-N+1} & \cdot & \cdot & \cdot & \cdot & \cdot & \cdot \\ \mathbf{0}_{N-3} & w_{2,P-N+2} & & & & & \cdot \\ 0 & \mathbf{0}_{N-3} & & & & & \cdot \\ 0 & 0 & \cdot & \cdot & \cdot & \cdot & w_{N,P} \end{bmatrix} \tag{3.13}$$

where $\mathbf{W}$ is $P \times N$ matrix of weights and $w_{n,p}$ is the weight of p^{th} element of n^{th} subarray and $\mathbf{0}_{N-3}$ represent a vector of $N-3$ zeros.

The baseband waveforms transmitted by antenna elements are

$$\{s_n(k) = \sqrt{\frac{1}{T}} e^{j2\pi(\frac{n}{T})k}\}_{n=1}^{N} \tag{3.14}$$

These signals maintains orthogonality for different Doppler shifts and time delays, if we select a pulse width T and a proper frequency increment $\Delta f = f_{n+1} - f_n$ for s_n and s_{n+1} in such a way that they satisfy $\Delta f >> 1/T$.

Moreover, for the proposed fully overlapped subarrays scheme, each antenna element will transmit a linear combinations of orthogonal waveforms. Therefore, the combination of signal sent by P antenna elements can be expressed as

$$\boldsymbol{\gamma}(\mathbf{k}) = \rho \mathbf{W}^* \mathbf{s}_N(k) \tag{3.15}$$

$\boldsymbol{\gamma}(\mathbf{k})=[\gamma_1(k),.....\gamma_P(k)]^T$ is the $P\times 1$ vector of waveforms transmitted by P antenna elements. $\mathbf{W}=[\mathbf{w}_1,\mathbf{w}_2.....\mathbf{w}_N]$ is the weight matrix of dimension $P\times N$ and '**s**' are the waveforms. Signal transmitted through each antenna element will be given as

Antenna 1: $$\gamma_1=\rho\left(w_{1,1}^{*}s_1+w_{2,1}^{*}s_2.....w_{N,1}^{*}s_N\right) \tag{3.16a}$$

Antenna 2: $$\gamma_2=\rho\left(w_{1,2}^{*}s_1+w_{2,2}^{*}s_2.....w_{N,2}^{*}s_N\right) \tag{3.16b}$$

$$\vdots \qquad \vdots \qquad \vdots$$

Antenna $P-1$: $$\gamma_{P-1}=\rho\left(w_{N,P-1}^{*}s_{N-1}+w_{N,P}^{*}s_N\right) \tag{3.16c}$$

Antenna P : $$\gamma_P=\rho\left(w_{N,P}^{*}s_N\right) \tag{3.16d}$$

Each antenna element will send a combination depending upon the weights. If a particular element is not part of a subarray, it will not send waveform of that particular subarray due to zero weight.

In practical considerations, proposed design has challenges like uniform power distribution for each antenna element and signals with constant modulus property. Power distribution can be addressed by applying the constraint of uniform power distribution across each antenna element during optimization of $\mathbf{W}$. After finding a suitable $\mathbf{W}$, the waveform $\mathbf{s}_N(t)$ can be designed in such a way that it produces $\boldsymbol{\gamma}(t)$, which may satisfy constant modulus property. Additionally, non-overlapped subarray based HPMR-US may also resolve the power distribution and constant modulus issues, however, we will lose the extra coherent gain provided by overlapped subarrays, resulting in degradation of SINR.

3.2.3 Beamforming and SINR

This sub-section will give mathematical expressions for the beampattern and signal to interference noise ratio (SINR) of HPMR-US.

3.2.3.1 Conventional beamforming

For conventional beamforming, weight vector for transmitter side is

$$\mathbf{w}_n = \frac{\mathbf{u}_n(\theta_t)}{\left\|\mathbf{u}_n(\theta_t)\right\|}, \qquad n = 1,2,.....,N \tag{3.17}$$

For receiver side, weight vector will be of dimension $NR \times 1$ and given as

$$\mathbf{w}_r = \mathbf{z}(\theta_t) = \left[\mathbf{x}(\theta_t) \odot \mathbf{d}(\theta_t)\right] \otimes \mathbf{v}(\theta_t) \tag{3.18}$$

The normalized beam pattern can be

$$B(\theta) = \frac{\left|\mathbf{w}_r^H \mathbf{z}(\theta)\right|^2}{\left|\mathbf{w}_t^H \mathbf{z}(\theta_t)\right|^2} = \frac{\left|\mathbf{z}^H(\theta_t)\mathbf{z}(\theta)\right|^2}{\left\|\mathbf{z}(\theta_t)\right\|^4} \tag{3.19}$$

By using value of $\mathbf{z}$ from (3.10), the beampattern become

$$B_n(\theta) = \frac{\left|\left(\left[\mathbf{x}(\theta_t) \odot \mathbf{d}(\theta_t)\right] \otimes \mathbf{v}(\theta_t)\right)^H \left(\left[\mathbf{x}(\theta_t) \odot \mathbf{d}(\theta_t)\right] \otimes \mathbf{v}(\theta_t)\right)\right|^2}{\left\|[\mathbf{x}(\theta_t) \odot \mathbf{d}(\theta_t)] \otimes \mathbf{v}(\theta_t)\right\|^4} \tag{3.20}$$

Assuming a ULA i.e. $\mathbf{u}_1^H(\theta_t)\mathbf{u}_1(\theta) = \mathbf{u}_2^H(\theta_t)\mathbf{u}_2(\theta) = ... = \mathbf{u}_N^H(\theta_t)\mathbf{u}_N(\theta)$, beampattern can be further simplified and written as

$$B_n(\theta) = \frac{\left|\mathbf{u}_n^H(\theta_t)\mathbf{u}_n(\theta)\right|^2}{\left\|\mathbf{u}_n^H(\theta_t)\right\|^4} \cdot \frac{\left|\mathbf{d}_n^H(\theta_t)\mathbf{d}_n(\theta)\right|^2}{\left\|\mathbf{d}_n^H(\theta_t)\right\|^4} \cdot \frac{\left|\mathbf{v}^H(\theta_t)\mathbf{v}(\theta)\right|^2}{\left\|\mathbf{v}(\theta_t)\right\|^4} \tag{3.21}$$

For HPMR-US, we will choose number of subarrays in the beginning and then calculate the number of elements in a subarray by varying "n". Resultant beampattern can be expressed by

$$B_n(\theta) = \frac{\left|\mathbf{u}_n^H(\theta_t)\mathbf{u}_n(\theta)\right|^2}{(P-N+n)^2} \cdot \frac{\left|\mathbf{d}_n^H(\theta_t)\mathbf{d}_n(\theta)\right|^2}{N^2} \frac{\left|\mathbf{v}^H(\theta_t)\mathbf{v}(\theta)\right|^2}{R^2} \tag{3.22}$$

Where $\|\mathbf{u}_n(\theta_t)\|^2 = P-N+n$, $\|\mathbf{d}_n(\theta_t)\|^2 = N$ and $\|\mathbf{v}(\theta_t)\|^2 = R$. For HPMR-ES, the resultant beampattern can be written as

$$B_n(\theta) = \frac{\left|\mathbf{u}_n^H(\theta_t)\mathbf{u}_n(\theta)\right|^2}{(P-N+1)^2} \cdot \frac{\left|\mathbf{d}_n^H(\theta_t)\mathbf{d}_n(\theta)\right|^2}{N^2} \frac{\left|\mathbf{v}^H(\theta_t)\mathbf{v}(\theta)\right|^2}{R^2} \tag{3.23}$$

3.2.3.2 Adaptive beamforming

The objective of adaptive beamforming is to maximize the output SINR at the received antenna array. Minimum variance distortionless response (MVDR) beamformer is used to give the distortionless response in target direction and minimize the interference plus noise. The optimization problem is as follows

$$\min_{\mathbf{w}_r} \mathbf{w}_r^H \mathbf{C}_{i+n} \mathbf{w}_r \qquad \text{subject to} \qquad \mathbf{w}_r^H \mathbf{z}(\theta_t) = 1 \tag{3.24}$$

The solution of (3.24) is given in [27] as

$$\mathbf{w}_r = \frac{\mathbf{C}_{i+n}^{-1}(\theta)\mathbf{z}(\theta_t)}{\mathbf{z}^H(\theta_t)\mathbf{C}_{i+n}^{-1}(\theta)\mathbf{z}(\theta_t)} \tag{3.25}$$

$\mathbf{C}_{i+n}$ is the interference plus noise covariance matrix for HPRM-US, which can be estimated as $\hat{\mathbf{C}} = \sum_{j=1}^{J} \mathbf{d}_j \mathbf{d}_j^H$,where $\mathbf{d}_j$ is the data acquired from J different pulses of proposed radar. Finally, the beampattern for an adaptive beamformer can be given as

$$B(\theta) = \left|\mathbf{w}_r^H \mathbf{z}(\theta)\right|^2 \tag{3.26}$$

3.2.3.3 SINR

Signal to interference plus noise ratio can be given as

$$SINR = \frac{\rho^2 \beta_t^2 \left| \mathbf{w}_r^H \mathbf{z}(\theta_t) \right|^2}{\mathbf{w}_r^H \mathbf{C}_{t+n} \mathbf{w}_r} \tag{3.27}$$

The $\mathbf{C}_{t+n}$ matrix can be given as

$$C_{t+n} = \sum_{t=1}^{Q} \rho^2 \beta_t^2 \mathbf{z}(\theta_t) \mathbf{z}^H(\theta_t) + \beta_{\bar{n}}^2 I \tag{3.28}$$

By substituting $\mathbf{C}_{t+n}$ and $\mathbf{w}$ in equation (40), we get

$$SINR = \frac{\rho^2 \beta_t^2 \left| \left\| \mathbf{u}_n(\theta_t) \right\|^2 \left\| \mathbf{d}_n(\theta_t) \right\|^2 \left\| \mathbf{v}(\theta_t) \right\|^2 \right|^2}{\mathbf{z}^H(\theta_t) (\sum_{t=1}^{Q} \rho^2 \beta_t^2 \mathbf{z}(\theta_t) \mathbf{z}_t^H(\theta_t) + \beta_{\bar{n}}^2 \mathbf{I}) \mathbf{z}(\theta_t)} \tag{3.29}$$

where β_t^2 and $\beta_{\bar{n}}^2$ are the variances of reflection coefficient from target and noise, respectively. By further simplifying (3.29), we will get the final relation for SINR

$$SINR_{HPMR-US} = \frac{\rho^2 \beta_t^2 (P - N + n)^2 N^2 R^2}{\sum_{t=1}^{Q} \rho^2 \beta_t^2 \left| \mathbf{z}^H(\theta_t) \mathbf{z}(\theta_t) \right| + \beta_{\bar{n}}^2 (P - N + n) R} \tag{3.30}$$

Since we are considering interference dominant case, (3.30) can be simplified to

$$SINR_{HPMR-US} = \frac{\rho^2 \beta_t^2 (P - N + n)^2 N^2 R^2}{\sum_{t=1}^{Q} \rho^2 \beta_t^2 \left| \mathbf{z}^H(\theta_t) \mathbf{z}(\theta_t) \right|} \tag{3.31}$$

For conventional Phased MIMO radar, i.e. Phased MIMO radar with equal subarrays (HPMR-ES), SINR can be given as

$$SINR_{HPMR-ES} = \frac{\rho^2 \beta_t^2 (P-N+1)^2 N^2 R^2}{\sum_{t=1}^{Q} \rho^2 \beta_t^2 \left| \mathbf{z}^H(\theta_t)\mathbf{z}(\theta_t) \right|} \tag{3.32}$$

Using $N=1$ and $N=P$ in (3.32), we will get SINR of PAR and MIMO respectively

$$SINR_{PAR} = \frac{\rho^2 \beta_t^2 P^2 R^2}{\sum_{t=1}^{Q} \rho^2 \beta_t^2 \left| \mathbf{z}^H(\theta_t)\mathbf{z}(\theta_t) \right|} \tag{3.33}$$

$$SINR_{MIMO} = \frac{\rho^2 \beta_t^2 P^2 R^2}{\sum_{t=1}^{Q} \rho^2 \beta_t^2 \left| \mathbf{z}^H(\theta_t)\mathbf{z}(\theta_t) \right|} \tag{3.34}$$

It can be concluded from (3.33) and (3.34) that the SINR of PAR and MIMO radar are equal to each other, which means PAR and MIMO radar has same robustness against interferences present in region of interest.

3.2.4 Simulation Results

In this subsection, we have plotted results of HPMR-US, HPMR-ES, PAR and MIMO radar in term of beampatterns and signal to interference plus noise ratio (SINR). First part presents the comparison of proposed radar with PAR and MIMO radar, while the second part gives a detailed comparison of proposed radar with existing HPMR-ES. In both parts of simulations, we use $P=15$ elements for transmit array, $N=7$ subarrays with full overlapping and $N=15$ receiving elements. Inter element Spacing is assumed to be $\lambda/2$ for both transmit and receive side. The desired target is assumed to be reflecting a wave from an angle $\theta_t = 0^\circ$ and there are four interfering targets at $-40^\circ, -20^\circ$, 20° and 40°. Complex Gaussian noise has been used as additive noise with zero mean spatially and

temporally white random sequence having same variance on each antenna element. In the coming simulations, we have illustrated the results of conventional beamforming, adaptive beamforming and SINR respectively

3.2.4.1. Comparison with PAR and MIMO

Hybrid Phased MIMO radars in literatures have shown improvements compared to PAR and MIMO alone. This section is dedicated to show the superiority of HPMR-US over PAR [18] and MIMO [101] before entering into the comparison with HPMR-ES [116]. First of all, the beampattern comparison of HPMR-US, PAR and MIMO radar is presented in Fig 3.2. It can be observed that the proposed radar shows a better overall beampattern as compared to other two radars. PAR and MIMO show almost same beampattern due to same overall response in terms of combined gain and waveform diversity i.e. PAR has maximum gain and only one waveform, while MIMO radar has maximum waveform diversity and unity gain. Therefore, more gain in PAR is compensated through diversity in MIMO, resulting in same overall effect for both radars. Improvement in HPMR-US beampattern can be attributed to combination of focused beams and waveform diversity provided by the proposed radar system.

Likewise, SINR of proposed radar is better than PAR and MIMO radar. Fig. 3.3 shows output SINR versus SNR for PAR, MIMO radar and HPMR-US. SINR for PAR and MIMO radar is almost same due to same sidelobes levels and thus same interference suppression capability. Proposed radar has a much higher SINR due to better side lobes levels (SLL) as shown in Fig. 3.2. Since we are considering the case of dominant interferences, therefore, proposed system is more robust to background interference as compared to other two radars.

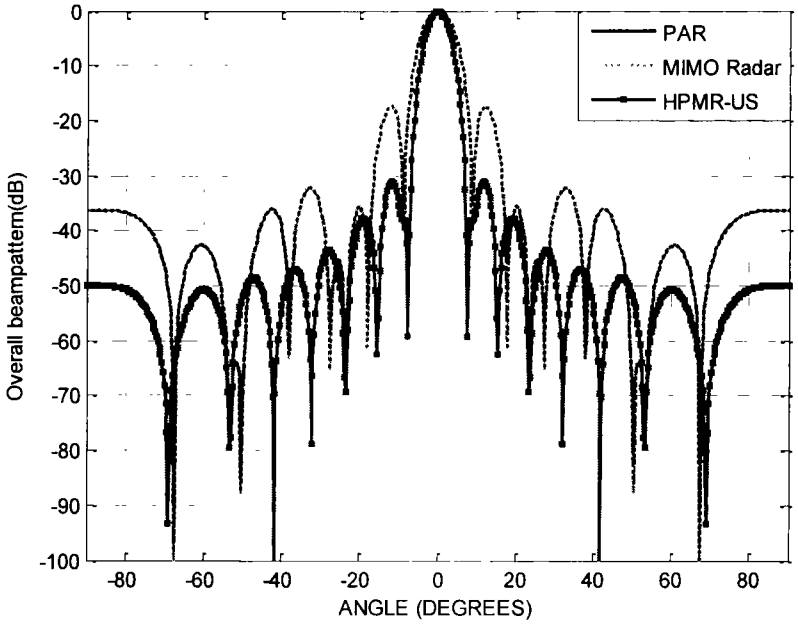

Fig. 3.2 Overall beampattern of PAR, MIMO and HPMR-US by using a conventional beamformer

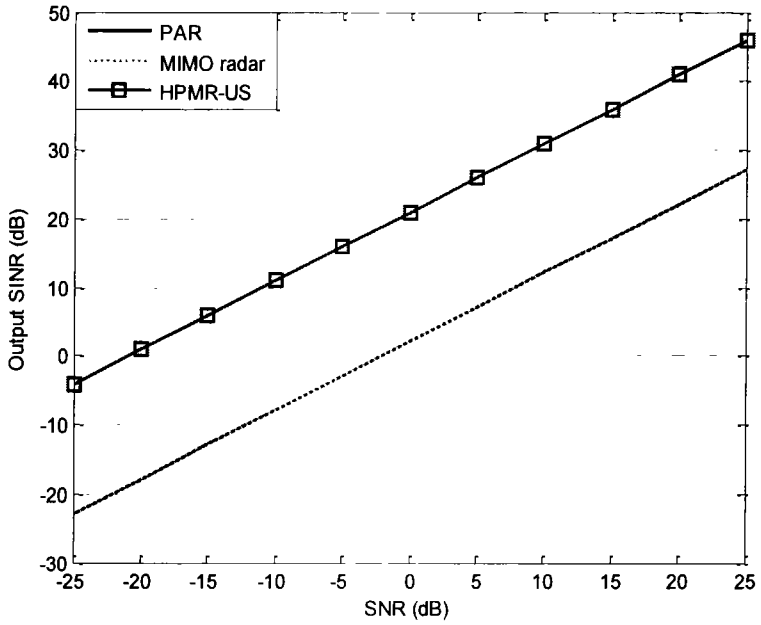

Fig. 3.3 SINR versus SNR of PAR, MIMO and HPMR-US by using a conventional beamformer

3.2.4.2. Comparison with HPMR-ES

In this subsection, proposed unequal subarray based system is compared with existing equal subarray based systems in terms of transmit/ received beampattern and output SINR by applying a conventional beamformer as well as adaptive beamformer. First of all, a conventional beamformer has been used on the transmit side to observe the maximum gain provided by of HPMR-ES and HPMR-US. Maximum gain provided by HPMR-ES is same for each subarray, as each subarray has same number of elements. On the contrary, the HPMR-US can offer additional gain due to more number of element in subarrays. Fig 3.4 confirms that maximum transmit gain of HPMR-US is a lot better than HPMR-ES due to extension in transmit aperture for most of the subarrays. The beam of proposed radar is a lot sharper than HPMR-ES.

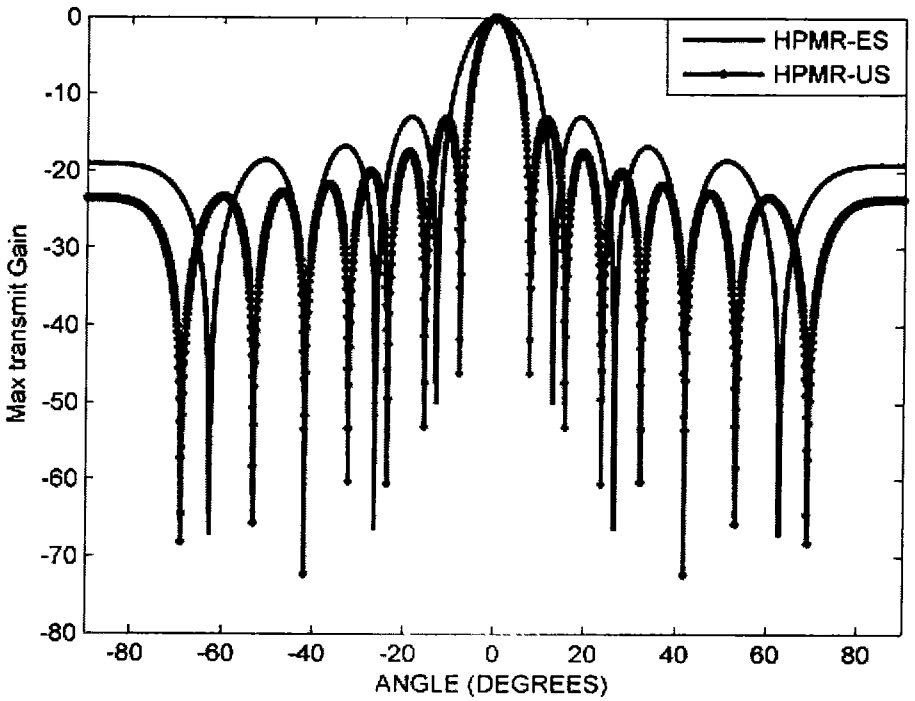

Fig. 3.4 Transmit beampattern of HPMR-ES and HPMR-US using a conventional beamformer

Fig 3.5 presents the overall beampattern for both HPMR-US and HPMR-ES. The performance of proposed radar, compared to HPMR-ES, is better in terms of side lobes level. Improvements can again be attributed to extra gain provided at the transmit side. In adaptive beamforming, the result of MVDR beamformer for both radars is shown in Fig 3.6. Clearly, both radars have effectively cancelled the interferences, however, the HPMR-US has an edge over HPMR-ES in the side lobes region. This enhancement is due to more focused beams at the transmit side, which results in better reflections from the target. Moreover, it is also important to realize that virtual extension for both radars system is same, however, the higher gain of HPMR-US at transmit side makes it more effective compared to HPMR-ES, as shown in above mentioned discussion of results.

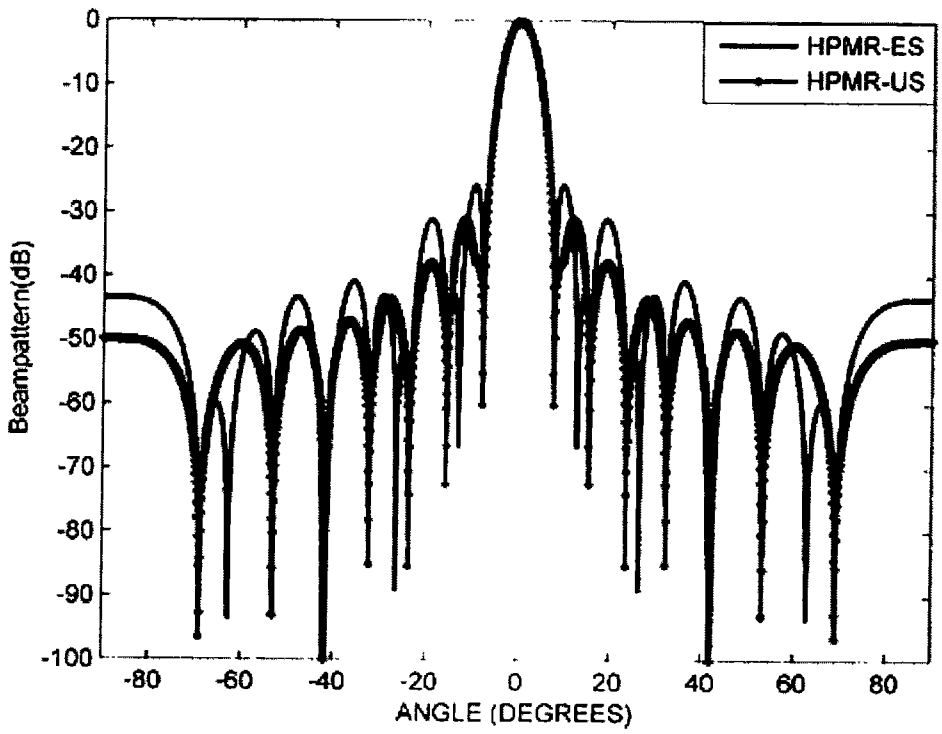

Fig. 3.5 Overall beampattern of HPMR-ES and HPMR-US using a conventional beamformer

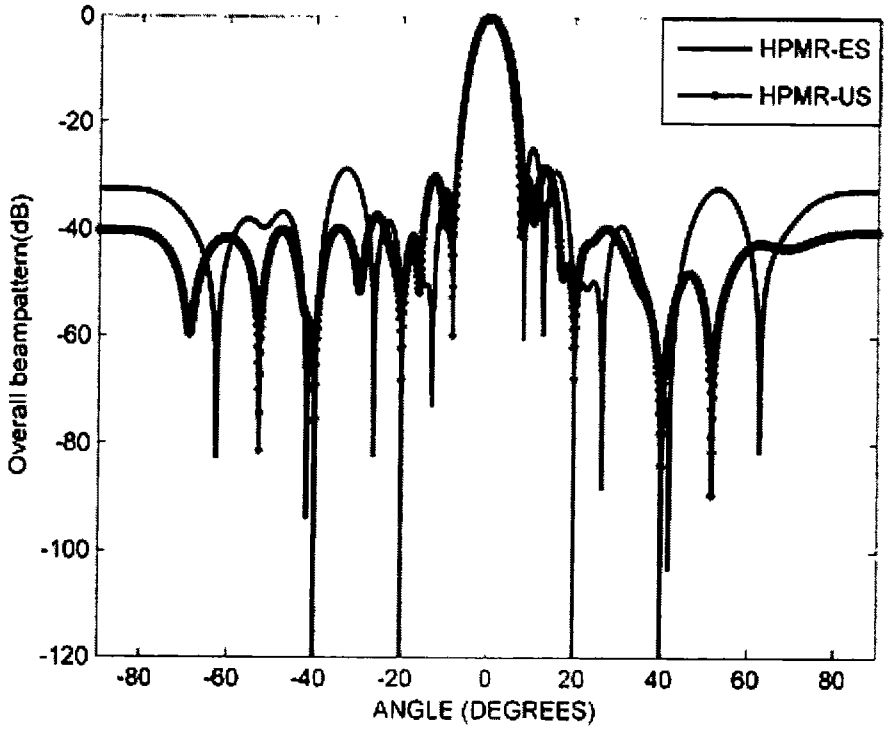

Fig. 3.6 Overall beampattern of HPMR-ES and HPMR-US using an adaptive beamformer

Finally, output SINR of both schemes is presented, where SINR is plotted against SNR. Both conventional and adaptive beamformers are used by keeping the interfernce level at 30dB. The SINR result of both the radars systems using a conventional beamformer is illustrated in Fig. 3.7. HPMR-US has better SINR than HPMR-ES, which can again be linked to the lengthy subarrays at the transmitter HPMR-US. Furthermore, Fig. 3.8 gives the SINR vs SNR plot for MVDR beamformer. HPMR-US again outperform HPMR-ES due to enhanced gain and slightly better interference cancellation capability. This improvement proved that proposed radar has a better robustness against interferences in the region of interest.

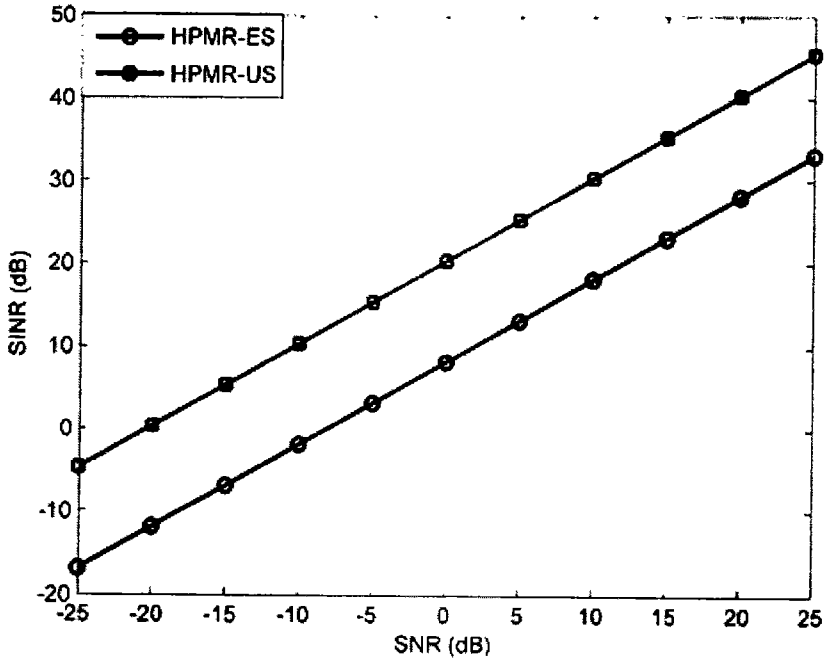

Fig. 3.7 SINR vs SNR of HPMR-ES and HPMR-US using the conventional beamformer

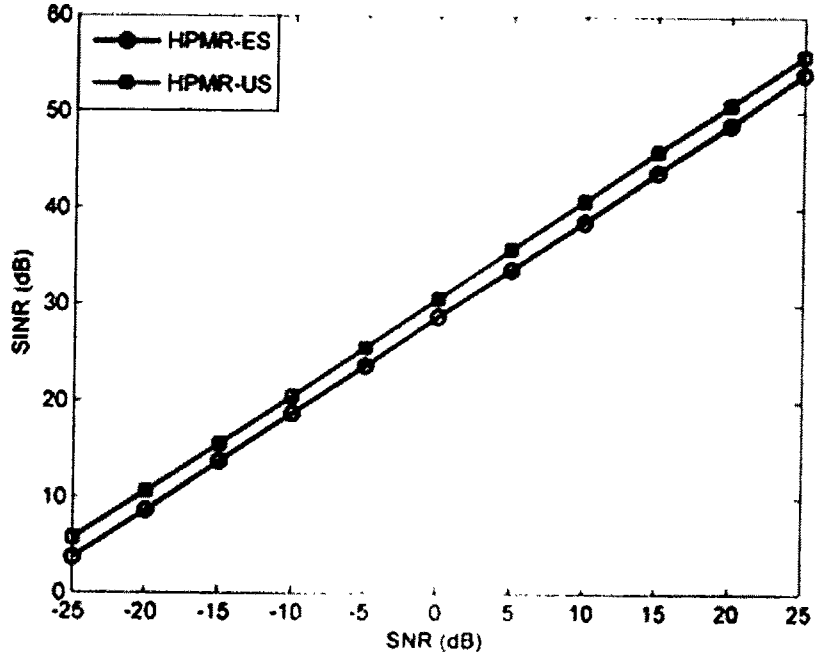

Fig. 3.8 SINR vs SNR of HPMR-ES and HPMR-US using the MVDR bemformer

All the above results have shown improvement in term of beampatterns and SINR, over existing radars, by applying an unequal subarrays approach. In terms of interference cancelltion, both HPMR-US and HPMR-ES have almost same capability. In order to get an extra edge, the waveform diversity should be increased in any proposed system. Therefore, another new variant of Phased MIMO radar system with increased waveform diversity will be presented in next section.

3.3 Phased MIMO Radar with Full Waveform Diversity

In this section, Phased MIMO radar with full waveform diversity is proposed, which applies fully overlapped partitioning to transmit array in such a way that the number of subarrays are equal to number of transmitting elements. The proposed Full Waveform Diverse Phased MIMO (FWD-PMIMO) radar not only provides some directional gain like PAR but also provides the waveform diversity equivalent to that of MIMO radar. It has the capability of cancelling same number of interferences as MIMO radar and can cancel more interferences than PAR and Phased MIMO radar.

Although MIMO and FWD-PMIMO transmit same number of waveforms but FWD-PMIMO is slightly different from MIMO in a way that MIMO uses only one antenna element to send out a waveform, whereas FWD-PMIMO uses different number of elements in a subarray for transmitting a waveform. The size of subarray in our design is variable ranging from 1 antenna element in first subarray to P antenna elements in last subarray. Proposed design matches MIMO in terms of interference suppression while maintaining a coherent gain at transmit side, which is very useful for getting better information about target. The performance of proposed FWD-PMIMO is examined in an environment with large number of distributed interferers. FWD-PMIMO can be considered as special case of

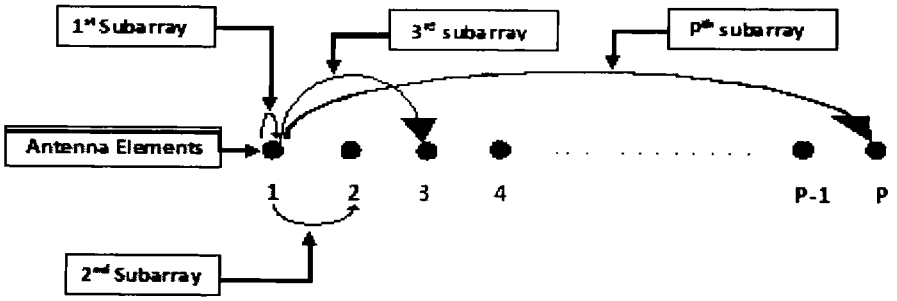

Fig. 3.9 Full waveform diverse Phased MIMO (FWD-PMIMO) radar

HPMR-US that is more focused on cancellation of maximum number of interferences. Keeping this fact in view, the signal model for radar under consideration will be similar to that of HPMR-US. Therefore, only a brief signal model will be presented before the simulations and comparison of proposed FWD-PMIMO radar with existing radars.

3.3.1 Signal Model

For signal model, a ULA comprising P antennas has been divided into P subarrays by using the partitioning scheme shown in Fig 3.9. Signal radiated by p^{th} subarray in the far field can be expressed as

$$m_p(k,\theta) = \rho\left[\mathbf{w}_p^H \mathbf{u}_p(\theta)\right] s_p(k) \qquad p = 1,2,\ldots\ldots,P \qquad (3.35)$$

Where $\mathbf{w}_p$ represents the weight vector of P^{th} subarray containing the weights belonging to only the active elements of this particular array and ρ is the energy given to each subarray. The reflected signal from a far field target at an angle θ can be given by

$$m_r(k,\theta) = \rho\alpha(\theta)\sum_{p=1}^{P} \mathbf{w}_p^H \mathbf{u}_p e^{j\tau_p}(\theta) s_p(k) \qquad (3.36)$$

Where $\alpha(\theta)$ represents complex valued reflection coefficient from the target and $\mathbf{u}_p$ is the

steering vector associated with P^{th} subarray. Applying a matched filter for the P different waveforms, an extended data vector of $PR \times 1$ is acquired, which can be written as

$$\mathbf{y} = \rho\alpha_t \mathbf{z}(\theta_t) + \sum_{i=1}^{Q} \rho\alpha_i \mathbf{z}(\theta_i) + \tilde{\mathbf{n}} \tag{3.37}$$

where $\mathbf{z}(\theta) = [\mathbf{x}(\theta) \odot \mathbf{d}(\theta)] \otimes \mathbf{v}(\theta)$ is the virtual steering vector of length $PR \times 1$. θ_t and θ_i represent the direction of target and interference respectively. The data vector $\mathbf{y}$ can be obtained by stacking the vectors from different subarrays. For a conventional phased MIMO in literature and HPMR-US in first section, virtual data vector can also be obtained in the same way as above, however, length of data vector for both of them will be $NR \times 1$ where $1 < N < P$. In other words, FWD-PMIMO radar enjoys a more extended aperture as compared to conventional phased-MIMO radar, which resulted in improved interference cancellation by proposed radar.

Since there are P different subarray in our proposed system, so we will get a weight matrix in which the columns of matrix represent vector corresponding to each subarray. The weight matrix is given as

$$\mathbf{W} = \begin{bmatrix} w_{1,1} & w_{2,1} & \cdot & \cdot & \cdot & \cdot & \cdot & w_{P,1} \\ 0 & w_{2,2} & \cdot & \cdot & \cdot & \cdot & \cdot & w_{P,2} \\ 0 & 0 & \cdot & \cdot & \cdot & \cdot & \cdot & \cdot \\ \cdot & \cdot & \cdot & \cdot & \cdot & \cdot & \cdot & \cdot \\ \cdot & \cdot & \cdot & \cdot & \cdot & \cdot & \cdot & \cdot \\ \cdot & \cdot & \cdot & \cdot & \cdot & \cdot & \cdot & \cdot \\ \cdot & \cdot & \cdot & \cdot & \cdot & \cdot & \cdot & \cdot \\ 0 & 0 & \cdot & \cdot & \cdot & \cdot & \cdot & w_{P,P} \end{bmatrix} \tag{3.38}$$

where $\mathbf{W}$ is $P \times P$ matrix of weights and $w_{i,k}$ is the weight of k^{th} element of i^{th} subarray.

Signal transmitted by P transmit antennas can be expressed as

$$\boldsymbol{\gamma}(\mathbf{k}) = \rho \mathbf{W}^{*} \mathbf{s}_{N}(k) \tag{3.39}$$

$\boldsymbol{\gamma}(\mathbf{k}) = \left[\gamma_1(k), \ldots\ldots\ldots\ldots \gamma_P(k)\right]^T$ is the $P \times 1$ vector of waveforms transmitted by P antenna elements. $\mathbf{W} = \left[\mathbf{w}_1, \mathbf{w}_2 \ldots\ldots\ldots \mathbf{w}_K\right]$ is the weight matrix of $P \times P$ and '$\mathbf{s}$' are transmitted waveforms from each subarray. The signal transmitted through each antenna element can be expressed as:

Antenna 1: $$\gamma_1 = \rho\left(w_{1,1}^{*} s_1 + w_{2,1}^{*} s_2 \ldots\ldots\ldots w_{P,1}^{*} s_P\right) \tag{3.40a}$$

Antenna 2: $$\gamma_2 = \rho\left(w_{2,2}^{*} s_2 + w_{3,2}^{*} s_3 \ldots\ldots\ldots w_{P,2}^{*} s_P\right) \tag{3.40}$$

$$\vdots \qquad \vdots \qquad \vdots$$

Antenna $P-1$: $$\gamma_{P-1} = \rho\left(w_{P-1,P-1}^{*} s_{P-1} + w_{P,P-1}^{*} s_P\right) \tag{3.40c}$$

Antenna P: $$\gamma_P = \rho\left(w_{P,P}^{*} s_P\right) \tag{3.40d}$$

It can be noted that if an element is not part of a particular subarray, then it will not send waveform associated with that subarray. Moreover, the linear combination of signals transmitted by first few antenna element are different from signals transmitted by HPMR-US given in section 3.2.

3.3.2 Beamforming and SINR of FWD-PMIMO

A conventional Beamformer is used for transmit side to show improvement in transmit beampattern, while an adaptive beamformer is used at receiver to verify the interference rejection capability of proposed FWD-PMIMO radar. MVDR beamformer is used for proposed. Beamforming weight vector for transmit side can be expressed as

$$\mathbf{w}_p = \frac{\mathbf{u}_p(\theta_t)}{\left\|\mathbf{u}_p(\theta_t)\right\|} \tag{3.41}$$

The weight vector for MVDR can be given as

$$\mathbf{w}_r = \frac{\mathbf{C}_{t+n}^{-1}(\theta)\mathbf{z}(\theta_t)}{\mathbf{z}^H(\theta_t)\mathbf{C}_{t+n}^{-1}(\theta)\mathbf{z}(\theta_t)} \tag{3.42}$$

$\mathbf{C}_{t+n}$ is interference plus noise covariance matrix for proposed FWD-PMIMO radar subarray. The beampattern for transmit side can be given as

$$B_p(\theta) = \left|\mathbf{w}_p^H \mathbf{z}(\theta)\right|^2 \tag{3.43}$$

The beampattern for adaptive beamformer at receiver side can be given as

$$B_r(\theta) = \left|\mathbf{w}_r^H \mathbf{z}(\theta)\right|^2 \tag{3.44}$$

Signal to interference plus noise ratio can be given as

$$SINR_{FWD-PMIMO} = \frac{\rho^2 \beta_t^2 \left|\mathbf{w}_r^H \mathbf{z}(\theta_t)\right|^2}{\mathbf{w}_r^H \mathbf{C}_{t+n} \mathbf{w}_r} \tag{3.45}$$

By substituting $\mathbf{C}_{t+n}$ and $\mathbf{w}$ in equation (28), we get

$$SINR_{FWD-PMIMO} = \frac{\rho^2 \beta_t^2 \left|\left\|\mathbf{u}_p(\theta_t)\right\|^2 \left\|\mathbf{d}_p(\theta_t)\right\|^2 \left\|\mathbf{v}(\theta_t)\right\|^2\right|^2}{\mathbf{z}^H(\theta_t)(\sum_{t=1}^{Q} \rho^2 \beta_t^2 \mathbf{z}(\theta_t)\mathbf{z}_t^H(\theta_t) + \beta_{\bar{n}}^2 \mathbf{I})\mathbf{z}(\theta_t)} \tag{3.46}$$

where β_t^2 and $\beta_{\bar{n}}^2$ are the variances of reflection coefficient from target and noise, respectively. After simplifying (3.46) we will get final relation for the SINR given as

$$SINR_{FWD-PMIMO} = \frac{\rho^2 \beta_t^2 p^2 R^2}{\sum_{t=1}^{Q} \rho^2 \beta_t^2 \left|\mathbf{z}^H(\theta_t)\mathbf{z}(\theta_t)\right|^2 + \beta_{\bar{n}}^2 pR} \tag{3.47}$$

For interference dominant case, we consider only the interference part. Thus SINR can be given as

$$SINR_{FWD-PMIMO} = \frac{\rho^2 \beta_t^2 p^2 R^2}{\sum_{i=1}^{Q} \rho^2 \beta_t^2 \left| \mathbf{z}^H(\theta_t) \mathbf{z}(\theta_t) \right|^2} \tag{3.48}$$

$\mathbf{z}(\theta_t)$ for PAR, MIMO radar and FWD-PMIMO radar has dimension of $R \times 1$, $PR \times 1$ and $PR \times 1$, respectively. Although MIMO and FWD-PMIMO have same dimension for virtual steering vector but MIMO has no gain at the transmit side, while FWD-PMIMO does have some gain at transmit side. Conventional Phased MIMO radar, on the other hand, has lesser dimension compared to proposed radar, since the number of subarrays in Phased-MIMO radar are always less than the proposed radar. As a result, the proposed radar outperform PAR, MIMO radar and phased MIMO radar (HPMR-ES) in terms of SINR for larger number of interferences. For PAR, MIMO and HPMR-ES, we will use the same SINR relations as given in section 3.2.

3.3.3 Simulation Results

For simulation, $P = 5$ antennas on transmitter have been divided into P fully overlapped subarrays. Receiver array also contains $R = 5$ antenna elements and both transmitter and receiver elements are at half wavelength from each other. Small transmit array has been chosen to give a better insight in to interference cancellation capability of the proposed system. Throughout the simulation target is assumed to be at an angle of 0^o but the interferences are assumed at many different angles. The number of interferences are kept high since the proposed scheme is designed for large number of interferences around the target. Complex Gaussian noise with zero mean is considered as the additive noise. Moreover, the results are presented in two different parts. First part deals with

beamforming at transmit side of proposed radar, whereas, second part presents beampattern and SINR using an MVDR Beamformer. Proposed scheme is also compared with PAR, MIMO radar and existing Phased MIMO radar.

3.3.3.1 Results on Transmit side

In this part, results have been presented in terms of beampattern for maximum transmit gain, beampattern for waveform diversity and the overall beampattern for PAR [21], MIMO radar [101], Phased MIMO (PMIMO) radar [116] and Full Waveform diverse Phased MIMO (FWD-PMIMO) radar. Figure 3.10 shows maximum transmit gain provided by all radar systems. It can be observed that phased array has the best transmit gain due to focusing of all the energy in one direction. FWD-PMIMO radar and Phased MIMO (PMIMO) radar has lesser gain compared to phased array but a lot better gain than the

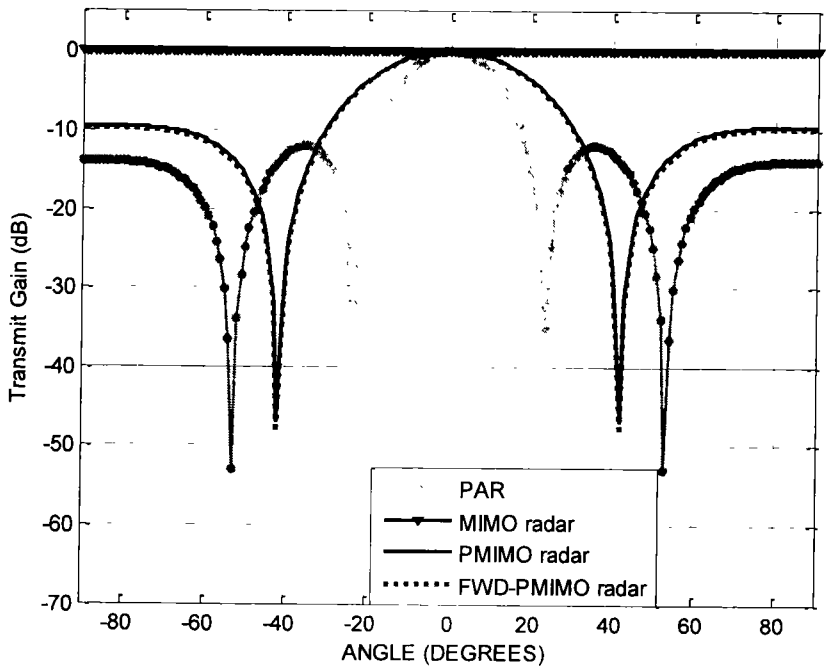

Fig. 3.10 Transmit beampattern of PAR, MIMO, PMIMO and FWD-PMIMO radar

MIMO radar which shows a flat line because of no transmit gain. The transmit gain provided by PMIMO and FWD-PMIMO is due to number of subarrays made at the transmitter, which give focused beams instead of omnidirectional transmission.

The waveform diversity beampattern is illustrated in figure 3.11, which shows that the diversity gain of both MIMO and FWD-PMIMO is equal and at its maximum value. PAR offers no diversity at all, which is quite clear from the plot of PAR. Furthermore, the PMIMO radar gives better diversity gain then PAR but less than MIMO radar and FWD-PMIMO radar. The reason for flat graph of PAR is that it uses only one waveform with phased shift at each antenna element. On the other hand, MIMO radar and FWD-PMIMO radar transmit P unique waveforms and PMIMO radar used less than P unique waveforms. Thus, more waveforms means sharper waveform diversity beampattern.

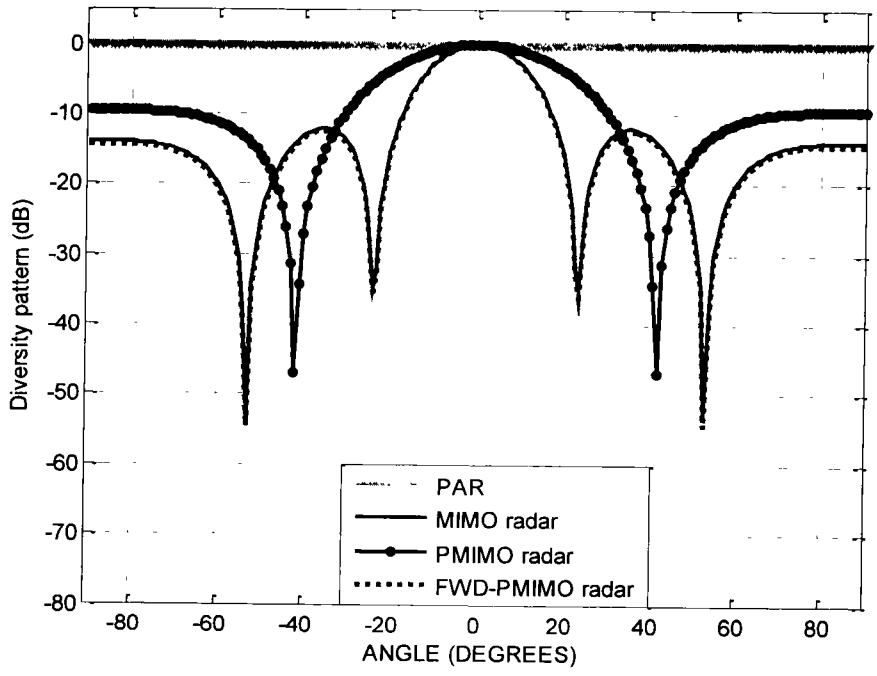

Fig. 3. 11 Waveform diversity beampattern of PAR, MIMO, PMIMO and FWD PMIMO radar

The overall beampattern, depicted in Fig. 3.12, is resultant of both gain beampattern and diversity beampattern. The corresponding values of both beampattern are multiplied (added in dB) to get the overall beampattern, which can been named as Gain Diversity product. Fig 3.12 clearly shows the improvement in overall beampattern of proposed radar compared to PAR, MIMO radar and PMIMO radar. This improvement can be understood from first two simulation results, which indicate that proposed radar contributes to both the plots in term of gain and diversity. It is also interesting to note that the overall beampattern of PAR and MIMO radar is exactly the same due to same contribution in first two plots i.e. PAR contribute with directional gain of 5 elements, while MIMO contribute with five orthogonal waveforms. The PMIMO also contribute to both plots but its diversity is less than proposed radar.

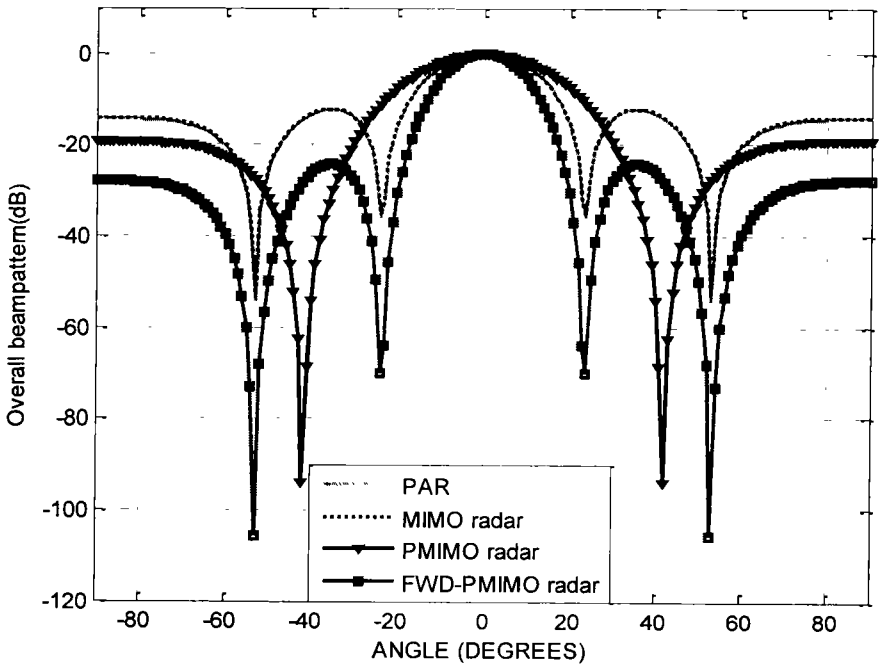

Fig. 3. 12 Overall beampattern of PAR, MIMO, PMIMO and FWD-PMIMO radar

3.3.3.2 Results on received side

This part of the simulation gives results of beamforming and SINR of an adaptive beamformer. We assume a target at 0^{o} and eight interferences at -70° -60° $-40^{\circ}, -20^{\circ}, 20^{\circ}$, 40° 60° and 70°. The result in Fig 3.13 shows that both MIMO and FWD-MIMO cancel all the interferences. However, the cancellation of proposed radar is slightly better i.e. Nulls placed by proposed radar are a lot deeper than that of MIMO radar. PAR on the other hand fails to cancel the interferences, since it does not have a virtual extension of array at receiver. PMIMO also fail to cancel all the interferences due to less virtual extension in received array. The SINR comparison of all techniques is illustrated in Fig 3.14, which clearly exhibit better SINR of FWD-PMIMO compared to other radars. This improvement can definitely be attributed to transmit gain and received virtual array extension.

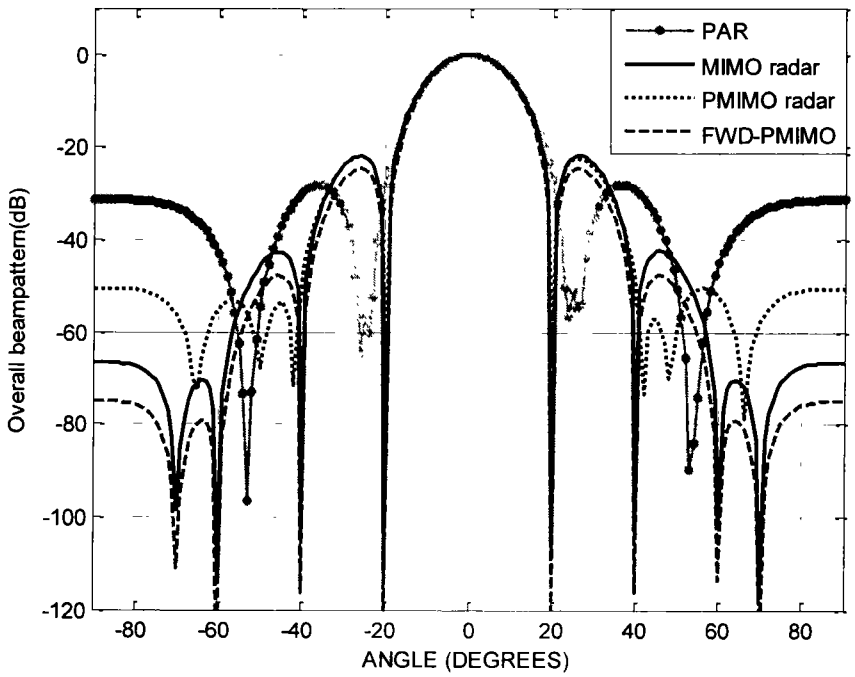

Fig. 3.13 MVDR Beampattern of PAR, MIMO, PMIMO and FWD-PMIMO for Q=8 interferences

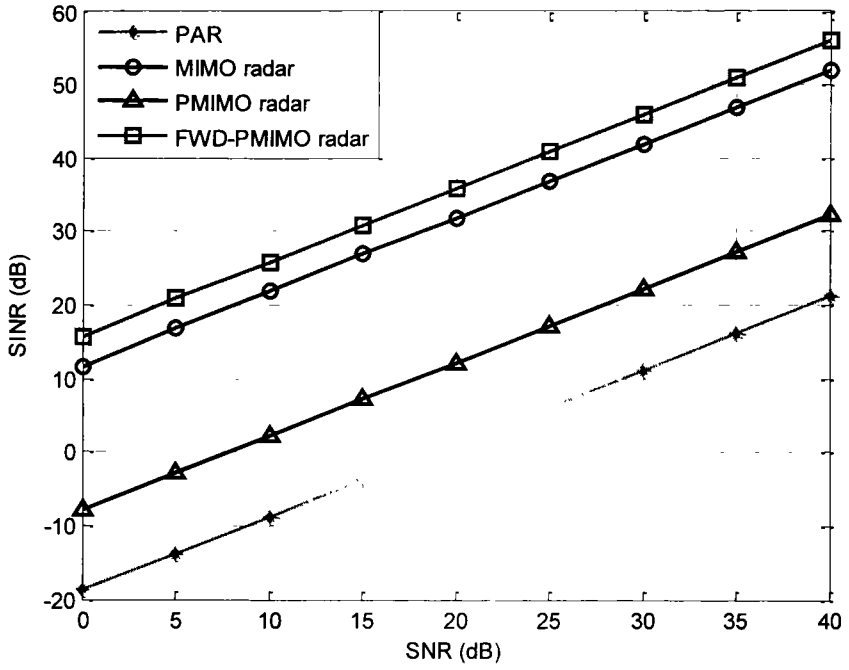

Fig. 3.14 Output SINR versus SNR of PAR, MIMO, PMIMO and FWD-PMIMO radar for Q=8 interferences

3.4 Summary of Chapter

Unlike conventional Phased MIMO radar, the proposed schemes used unequal subarrays to focus the beam on target of interest. First proposed scheme has used same number of subarrays as conventional Phased MIMO radar, however, variable sizes of subarrays enhanced the returns from the target. As a result, the improvements in beampatterns as well as SINR for proposed radar has been observed. The second proposed scheme has applied unequal subarrays in a different way to attain full waveform diversity. The essence of this second scheme is to attain the waveform diversity equal to a MIMO radar for cancelling maximum number of interferences. Results have confirmed the better results of proposed scheme in terms of beampatterns, SINR and interference cancellation.

Chapter 4

New Schemes in MIMO-FDA Radar using Uniform Frequency Offset

4.1 Introduction

In the previous chapter, we have investigated the unequal subarrays for Phased MIMO radar to provide better received beampatterns, improved SINR, low side lobes level and superior interference cancellation. However, it can be observed that all the improvements are in angle dimension only. In order to further enhance its capabilities, the hybrid radar must also offer improvements in range dimension along with angle dimension. To accomplish it, this chapter has presented two new schemes for MIMO-FDA radar. In both designs, we assume a linear frequency offset among the antenna elements.

First scheme uses unequal subarrays for transmit side of a MIMO-FDA radar. Idea is to illuminate the region of interest with beams of variable width to get better information about the target in terms of range and angle. Therefore, the proposed Unequal Subarray based MIMO-FDA (US-MIMO-FDA) radar shows an improvement in range dimension as well as angle dimension. Moreover, Frequency increment can be adjusted in such a way that it produces maxima at desired range-angle pair. MIMO radar contributes in terms of applying different waveforms to overlapped subarray structure and achieving virtual array extension at the receiver, resulting in improved patterns in range and angle dimension as compared to FDA radar and Equal Subarray based MIMO-FDA (ES-MIMO-FDA) radar.

Performance analysis of proposed radar has also been done in terms of output SINR and probability of detection.

Second proposed scheme uses double pulse concept in MIMO-FDA i.e. (DP-MIMO-FDA) for better target localization in range-angle dimension, as compared to existing FDA radar systems. Due to strong range angle coupling of FDA beampattern, it is difficult to determine ranges and angles directly from the peaks of beampattern, thus a two stage process is presented. First stage estimates angle of target by sending a pulse of zero frequency offset across the subarrays, followed by a pulse of suitable frequency increment across the subarrays to estimate range. As a result, we can accurately estimate angle and range from the peak of beampattern. Proposed scheme has been simulated and compared with existing double pulse FDA (DP-FDA) radar to show that MIMO-FDA scheme is superior to FDA scheme. Performance analysis has also been done in terms of CRLB to demonstrate better range and angle estimation by DP-MIMO-FDA radar.

4.2 MIMO-FDA radar with Unequal Subarrays

In this section, MIMO-FDA with unequal subarrays has been formulated and discussed. The transmit array of a FDA radar is divided into number of subarrays that are fully overlapped and contains variable number of antenna elements in each subarray. Like HPMR-US, first subarray will contain least number of elements followed by other subarray with one more number of element in each subarray. Last subarray will have all the antenna elements present in transmit array. Each subarray coherently transmits unique waveform and form a beam by using frequency increment across the elements of subarray. Each beam has a different width due to variable number of elements in each subarray, which is in contrast to equal subarrays size of ES-MIMO-FDA radar.

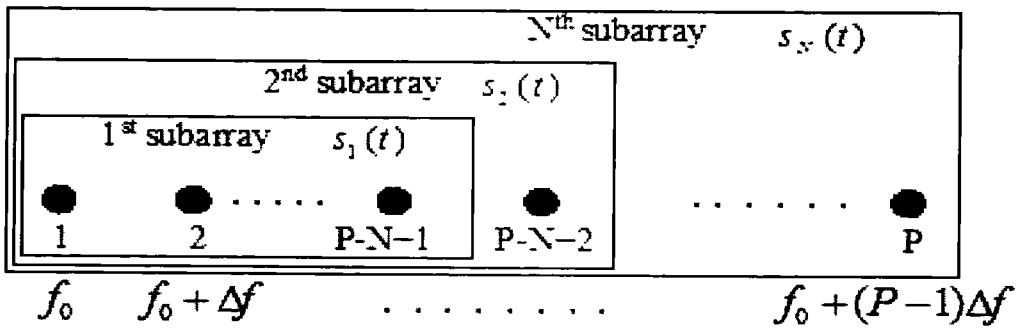

Fig. 4.1 MIMO-Frequency diverse array radar with unequal subarrays

4.2.1 Signal Model

For signal model, an array of P elements with N subarrays is considered as shown in Fig. 4.1. The baseband equivalent signal of n^{th} subarray at transmitter can be written as

$$\left[\mathbf{c}_n \odot \mathbf{u}(\theta,r)\right]^* s_n(k) \tag{4.1}$$

Where $\mathbf{c}_n$ is the vector used to determine length of subarray by using 1's for active elements in a subarray and 0's for inactive elements in a subarray. $\mathbf{u}(\theta,r)$ is the steering vector, $s_N(k)$ is the n^{th} baseband waveform with k being the sample within a pulse, $\odot$ is the element-by-element product and $(.)^*$ represents the complex conjugate. Signal arriving at the far-field point from this radar can be expressed as

$$\mathbf{u}(\theta,r)^H \left[\mathbf{c}_n \odot \mathbf{u}(\theta,r)\right]^* s_n(k) \tag{4.2}$$

where $\mathbf{u}(\theta,r)^H$ is vector obtained due to propagation effects. This vector has the same form as a steering vector [136]. Equation (4.2) can be written as takes

$$\left[\mathbf{w}_n{}^H \mathbf{u}(\theta,r)\right] s_n(k) \tag{4.3}$$

where $\mathbf{w}_n = \mathbf{c}_n \odot \mathbf{u}(\theta,r)$ represents the beamspace weight vector for N^{th} subarray. The

proper design of this weight vector allows us to focus energy in desired angle and range pair. Furthermore, sum of all subarrays in far field can be given as

$$m(k,\theta,r)=\sum_{n=1}^{N}\left[\mathbf{w}_n{}^{H}\mathbf{u}(\theta,r)\right]s_n(k) \tag{4.4}$$

Unlike ES-MIMO-FDA radar, the size of $\mathbf{w}$ for each subarray is different and the number of elements in each subarray of US-MIMO-FDA radar can be given by $L=P-N+n$, with $n=1,2\ldots\ldots N$. The signal in (4.4) can also be written as

$$m(k,\theta,r)=\left[\mathbf{W}^{H}\mathbf{u}(\theta,r)\right]^{T}\mathbf{s}_N(k) \tag{4.5}$$

$\mathbf{W}=[\mathbf{w}_1,\mathbf{w}_2\ldots\ldots\mathbf{w}_N]$ is $P\times N$ weight matrix and $\mathbf{s}_N(\mathbf{k})=[\mathrm{s}_1(k),\mathrm{s}_2(k)\ldots\ldots\mathrm{s}_N(k)]$ is the waveform vector of length $N\times 1$. The suitable value of each weight vector is important for beam steering to desired range and angle pair. The equivalent waveforms transmitted from transmit array can be

$$\boldsymbol{\gamma}(\mathbf{k})=\mathbf{W}^{*}\mathbf{s}_N(k) \tag{4.6}$$

$\boldsymbol{\gamma}(\mathbf{k})=[\gamma_1(k),\ldots\ldots\ldots\gamma_P(k)]^T$ is the $P\times 1$ vector of waveforms transmitted by P antenna elements and $(.)^*$ denote the complex conjugate. It can be observed that if we can find beamspace matrix $\mathbf{W}$, then the waveform can be specifically designed.

At the receiving end, we will use a simple phased array to receive the reflected signal. The steering vector for the receiver will be

$$\mathbf{v}(\theta)=\begin{bmatrix}1 & e^{-j\left(\frac{2\pi f_1 d\sin\theta}{c_0}\right)} & \ldots\ldots\ldots & e^{-j\left(\frac{2\pi f_1(n-1)d\sin\theta}{c_0}\right)}\end{bmatrix} \tag{4.7}$$

Now, if we assume target and Q interferences in area of interest, the signal at receiver array will be

$$m_r(k,\tau) = \alpha(\tau)[(\mathbf{W}^H\mathbf{u}(\theta_t,r_t)^T\mathbf{s}_N(k))]\mathbf{v}(\theta_t) + \sum_{q=1}^{Q}\alpha_q(\tau)[(\mathbf{W}^H\mathbf{u}(\theta_q,r_q)^T\mathbf{s}_N(k))]\mathbf{v}(\theta_q) + \mathbf{n}(k,\tau) \tag{4.8}$$

where τ is used for the time delay, $\alpha_q(\tau)$ are the complex reflection coefficients from the targets, $s_N(k)$ is the n^{th} waveform and $\mathbf{n}(k,\tau)$ is the Gaussian noise. The received signal can be match filtered for each waveform $s_n(k)$ as

$$\mathbf{y}_n(\tau) = \frac{\int_{T_p}\mathbf{m}_r(k,\tau)s_n^*(k)dk}{\int_{T_p}\left|s_n^*(k)\right|^2 dk} \tag{4.9}$$

$$\mathbf{y}_n(\tau) = \alpha(\tau)[(\mathbf{w}_n{}^H\mathbf{u}(\theta_t,r_t))]\mathbf{v}(\theta_t) + \sum_{t=1}^{Q}\alpha_t(\tau)[(\mathbf{w}_n{}^H\mathbf{u}(\theta_t,r_t))]\mathbf{v}(\theta_t) + \mathbf{n}_n(t,\tau) \tag{4.10}$$

where $\mathbf{n}_n(\tau)$ noise is term for n^{th} subarray and $\mathbf{y}_n(\tau)$ is the data vector associated with N^{th} subarray. Data vector received from each subarray can be stacked in single vector to get total data vector for all subarrays. This new data vector can be given as

$$\mathbf{y}(\tau) = \alpha(\tau)\mathbf{x}(\theta_t,r_t)\otimes\mathbf{v}(\theta) + \sum_{t=1}^{Q}\alpha_t(\tau)\mathbf{x}(\theta_t,r_t)\otimes\mathbf{v}(\theta) + \tilde{\mathbf{n}}_N(\tau) \tag{4.11}$$

where $$\mathbf{x}(\theta,r) = [\mathbf{w}_1^H\mathbf{u}_1(\theta,r),\mathbf{w}_2^H\mathbf{u}_2(\theta,r),.....\mathbf{w}_v^H\mathbf{u}_N(\theta,r)]^T \tag{4.12}$$

The dimension of data vector is $NR\times1$ and it can be further written as

$$\mathbf{y} = \alpha(\tau)\mathbf{z}(\theta_t,r_t) + \sum_{t=1}^{Q}\alpha_t(\tau)\mathbf{z}(\theta_t,r_t)\alpha_q(\tau)\mathbf{z}(\theta_t,r_t) + \tilde{\mathbf{n}}_N(\tau) \tag{4.13}$$

The data vector consists of $NR\times1$ signal term, $NR\times1$ interference term and $NR\times1$ noise term. $\mathbf{z}(\theta)$ is actually $NR\times1$ virtual steering vector for MIMO-FDA and given as

$$\mathbf{z}(\theta,r) = \mathbf{x}(\theta,r)\otimes\mathbf{v}(\theta) \tag{4.14}$$

This virtual steering vector is a very important feature of conventional MIMO radar. Although the length of virtual steering vector in a MIMO-FDA is less than that of MIMO radar, however, the gain obtained at the transmitter side due to subarray structure has been exploited to get better result for proposed radar. The unequal subarrays also provide an extra degree of freedom by producing beams of variable width at the target in contrast to Equal subarray based MIMO-FDA, which illuminate the target with same beams.

4.2.2 Beamforming for Proposed Radar

A non-adaptive beamformer has been used to generate a beampattern. Weight vector for this beamformer can be given by

$$\mathbf{w}_R = \mathbf{z}(\theta_t, r_t) \tag{4.15}$$

Where θ_d and r_d is the angle and range of desired target. The normalized received beampattern can be written as

$$B(\theta, r) = \frac{\left|\mathbf{w}_r^H \mathbf{z}(\theta, r)\right|^2}{\left|\mathbf{w}_r^H \mathbf{z}(\theta_t, r_t)\right|^2} = \frac{\left|\mathbf{z}^H(\theta_t, r_t)\mathbf{z}(\theta, r)\right|^2}{\left\|\mathbf{z}(\theta_t, r_t)\right\|^4} \tag{4.16}$$

4.2.3 Performance analysis of Proposed Radar

In this section, performance analysis of US-MIMO-FDA radar has been done in terms of output SINR and probability of detection.

4.2.3.1 SINR

SINR for MIMO-FDA can be given as

$$SINR = \frac{\beta_t^2 \left|\mathbf{w}_r^H \mathbf{z}(\theta_t, r_t)\right|^2}{\mathbf{w}_r^H \mathbf{C}_{i+n} \mathbf{w}_r} \tag{4.17}$$

The $\mathbf{C}_{i+n}$ matrix can be given as

$$C_{i+n} = \sum_{i=1}^{Q} \beta_i^2 \mathbf{z}(\theta_i, r_i)\mathbf{z}_i^H(\theta_i, r_i) + \beta_n^2 I \tag{4.18}$$

where β_t^2 and β_n^2 are the variances of reflection coefficient for target and noise, respectively. By substituting the values of $\mathbf{C}_{i+n}$ and $\mathbf{w}$ for both ES-MIMO-FDA radar and US-MIMO-FDA radar, we will get the SINR for both the radars.

4.2.3.2 Detection Performance

For detection performance of MIMO-FDA, the signal from target can be modified to express it as

$$\mathbf{y}(k) = \alpha(\tau)[(\mathbf{W}^H\mathbf{u}(\theta_t, r_t)^T \mathbf{s}_N(k))]\mathbf{v}(\theta_d) + \mathbf{n}(k) = \mathbf{h}(k) + \mathbf{n}(k) \tag{4.19}$$

where $\mathbf{h} = \alpha(\tau)[(\mathbf{W}^H\mathbf{u}(\theta_t, r_t)^T \mathbf{s}_N(k))]\mathbf{v}(\theta_d)$ and $\mathbf{n}(t)$ is the white Gaussian noise. The hypothesis problem can be given as

$$\begin{cases} H_0 : \mathbf{y}(k) = \mathbf{n}(k) \\ H_1 : \mathbf{y}(k) = \mathbf{h}(k) + \mathbf{n}(k) \end{cases} \tag{4.20}$$

The assumption for the noise process is to be Gaussian and independent and identically distributed (i.i.d). The probability density function (PDF), i.e. the likelihood for a random variable $\mathbf{y}$ to have a given value of H_0 and H_1, can be given as

$$p(y(k); H_0) = \exp\left(-\frac{\|\mathbf{y}(k)\|^2}{\sigma_n^2} \right) \tag{4.21}$$

$$p(y(k); H_1) = \exp\left(-\frac{\|\mathbf{y}(k)\|^2}{\sigma_n^2} \right) \times \exp\left(-\frac{\|\mathbf{h}(k) + \mathbf{n}(k)\|^2}{2\sigma_n^2} \right) \tag{4.22}$$

The likelihood ratio test can be given as

$$\Lambda = \frac{p(y(k);H_1)}{p(y(k);H_0)} \begin{matrix} H_1 \\ > \\ < \\ H_0 \end{matrix} \delta \tag{4.23}$$

where δ is the threshold for detection. Furthermore. the probability of false alarm and probability of detection can be given as

$$p_{fa} = p(\Lambda > \delta \mid H_0) = 1 - F_{\chi^2_{(2)}}\left(\frac{2\delta}{\sigma_n^2}\right) \tag{4.24}$$

$$p_d = p(\Lambda > \delta \mid H_1) = 1 - F_{\chi^2_{(2)}}\left(\frac{\sigma_n^2 F^{-1}_{\chi^2_{(2)}}(1-p_{fa})}{\sigma_t^2 (P-N+n)^2 R^2 + \sigma_n^2}\right) \tag{4.25}$$

$F(.)$ is the cumulative distributive function, $\chi^2_{(2)}$ is the chi-square distribution, $P-N+n$ is the number of elements in n^{th} array and R is the number of elements in receiver array.

4.2.4 Simulation Results

In the simulations, we have assumed transmit array of $P=15$elements divided into $N=7$ subarrays with full overlapping. The receiver array consists of $R=15$elements and the distance between antenna elements for both transmitter and receiver is taken as $\lambda/2$. Fundamental frequency used is $f_1=10GHz$ and frequency increment is taken as $\Delta f=15KHz$. Additive noise is Complex Gaussian noise with zero mean spatially and temporally white random sequence having same variance on each antenna element. Target is assumed to be present at the 0° in angle dimension and at 11 km in range dimension. In the first part, maximum gain of ES-MIMO-FDA and US-MIMO-FDA are compared followed by and received beampatterns of FDA radar [40], ES-MIMO-FDA radar [59] and US-MIMO-FDA radar. In the second part, performance of both the radars are compared in

terms of output SINR and detection probability.

First of all the transmit beampatterns for ES-MIMO-FDA and US-MIMO-FDA radar is presented in figure 4.2(a) and 4.2(b) to show the maximum gain provided by both the radars. It can be observed that both the radars exhibit almost same beampattern in combined range-angle beam pattern, however, the beam produced by US-MIMO-FDA radar is a little sharp. In order to compare both the radars systems, the 1-D profiles of maximum gain is given in the next simulations. 1-D profiles are simply the cuts of Fig. 4.2, where angle dimension and range dimension is plotted separately to show the performance of proposed system compared to existing radar system. In Fig. 4.3, angle profile of both ES-MIMO-FDA and US-MIMO-FDA have been plotted. It can be seen that maximum gain provided by proposed radar is better than ES-MIMO-FDA. The beampattern for proposed radar is more focused due to the extra number of elements in the subarrays of proposed radar. Likewise, figure 4.4 gives the result for the range profile of both the radars. Once again the transmit gain of proposed radar is better in range dimension due to extension in subarrays.

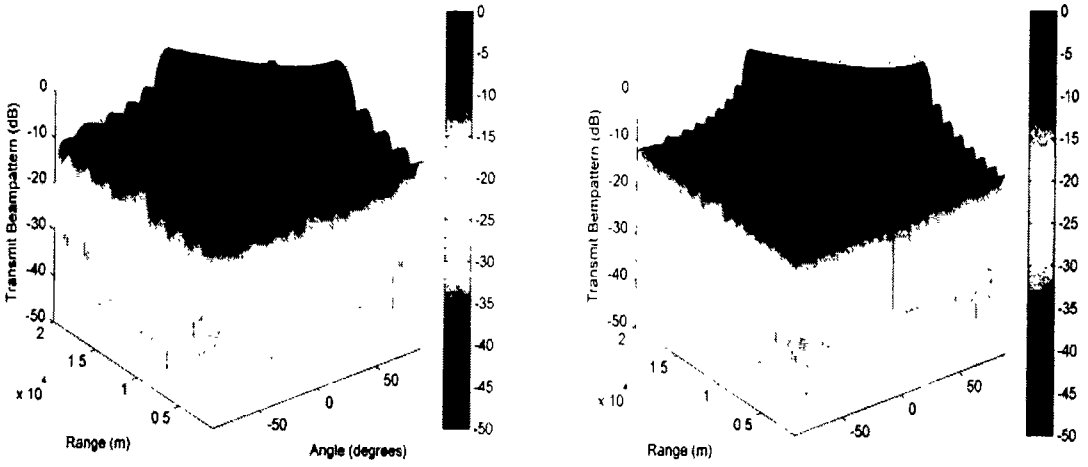

(a) ES-MIMO-FDA (b) US-MIMO-FDA

Fig. 4.2 Beampatterns for transmit side of (a) ES-MIMO-FDA (b) US-MIMO-FDA

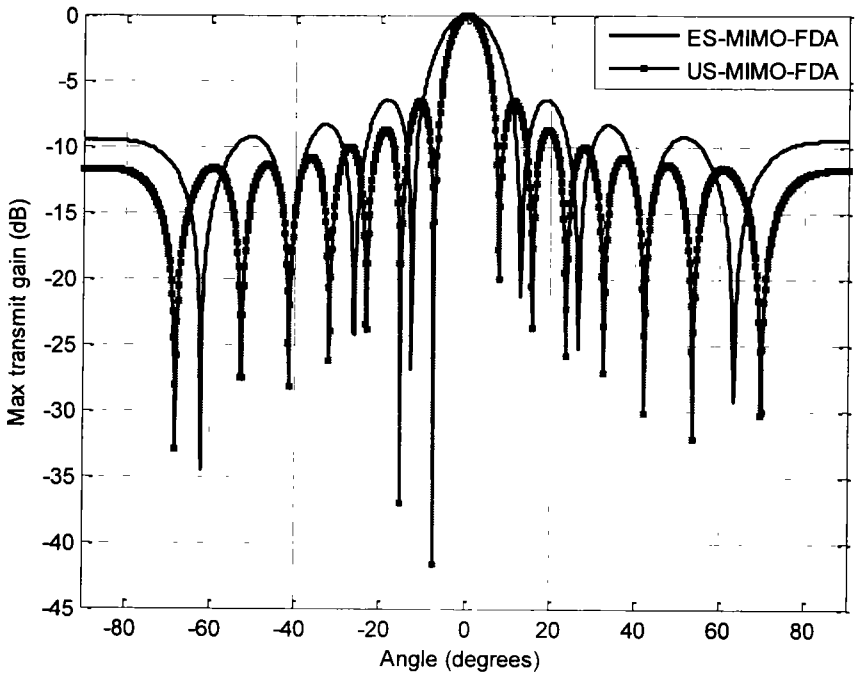

Fig. 4.3 Comparison of Angle profile for ES-MIMO-FDA and US-MIMO-FDA radar beampatterns on the transmit side

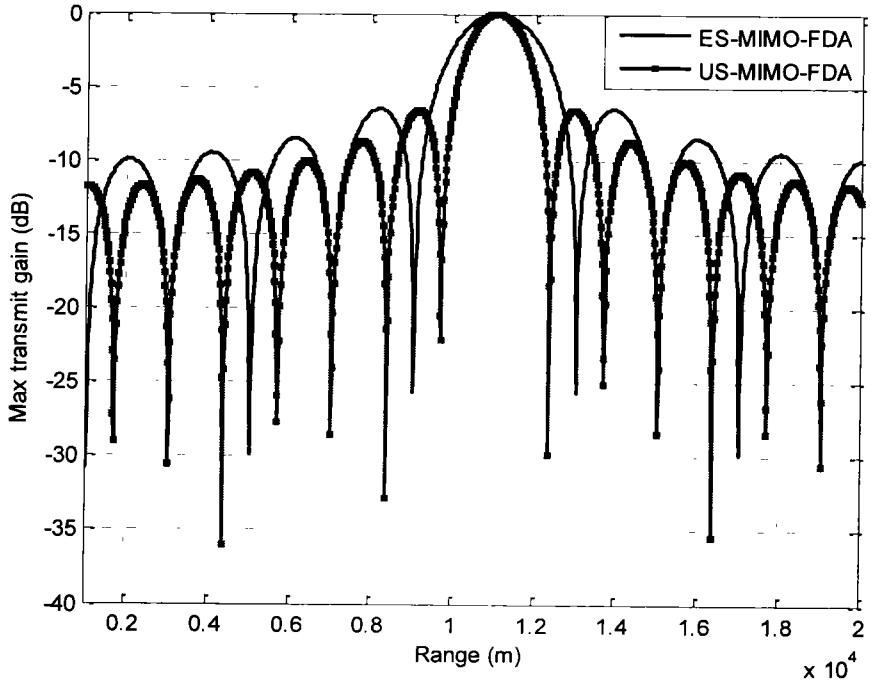

Fig. 4.4 Comparison of range profile for ES-MIMO-FDA and US-MIMO-FDA radar beampatterns on the transmit side

Figures 4.5(a) and 4.5(b) show the received joint range-angle beampattern plot for FDA, US-MIMO-FDA and ES-MIMO-FDA radar respectively. It can be observed that maxima in these plots is a lot sharper in these beampattern as compared to the transmit side plots. This sharpness is due to multiple waveforms used at transmit side, which contribute

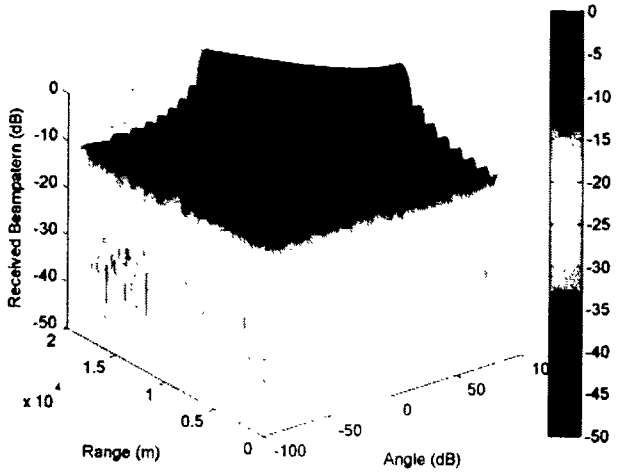

(a) FDA radar

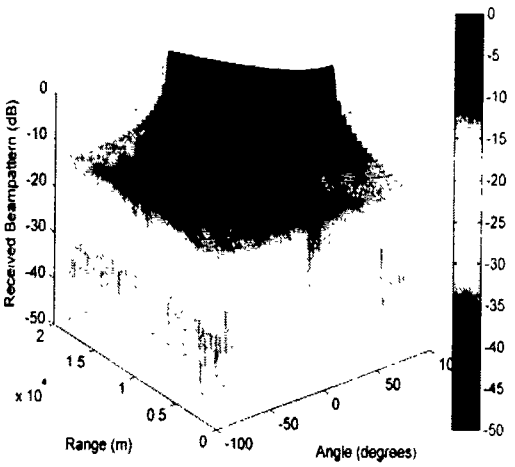

(b) ES-MIMO-FDA

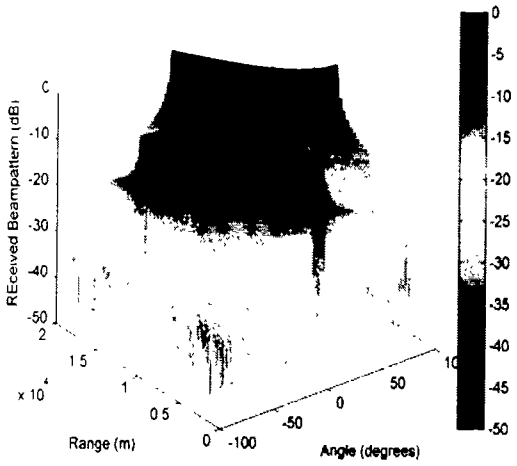

(c) US-MIMO-FDA

Fig. 4.5 Received beampatterns for (a) FDA radar (b). ES-MIMO-FDA radar (c). US-MIMO-FDA radar

to the extended virtual steering vector. In order to clearly compare results of both radars, 1-D plots are again plotted for both angle and range dimension. Received beampattern for angle dimension of all three radars are shown in Fig. 4.6. It can be noticed that the proposed US-MIMO-FDA radar has a better beampattern compared to FDA radar and ES-MIMO-FDA. The improvement can be clearly observed in terms of less beam width and lower side lobes level. Likewise, the range profile comparison of beam patterns is shown in Fig 4.7, which illustrates the better result of proposed radar in terms of lower side lobes level. This improvement in angle and range dimension can be attributed to increase in length of subarrays at transmit side.

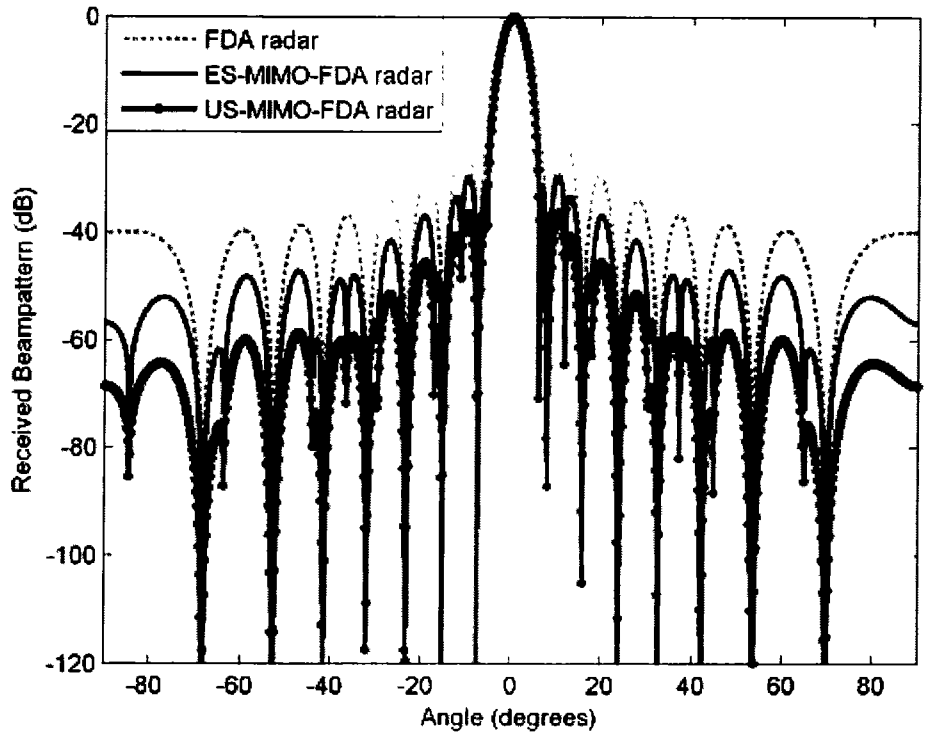

Fig. 4.6 Comparison of angle profile for the received beampatterns of FDA radar, ES-MIMO-FDA and US-MIMO-FDA radar

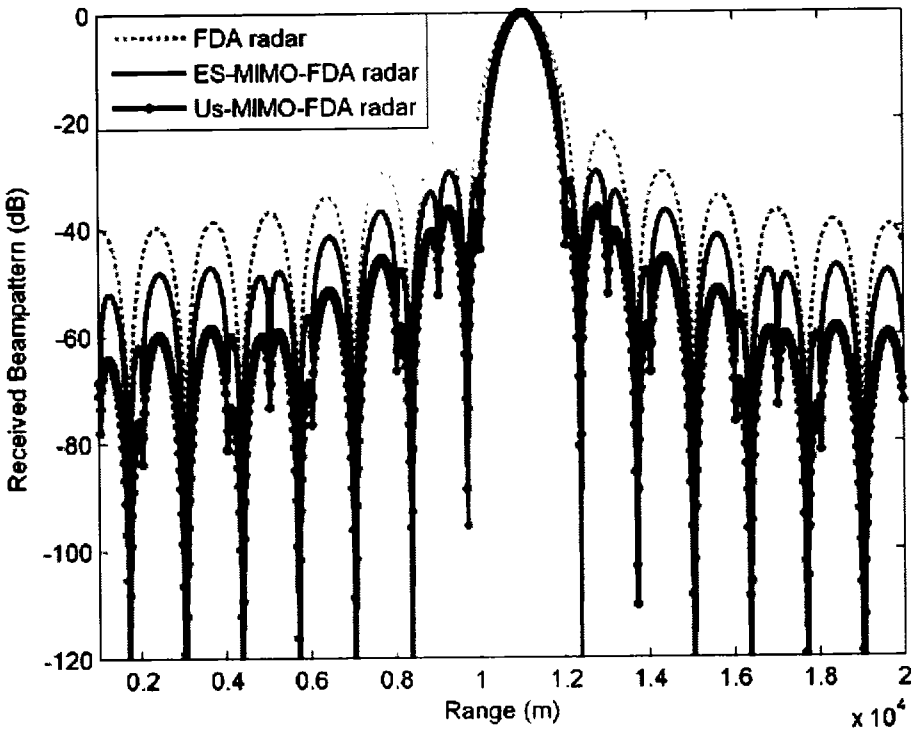

Fig. 4.7 Comparison of angle profile for the received beampatterns of FDA radar, ES-MIMO-FDA and US-MIMO-FDA radar

In the second part of simulation, performance analysis of proposed US-MIMO-FDA radar has been presented and compared with FDA radar and ES-MIMO-FDA radar. First the SINR versus SNR, in an interference dominant case, is simulated and plotted for both radars. Fig. 4.8 clearly shows that the proposed radar has higher SINR compared to FDA radar and ES-MIMO-FDA radar. In addition, detection performance of all the radars are also plotted and compared. Once again the US-MIMO-FDA has better detection performance compared to other two radars, as shown in Fig. 4.9. This superiority of US-MIMO-FDA in SINR and probability of detection can be attributed to more focused beams formed by extended aperture of subarrays at transmit side.

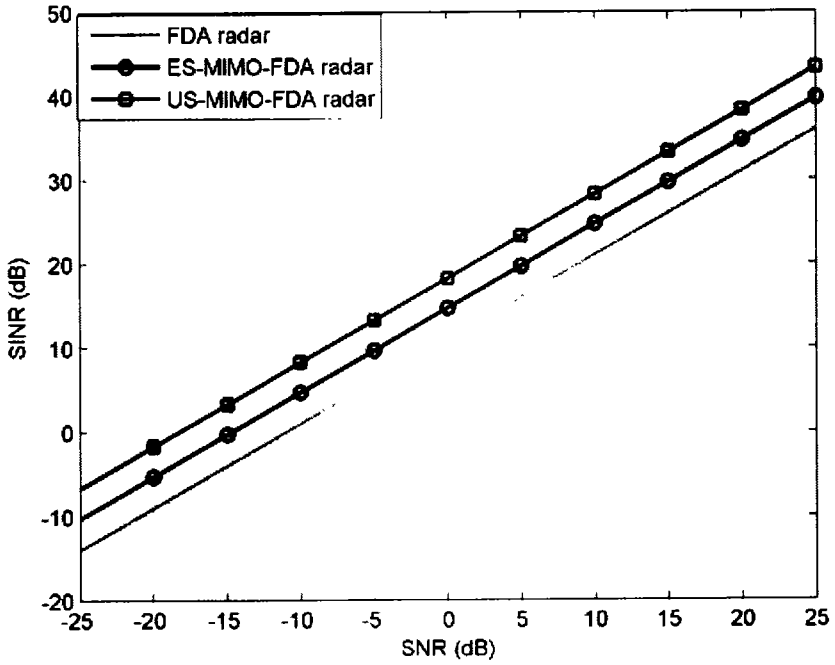

Fig. 4.8 SINR versus SNR performance of FDA radar, ES-MIMO-FDA and US-MIMO-FDA radar

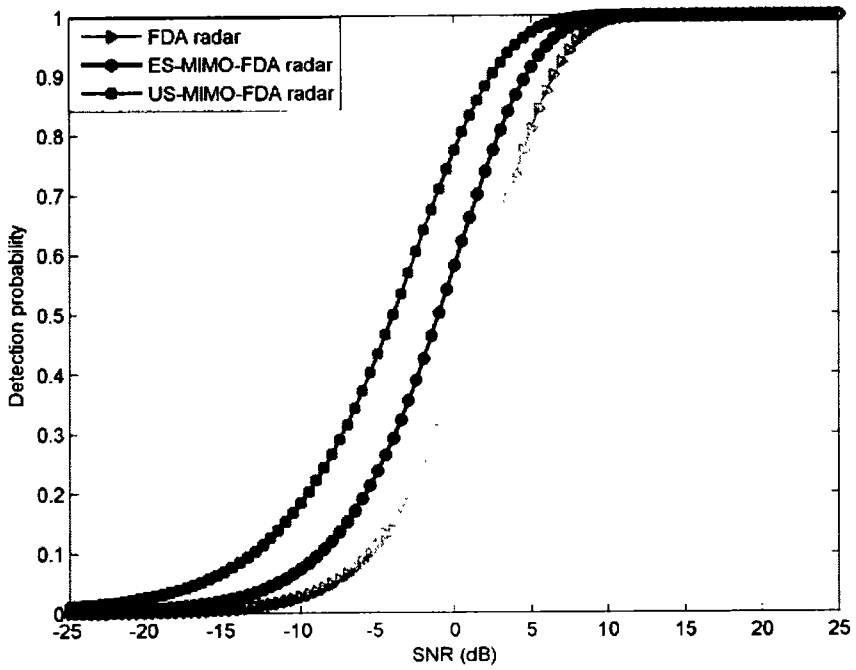

Fig. 4.9 Comparison of detection performance of FDA radar, ES-MIMO-FDA and US-MIMO-FDA radar

4.3 Double Pulse MIMO-FDA Radar

In this section, a double pulse MIMO-FDA (DP-MIMO-FDA) radar has been proposed to localize the target in both angle and range dimensions. In literature, FDA radar and MIMO-FDA have been explored to show their range-angle dependent beampattern. However, the strong coupling of beampattern in range and angle has made it difficult to localize the target in both dimensions. In other words, it is not possible to compute range and angle directly from the peaks of beampattern. To overcome this inability of former two radars, the proposed radar uses idea of double pulse for each subarray to perform angle and range localization. Fig. 4.10 shows the basic architecture of proposed DP-MIMO-FDA. Since our objective is simply to show the effectiveness of double pulse, therefore, we will use conventional MIMO-FDA radar for introducing and validating this idea. In addition, the comparison has been carried out only with DP-FDA radar because the single pulse FDA and MIMO-FDA radar are unable to produce uncoupled responses.

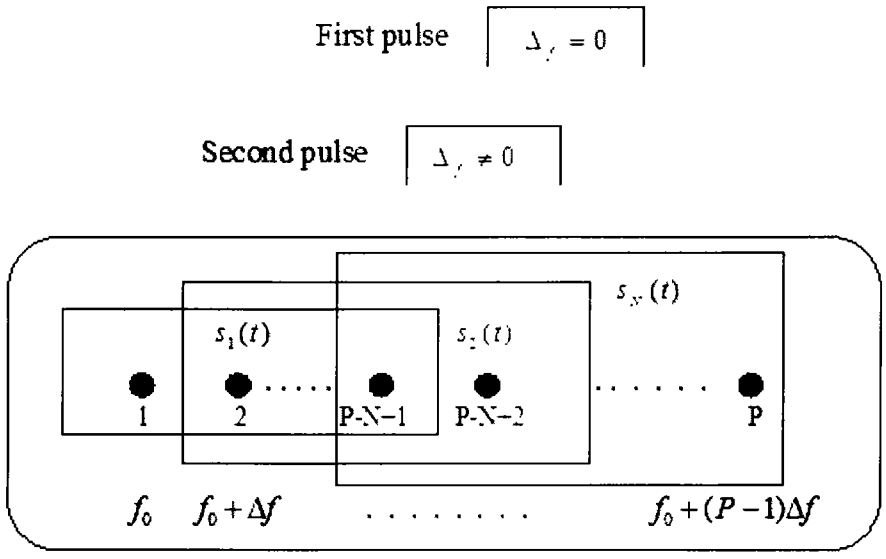

Fig. 4.10 Basic concept of Double pulse MIMO-FDA radar

4.3.1 Preliminary Data Model

Preliminary signal model involves P elements divided into N subarrays of equal size. The signal arrived in the far field at (θ, r) due to n^{th} subarray can be written as

$$m(k,\theta,r) = \rho[\mathbf{w}_n{}^H \mathbf{u}_n(\theta,r)]s_n(k) \tag{4.26}$$

Where $\mathbf{w}_n$ and $\mathbf{u}_n(\theta,r)$ are weight vector and steering vector respectively. The equivalent signal at received array is the sum of signals from all the subarrays and can be given as

$$\mathbf{m}_r(\tau) = \rho\alpha_t(\tau)\left[\sum_{n=1}^{N} \mathbf{w}_n{}^H \mathbf{u}_n(\theta_t, r_t)s_n(k)\right]\mathbf{v}(\theta_t) + \mathbf{n}(k,\tau) \tag{4.27}$$

Where θ_d and r_d is desired target direction and range respectively, ρ is energy given to each subarray, τ is time delay, $\alpha(\tau)$ is the reflection from target, $\mathbf{v}(\theta_d)$ is received steering vector and $\mathbf{n}(k,\tau)$ is the Gaussian noise. After matched filtering, we get

$$\mathbf{y}_n(\tau) = \rho\alpha_t(\tau)[(\mathbf{w}_n{}^H \mathbf{u}_n(\theta_t, r_t))]\mathbf{v}(\theta_t) + \mathbf{n}_n(\tau) \tag{4.28}$$

By stacking all vectors after matched filtering, resultant data vector can be written as

$$\mathbf{y}(\tau) = [\mathbf{y}_1^T(\tau) \;\; \mathbf{y}_2^T(\tau) \;\ldots\ldots\; \mathbf{y}_N^T(\tau)]^T \tag{4.29}$$

$$\mathbf{y} = \rho\alpha_t \mathbf{z}(\theta_t, r_t) + \tilde{\mathbf{n}} \tag{4.30}$$

$\mathbf{z}(\theta,r) = [\mathbf{w}_1^H \mathbf{u}_1(\theta,r), \mathbf{w}_2^H \mathbf{u}_2(\theta,r), \ldots\ldots\ldots \mathbf{w}_N^H \mathbf{u}_N(\theta,r)] \otimes \mathbf{v}(\theta)$ is $NR \times 1$ virtual steering vector due to multiple waveforms used at the transmit array. This virtual steering vector has been used for upcoming analysis of double pulse MIMO-FDA radar.

4.3.2 Double Pulse MIMO-FDA radar for Localization

In a DP-MIMO-FDA, the angle of desired target can be found by transmitting a pulse with zero frequency increment in the first step. After processing these returns through a

non-adaptive beamformer for desired angle, the second step involves the transmission of a pulse with suitable frequency increment in the direction obtained in the first step. The new returns are once again processed by a non-adaptive beamformer to get the desired range. It is worth mentioning that the exact angle estimated in the first step plays a vital role in properly estimating the range of target. Moreover, the two steps can be also be interpreted in terms of data vector and steering vector as given below:

1. In the first step quantified above, the signal is sent with $\Delta f = 0$ to get the estimate of angle. Data vector in (4.30) will then be reduced to

$$\mathbf{y}_{ang} = \rho\alpha_t \mathbf{z}(\theta_t) + \tilde{\mathbf{n}} \tag{4.31}$$

Furthermore, the steering vector will also be reduce to

$$\mathbf{z}_{ang}(\theta_t) = \mathbf{z}(\theta_t, r_t)|_{\Delta f=0} = [\mathbf{w}_1^H \mathbf{u}_1(\theta_t), \mathbf{w}_2^H \mathbf{u}_2(\theta_t), \ldots\ldots\ldots \mathbf{w}_N^H \mathbf{u}_N(\theta_t)] \otimes \mathbf{v}(\theta_t) \tag{4.32}$$

where $\mathbf{z}_{ang}(\theta_t)$ denotes the steering vector for estimation of angle. It can be clearly observed that the range dimension simply disappears and we are left with subarrayed MIMO i.e. Phased MIMO radar, transmitting different waveforms towards a target in a particular direction. Applying a non-adaptive beamformer with weight vector $\mathbf{w}_{R_{ang}} = \mathbf{z}(\theta_t)$, the angle can be estimated as

$$\hat{\theta} = \arg\{\max_{\theta_t} \left| \mathbf{w}_{R_{ang}}^H \mathbf{z}_{ang}(\theta_t) \right|^2\} \tag{4.33}$$

2. In the second step, signal with $\Delta f \neq 0$ is sent which produces following data vector

$$\mathbf{y}_{range} = \rho\alpha_t \mathbf{z}(\theta_t, r_t) + \tilde{\mathbf{n}} \tag{4.34}$$

The steering vector for this case can be written as

$$\mathbf{z}_{range}(\theta_t, r_t) = [\mathbf{w}_1^H \mathbf{u}_1(\theta_t, r_t), \mathbf{w}_2^H \mathbf{u}_2(\theta_t, r_t), \ldots\ldots\ldots \mathbf{w}_N^H \mathbf{u}_N(\theta_t, r_t)] \otimes \mathbf{v}(\theta_t) \tag{4.35}$$

For a weight vector $\mathbf{w}_{R_{range}} = \mathbf{z}(\theta_t, r_t)$, the range can be estimated as

$$\hat{r} = \arg\{\max_{r_t} \left| \mathbf{w}_{R_{range}}^H \mathbf{z}_{range}(\theta_t, r_t) \right|^2 \} \tag{4.36}$$

After two step processing, we have the estimates in both range and angle. Therefore, we can localize the target in angle and range dimension i.e. (θ_t, r_t).

The above mentioned scheme has allowed us to get beampattern for both angle and range dimensions in such a way that the peaks of beampattern represent the desired angle and range. Additionally, we can focus the target with multiple waveforms to get the useful waveform diversity, which can contribute in better localization and estimation of target parameters. Finally, the proposed scheme can also add some extra degree of freedom in terms of applying a suitable offset for different subarrays to get even better estimation of target. The proposed system has also been compared with the double pulse FDA radar in subsequent subsections. Due to subarrayed structure, i.e. waveform diversity, the DP-MIMO-FDA radar has shown a superior performance as compared to DP-FDA radar in both dimensions.

4.3.3 Performance Analysis of Proposed Scheme

In this sub-section, estimation performance of DP-MIMO-FDA has been analyzed by using Cramer-Rao Lower Bound (CRLB). The Cramér-Rao bound (CRB) has been used to assess the performance of unbiased estimators [137]–[140]. In particular, the deterministic CRB is used for target parameter estimation where for an increase in signal-to-noise ratio (SNR), the deterministic maximum likelihood estimator (MLE) attains this bound. Our aim here is to analyze the angle and range estimation performance of DP-

MIMO-FDA radar in terms of CRLB. To achieve this task, data vectors in (4.31) and (4.34) can be modified to get an extended data vector

$$\mathbf{d}_{ext} = \sqrt{SNR}\,\mathbf{z}_{ext}(\theta_t, r_t) + \mathbf{n} \tag{4.37}$$

where $\mathbf{d}_{ext}$ and $\mathbf{z}_{ext}$ are the extended data vector and steering vector of length $2NR \times 1$ and $\mathbf{n}$ is the normalized Gaussian noise vector with zero mean and unit variance. The extended length of steering vector can be achieved by simply stacking the virtual steering vectors of the two pulses and can be written as

$$\mathbf{z}_{ext}(\theta_t, r_t) = [\mathbf{z}(\theta_t, r_t)\big|_{\Delta f = 0}, \mathbf{z}(\theta_t, r_t)]^T \tag{4.38}$$

Since the vector $\mathbf{z}(\theta_t, r_t)$ is $NR \times 1$ virtual steering vector due to the N subarrays used at the transmit side. Therefore, by merging the first part i.e. $\mathbf{z}(\theta_t, r_t)\big|_{\Delta f = 0}$, and the second part i.e. $\mathbf{z}(\theta_t, r_t)\big|_{\Delta f \neq 0}$, the overall length of extended steering vector is $2NR \times 1$. Assuming $M = NR$, the steering vector for both steps can be written as

$$\mathbf{z}(\theta_t, r_t)\big|_{\Delta f = 0} = [1\ e^{-j\omega_0} \ldots e^{-j(M-1)\omega_0}] \tag{4.39}$$

$$\mathbf{z}(\theta_t, r_t)\big|_{\Delta f \neq 0} = [1\ e^{-j\omega_1} \ldots e^{-j(M-1)\omega_1}] \tag{4.40}$$

where

$$\omega_0 = \frac{2\pi f_1 d \sin\theta_t}{c} \tag{4.41a}$$

$$\omega_1 = \frac{2\pi f_1 d \sin\theta_t}{c} + \frac{2\pi \Delta_f d \sin\theta_t}{c} + \frac{2\pi \Delta_f r_t}{c} \tag{4.41b}$$

The mean μ and covariance R given vector can be written as

$$\mu = z_{ext}(\theta_t, r_t)\sqrt{SNR} \tag{4.42}$$

$$\mathbf{R}_n = E[\mathbf{n}\,\mathbf{n}^H] = \mathbf{I} \tag{4.43}$$

Now the Fisher information matrix can be derived as

$$\mathbf{J}_{DP-MIMO-FDA} = 2\,\mathrm{Re}\{D_{\Psi_i}^{H}(\Psi)(\mathbf{R}_n^{-1})D_{\Psi_j}(\Psi)\} = \begin{bmatrix} J_{\theta\theta} & J_{\theta r} \\ J_{r\theta} & J_{rr} \end{bmatrix} \tag{4.44}$$

Where $$\Psi = [\theta, r]^T \tag{4.45}$$

$$D_{\Psi_i}(\Psi) = \frac{\partial \mu(\Psi)}{\partial_{\Psi_i}} \tag{4.46}$$

$$J_{\theta\theta} = 2SNR.\frac{1}{c^2}[4\pi^2 f_1^2 d^2 \cos^2(\theta) + 4\pi^2 \Delta f^2 d^2 \cos^2(\theta)].N.\sum_{n=0}^{N-1} n^2 \tag{4.47}$$

$$J_{rr} = 2SNR.\frac{1}{c^2}[4\pi^2 \Delta f^2].N.\sum_{n=0}^{N-1} n^2 \tag{4.48}$$

$$J_{\theta r} = J_{r\theta} = 2SNR.\frac{1}{c^2}[4\pi^2 f_1 \Delta f d \cos(\theta)].N.\sum_{n=0}^{N-1} n^2 \tag{4.49}$$

The CRLB for target angle and range estimate can be given as the diagonal elements of the inverse FIM i.e.

$$CRLB_{\theta\theta_{DP-MIMO-FDA}} = \left[\mathbf{J}_{DP-MIMO-FDA}^{-1}\right]_{1,1} \tag{4.50}$$

$$CRLB_{rr_{DP-MIMO-FDA}} = \left[\mathbf{J}_{DP-MIMO-FDA}^{-1}\right]_{2,2} \tag{4.51}$$

These given CRLB of DP-MIMO-FDA radar have been compared with DP-FDA radar. The improvements offered by proposed design in angle and range dimensio have been shown in subsequent section.

4.3.4 Simulation Results

For simulations of proposed radar system, a ULA of $P = 15$ antenna element is assumed for the transmit side. This array is divided into $N = 6$ overlapped subarrays. The number of elements in each subarray are $P - N + 1$, while the receiver array consists of $R = 15$ antenna elements. A unique waveform has been steered by each subarray toward

the target of interest. Distance between two consecutive antenna elements of transmit as well as received array is half wavelength. A carrier frequency of $f_1 = 10GHz$ and frequency increment of $\Delta f = 30KHz$ is used. Target is assumed to be present at 10^o in angle and $12\,km$ in slant range. Noise is assumed to be additive Gaussian noise with zero mean spatially and temporally white random sequence having same variance at each antenna element. To localize the target in terms of this angle and range, the double pulse approach has been applied to produce the angle and range beampatterns respectively. Furthermore, proposed radar has also been compared with the DP-FDA radar [62] in terms of received beampattern followed by Cramer Rao Lower Bound (CRLB) analysis of both the radars.

4.3.4.1 Range and angle Beampatterns of DP-MIMO-FDA radar

In the first part, we have presented the received beampattern of proposed DP-MIMO-FDA. The conventional MIMO-FDA has been unable to achieve good localization in range and angle due to coupled response. The 2-D range-angle beampattern for a MIMO-FDA has been presented in Fig. 4.11. It can be observed that the angle and range dimensions are coupled and it is very difficult to separate the peaks of angle and range. To overcome this inability, the process given in section 4.3.3 has been implemented to treat the range and angle dimension separately. Fig 4.12 (a) exhibits the received beampattern for target direction. Clearly, a peak has been produced at 10^o, which is precisely the angle of desired target. This information about angle can be used in the next step, where the range estimation can be achieved by choosing a suitable frequency offset Δf. For the processing of this step, we have assumed a frequency increment of $\Delta f = 30KHz$. Range response for desired target has been presented in Fig 4.12 (b). It can be seen that the range response exhibits a peak at 12 km, which is our assumed range. In the end, both the responses can

be combined to localize the target in both angle and range dimension i.e. (10°, 12km). Moreover, results in Fig 4.12 (a)-(b) are estimated responses of angle and range, in contrast to angle and range profiles cuts given in section 4.2.

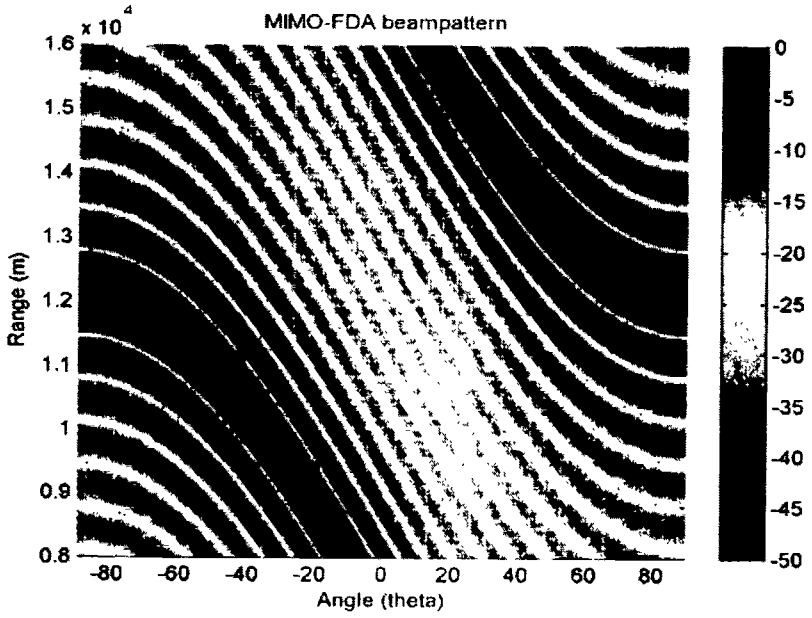

Fig. 4.11 Range-angle beampattern of DP-MIMO-FDA radar

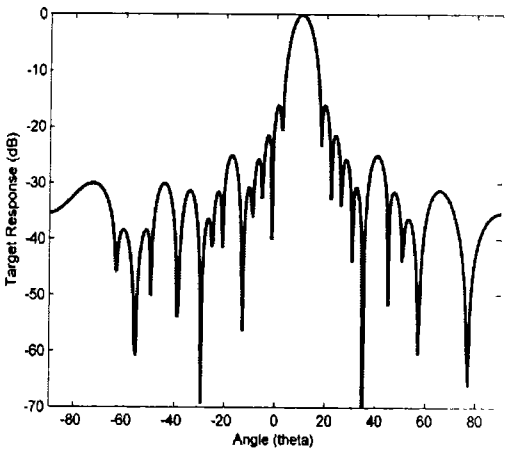

Fig. 4.12(a) Angle Response

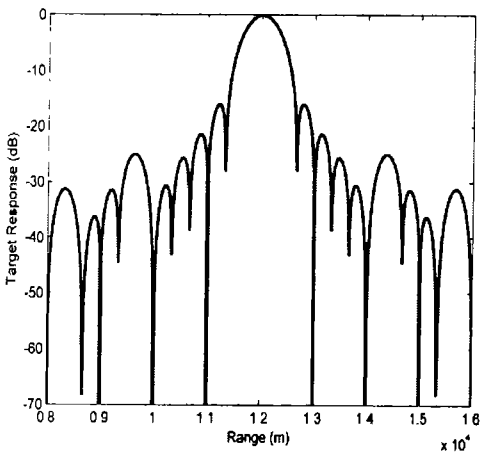

Fig. 4.12(b) Range Response

Fig. 4.12 DP-MIMO-FDA radar (a) Angle response (b) Range response

4.3.4.2 Comparison of DP-MIMO-FDA radar with DP-FDA radar

In this subsection, the beam patterns of proposed DP-MIMO-FDA radar have been compared with DP-FDA in both dimensions. It is important to note that the proposed DP-MIMO- FDA can be reduced to DP-FDA radar by choosing $N=1$ subarray. In that case a single waveform will be transmitted instead of multiple waveforms of DP-MIMO-FDA. The beampattern of both DP-FDA and DP-MIMO-FDA in angle dimension has been shown in Fig. 4.13. It can be clearly seen that, although, the main lobe width of both the radar is same, DP-MIMO-FDA outperform DP-FDA radar in terms of side lobe levels. The reduction in side lobes can be attributed to the extended virtual steering vector of DP-MIMO-FDA radar. Likewise, the range beampattern of DP-MIMO-FDA has also shown better performance compared to FDA radar. Fig. 4.14 clearly show the superiority of proposed radar in terms of side lobes level.

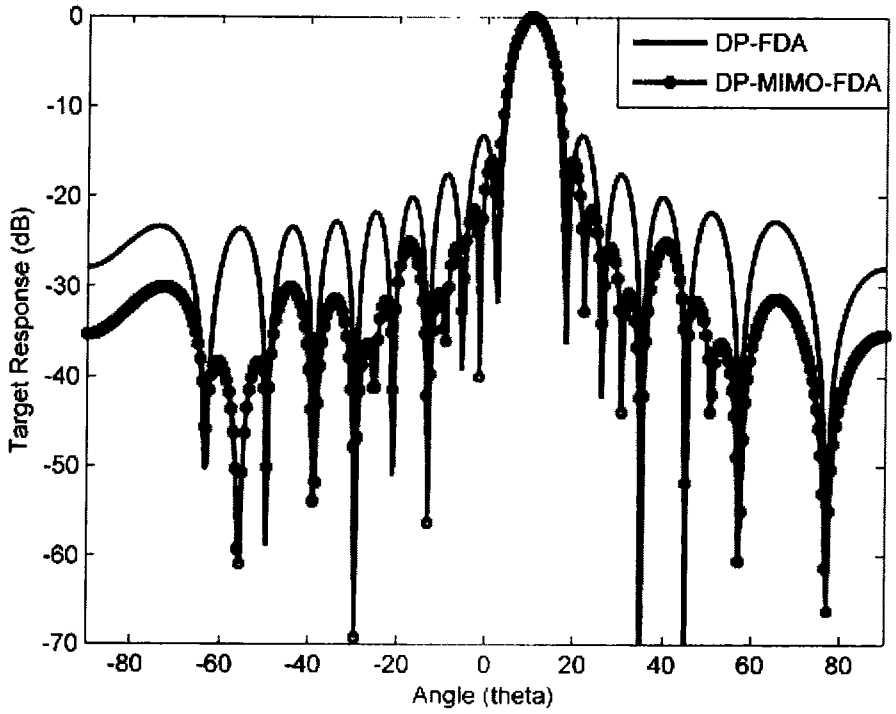

Fig. 4.13 Comparison of angle response of DP-FDA and DP-MIMO-FDA radar

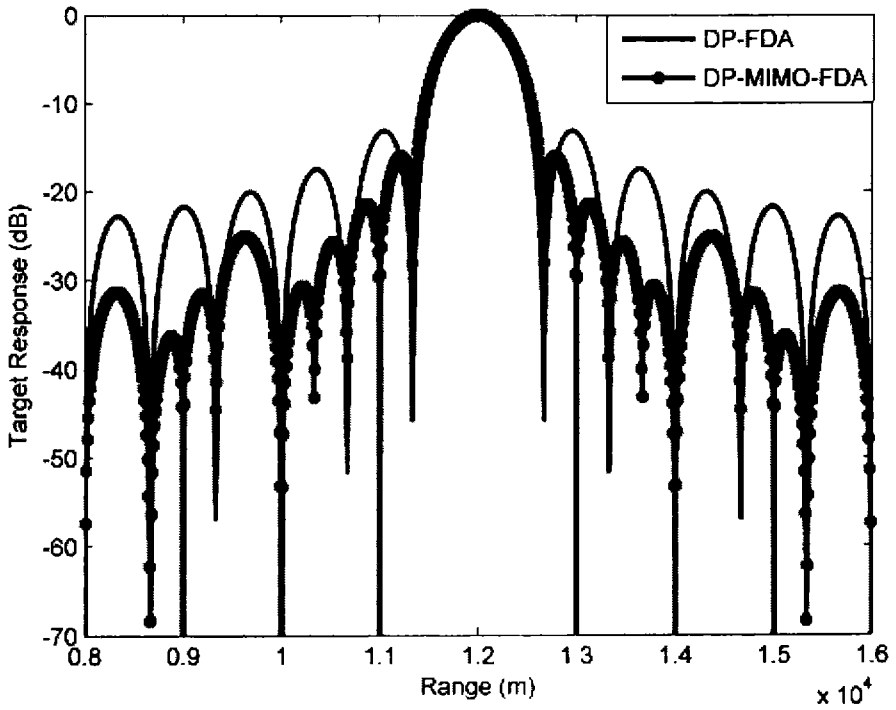

Fig. 4.14 Comparison of range response of DP-FDA and DP-MIMO-FDA radar

4.3.4.3 CRLB for DP-MIMO-FDA radar

In the final simulation, CRLB plots have been shown to analyze the estimation performance of DP- MIMO-FDA. Moreover, a comparison with double pulse FDA radar has also been given. CRLB of both radars has been plotted against SNR to prove that CRLB performance of double pulse MIMO-FDA is better than double pulse FDA. CRLB on target angle and range have been shown in Fig. 4.15 and Fig. 4.16 respectively. Both radars have presented good estimation in angle dimension, however, the proposed radar has shown better performance compared to the FDA radar as shown in Fig 4.15. Likewise, CRLB has been given in Fig. 4.16 for range estimation of both radars. Again performance of proposed scheme is better than DP-FDA radar. The improvement in DP-MIMO-FDA can be attributed to unique waveforms of MIMO and extended data vector at the receiver.

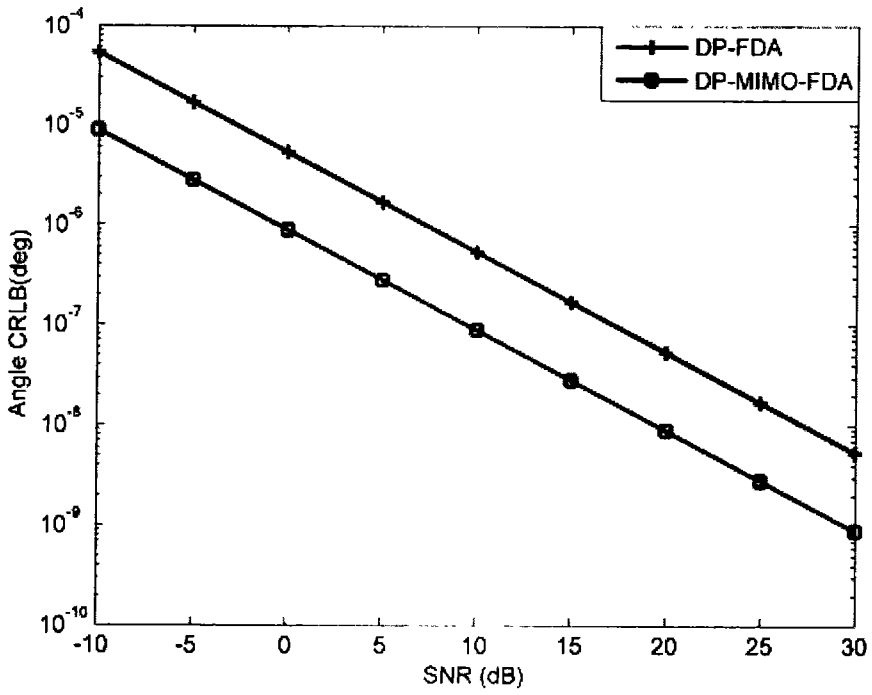

Fig. 4.15 Target angle CRLB for DP-FDA and DP-MIMO-FDA radar

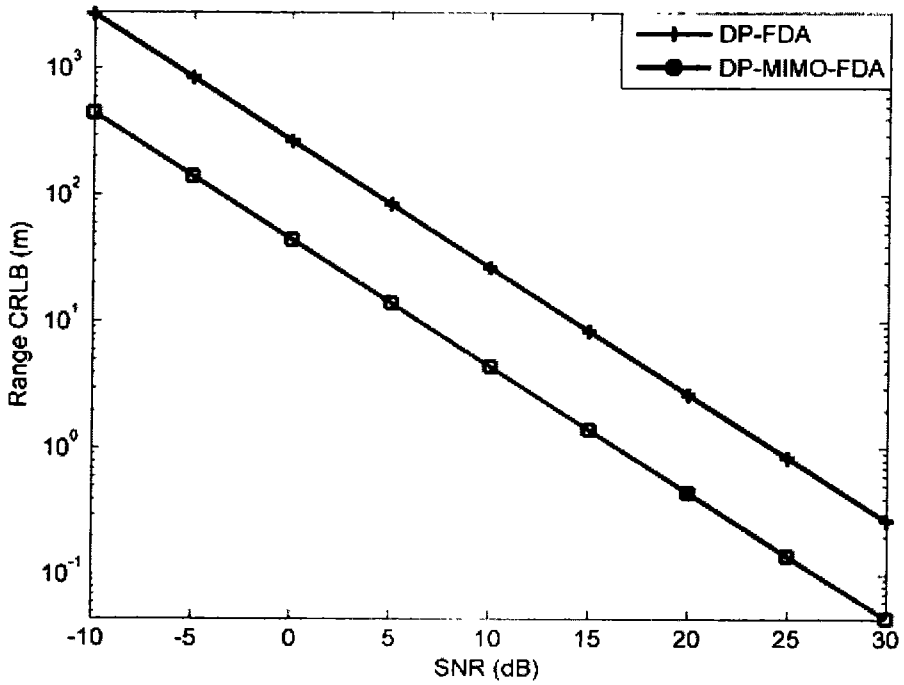

Fig. 4.16 Target range CRLB for DP-FDA and DP-MIMO-FDA radar

4.4 Summary of Chapter

This chapter has presented two new schemes for MIMO-FDA with uniform frequency offset between antenna elements. In the first scheme, the idea of unequal subarrays has been applied to MIMO-FDA radar to show improvements in range dimension as well as angle dimension interms of Beampatterns. Performance analysis has been provided in terms of better SINR and Probability of detection. The second schemes removes the range-angle coupling of FDA by using concept of double pulse i.e. pulse with no offset followed by a pulse of suitable offset. Improvement in localization has also been achieved through extended data vector achieved by using multiple waveforms at the transmit side. Results for beampattern and CRLB have verified the effectiveness of proposed scheme as compared to [62].

Chapter 5

Hybridization of MIMO Radar with FDA radar using Logarithmic Frequency Offset

5.1 Introduction

Frequency offset plays a very important role in performance of FDA and MIMO-FDA radar systems. In previous chapter, we have applied uniform frequency offset for transmit array to show improvements in localization of target. Since we are interested in localization of target, so we have used that particular value of frequency offset, which produces a single maxima for a desired range-angle pair. If we increase the value of frequency offset then the radar scene will exhibit multiple maxima in region of interest due to periodicity property of FDA [44]. To avoid multiple maxima for different values of frequency offset, the non-uniform offset can be applied to transmit subarrays, resulting in single maxima for a target.

This chapter presents the MIMO-FDA using logarithmic frequency offset i.e. non-uninform frequency offset instead of linear or uniform frequency offset. It has been observed in [68] that the logarithmic offset among the antenna elements removes the periodicity of FDA beampattern and produces exactly one maxima in region of interest. First part of the chapter presents a crisp idea of applying range bins and logarithmic offset in each subarray of MIMO-FDA. Resultant system allows us to place single maxima for each of the multiple targets present in different range bins. Moreover, Frequency offset for

MIMO-FDA with logarithmic offset can be adjusted to separate the targets present at different ranges.

Second part of chapter explores the idea of using variable logarithmic offset for each subarray of a MIMO-FDA radar. Since the increase in logarithmic offset directly increases the sharpness of beampattern, so a logarithmically increasing offset is applied in each subarray to get better localization of target. Transmit side of proposed MIMO-Log-FDA shows focusing of beampattern compared to existing FDA radars, which is followed by detailed signal model of the receiver side. It has been shown that the variable logarithmic offset in MIMO-Log-FDA not only produces single maxima, but also gives a sharper beampattern and better SINR due to focused beams at the transmit side. CRLB has been derived for proposed radar and compared with MIMO-FDA and Log-FDA radars.

5.2 Range Bins based MIMO-Log-FDA radar

In this section, a new scheme has been proposed for MIMO-FDA radar with logarithmic frequency offset. Proposed radars system can place exactly one maxima for each of the multiple targets present at different ranges. Inspiration for this idea comes from the fact that Log-FDA produces a single maxima for whole range dimension to remove the periodicity in FDA beampattern. However, in producing only one maxima in radar scene, it will ignore any other potential target present in the vicinity of first target. Therefore, using a subarray approach for multiple targets will be very helpful, since it will be able to produce single maxima for each of the target present at different range.

The basic idea of proposed radar is to divide FDA transmit array into multiple non-overlapping subarrays and apply logarithmic offset along with different waveform in each subarray. Resultant multiple beams are steered towards different region of interest. As a

result, we can focus energy on multiple targets present at different ranges in the space. The logarithmic offset in each subarray has allowed us to produce single maxima for a target in a particular range bin, whereas, the different waveforms will help in independence of signal from each subarray and proper match filtering of the target returns at the receiver

5.2.1 Preliminaries and Signal Model

For a frequency diverse array of P elements using a logarithmic offset among elements, the signal sent by p^{th} element is

$$s_p(t) = w_p e^{j2\pi f_p t} \tag{5.1}$$

The radiated frequency f_p will be

$$f_p = f_0 + \Delta f_p \tag{5.2}$$

where f_0 is the carrier frequency and the frequency offset Δf_p can be given as

$$\Delta f_p = \log(p+1).\delta \qquad p = 0,1,.....P-1 \tag{5.3}$$

Where δ is the configurable parameter for adjusting the logarithmic offset. It can be seen that the frequency offset across each antenna element in logarithmic instead of linear offset. Considering a point target in space, the pattern of transmitted signal can be written as

$$x(t;r_0,\theta) = \sum_{p=0}^{P-1} s_p\left(t - \frac{r_p}{c}\right) = \sum_{p=0}^{M-1} w_p e^{-j2\pi f_p\left(t - \frac{r_0 - pd\sin\theta}{c}\right)} \tag{5.4}$$

where $r_p = r_0 - pd\sin\theta$ is the range of target from p^{th} antenna element and c is speed of light. By applying f_p from (5.2) and the assumption that $f_0 >> \log(P)\delta$, we will get

$$x(t;r_0,\theta) = e^{j2\pi f_0(t - r_0/c)} \times \sum_{p=0}^{M-1} a_p e^{j2\pi\log(p+1)\delta(t - r_0/c)} e^{j2\pi f_0 pd\sin\theta/c} \tag{5.5}$$

The overall signal arrived at a far field point is given in (5.5). It will produce a single maxima at the target location and removes periodicity in maxima. Term inside summation can be taken as array factor and its magnitude square is the transmit beampattern. For a fixed value of t, it will become range-angle dependent beampattern. In our proposed radar, we consider a MIMO-FDA with non-overlapped subarrays and logarithmic offset in each subarray, as shown in Fig 5.1. A transmit array of P elements is divided into N equal non-overlapping subarrays. Number of elements for each subarray can be given by $L = P/N$. Signal radiated by n^{th} subarray in the far field is

$$x_n(t,\theta,r) = \rho\left[\mathbf{w}_n{}^H \mathbf{u}_n(\theta,r)\right] s_n(t) \tag{5.6}$$

$s_n(t)$ is the n^{th} waveform, while $\mathbf{w}_n$ and $\mathbf{u}_n$ are the weight vector and steering vector for n^{th} subarray. Weight vector for n^{th} transmit subarray can be configured as

$$\mathbf{w}_n = [e^{J\gamma_1}\ e^{J\gamma_2}\ \ldots\ldots\ e^{J\gamma_L}] \tag{5.7}$$

Where
$$\gamma_l = 2\pi\left[\frac{\left(l\log(l+1)\delta r_{t_n} - f_0\, ld\sin\theta_{t_n}\right)}{c}\right] \tag{5.8}$$

θ_{t_n} and r_{t_n} are the desired angle and range for n^{th} target.

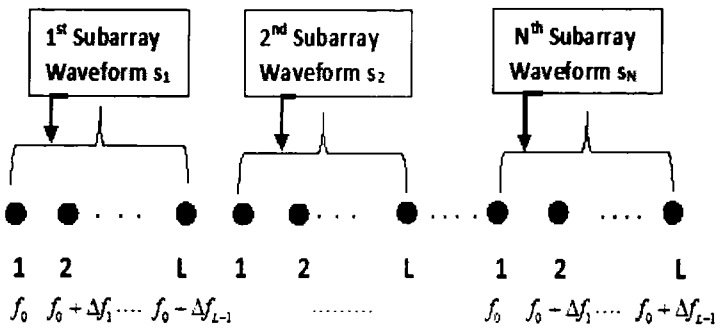

Fig. 5.1 MIMO-log-Frequency diverse array radar

The steering vector for transmit subarray can be given as

$$\mathbf{u}(\theta, r) = \left[e^{j\beta_1} \; e^{j\beta_2} \; \ldots\ldots \; e^{j\beta_L} \right] \tag{5.9}$$

where

$$\beta_l = 2\pi \left[\frac{\left(\log(l+1)\delta(r_0/c) + f_0 l d \sin\theta \right)}{c} \right] \tag{5.10}$$

In our proposed scheme, beam from each subarray will steer the whole region of interest, however, maxima can be produced in desired range by adjusting weights given in (5.7). Each subarray is modulated with a different waveform to separate the returns at receiver. Logarithmic offset in each subarray allows us to get single maxima at desired range-angle pair. The advantage of applying this scheme not only solves the problem of periodic maxima of MIMO-FDA but also improves the existing log-FDA by handling multiple targets simultaneously. Finally, MIMO-Log-FDA radar will become MIMO-FDA by replacing $\log(l+1)$ with l in (5.8) and (5.10).

5.2.2 Range Bins for MIMO-Log-FDA Radar

Range bins are range intervals in which a target is present and a maxima has to be placed for that target. For the case of log-FDA, we get only one maxima for whole range dimension. To place multiple maxima in range dimension, the range bin or intervals have to be fixed for each subarray to get one maxima for each target. Since we are using unique waveforms, so each waveform will place its maxima separately and will not be influenced by the waveform from other subarray. Assuming that the targets position is known, range bins formation can be done through following steps.

1. Select the total interval for the area of interest in range dimension. i.e. $r_0 \le r \le r_N$.

   where r_0 is the starting point of range interval and r_N is the final point.

2. Divide the total interval into N ranges because there are N subarrays. Boundary of each range bin can be given as $r_1, r_2 \ldots\ldots r_{N-1}$ .The range bins will be $r_{b_1} = r_1 - r_0$, $r_{b_2} = r_2 - r_1$, ... , $r_{b_{N-1}} = r_N - r_{N-1}$.

Selecting the size of a range bin is an issue of practical importance. In the system presented here, range bins are selected on the basis of spread of a particular maxima. Spread is the region covered in range dimension by beampattern peak and sides lobes with considerable values on both sides of peak. It has been shown in the upcoming simulation results that frequency offset has an inverse effect on the spread of maxima in range. For larger frequency offset, the spread is small, so we can set smaller range bins. Closer ranges are handled by first few subarrays, while the farthest range bins are handled by last few subarrays.

This idea of range bins has been applied to MIMO-log-FDA for determining the multiple two-dimensional spatial sections in which we want to maximize the energy using different subarrays. Signal transmitted by n^{th} subarray towards angle θ and N different ranges in different range bins can be given as

$$x_n(t,\theta,r) = \left[\mathbf{w}_n{}^H \mathbf{u}_n(\theta, r_n)\right] s_n(t) \tag{5.11}$$

$\mathbf{w}_n$ and $\mathbf{u}_n(\theta_n, r_n)$ are weight vector and the steering vector of MIMO-Log-FDA,(θ, r_n) represent the angle and range of N different targets. $s_n(t)$ is n^{th} waveform transmitted towards n^{th} range bin. The normalized transmit beam pattern for each of the subarray is

$$B_n(\theta,r) = \frac{\left|\mathbf{w}_n^H \mathbf{u}_n(\theta,r)\right|^2}{\left|\mathbf{w}_n^H \mathbf{u}_n\left(\theta_{t_n}, r_{t_n}\right)\right|^2} \tag{5.12}$$

Range bins are important for MIMO-log-FDA radar in given scenario of multiple targets.

Without range bins, we will get only one maxima for all the targets due to logarithmic offset i.e. single maxima for only one target can be achieved.

5.2.3 Simulation Results

Consider a uniform linear array of 32 elements divided into 4 non-overlapped subarrays, where each subarray consists of 8 elements. The fundamental frequency of $f_0 = 10GHz$ is used throughout the simulation. Configurable parameter of $\delta = 50KHz$ is used in all other simulation except the last plot which use different values of configuring parameter. We assume stationary point-like targets in this simulation and there is no mutual coupling between antenna elements. The distance between antenna elements is taken as $\lambda/4$ to avoid physical reallocation of antennas elements in case of changing parameter δ [68]. Range dimension is divided into four sub-ranges to match them with number of subarrays. Since the spread in maxima is around 10 km, so we have chosen the size of range bins as 12km each. We assume four targets present at $\theta = 10^0$ and four different ranges for MIMO-log-FDA radar, i.e. $r_1 = 10km$, $r_2 = 20km$, $r_3 = 30km$ and $r_4 = 40km$. However, the number of targets will vary for different simulations. Since we focus more on range dimension, the angle for each target is fixed at $\theta = 10^0$.

In Fig. 2, the results of our proposed scheme have been presented. Each subarray will scan the whole region and place maxima at different range-angle pair to give single maxima for multiple targets. The results shown in Fig 5.2.(a)- (d) exhibit a single maxima for each target. This single maxima can be attributed to the logarithmic offset used in each subarray. In the next simulation, we have given the results of MIMO-FDA radar [58] and MIMO-Log-FDA radar for only first subarray. Our objective is to show the superiority of proposed

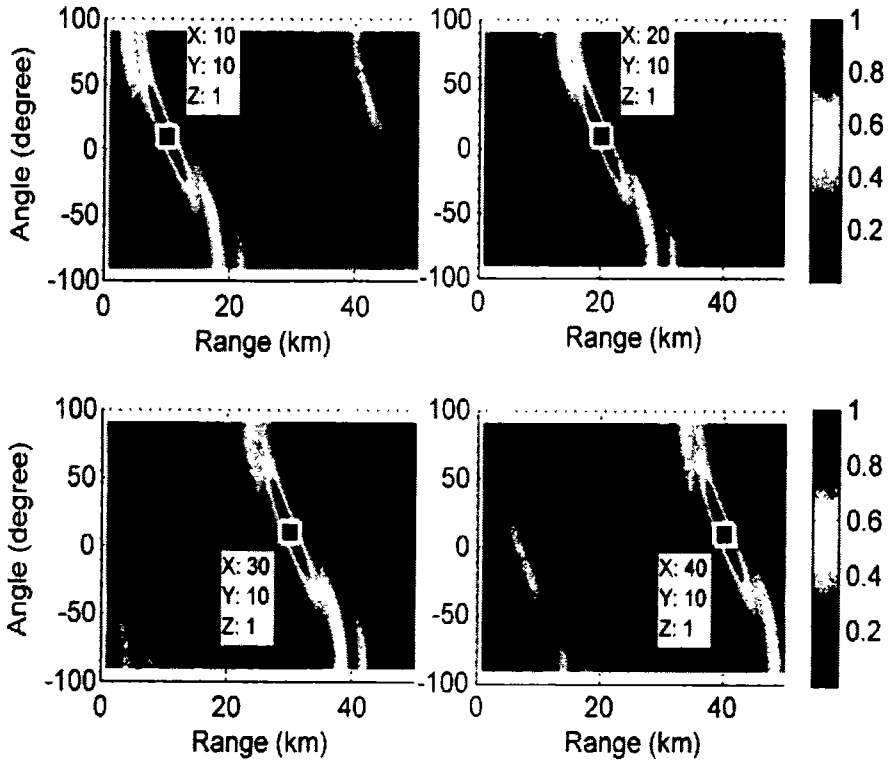

Fig. 5.2 Normalized beampatterns of MIMO-log-FDA for targets at $(10^o, 10km)$, $(10^o, 20km)$, $(10^o, 30km)$ and $(10^o, 40km)$

design over the traditional MIMO-FDA radar in terms of single maxima for a target instead of multiple peaks at periodic ranges. Target is assumed to be present at $(\theta_t, r_t) = (10^0, 24km)$. It can be seen in Fig 5.3. (a) that MIMO-FDA has produced a peak for the given range-angle pair, however, it has also exhibited other maxima within that range bin. This is due to the uniform frequency offset, which result in repetition of maxima after every c/Δ_f [2]. On the other hand, the same subarray produces a single maxima for MIMO-Log-FDA as shown in Fig 5.3. (b). which is due to non-uniform offset. It is also important to mention that both MIMO-FDA and MIMO-Log-FDA will produce similar results in rest of three subarrays.

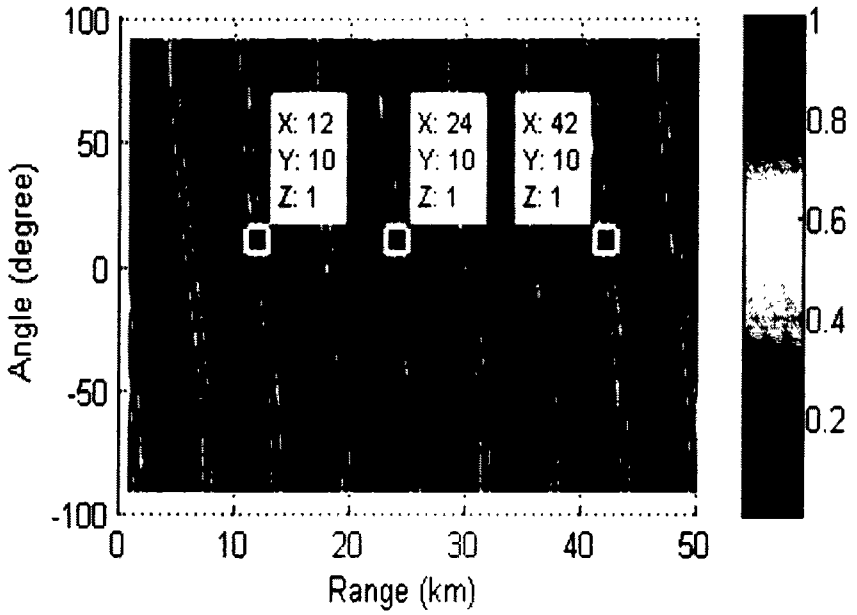

(a) MIMO-FDA beampattern

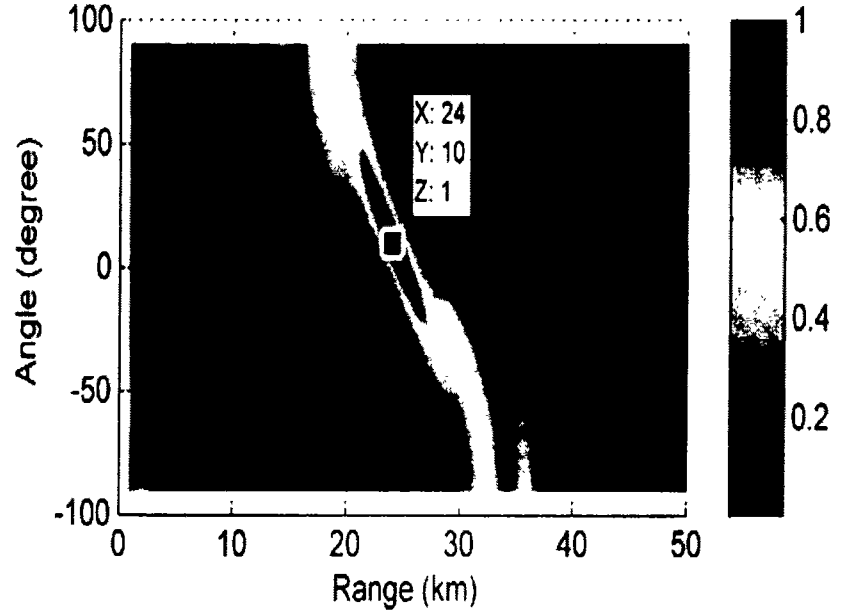

(b) MIMO-Log-FDA beampattern

Fig. 5.3 Normalized beampatterns of (a) MIMO-FDA (b) MIMO-Log-FDA. $L=8$

$(\theta_t, r_t) = (10^0, 24km)$ and $\delta = 50Khz$

In the next plot, MIMO-Log-FDA beampattern has been plotted for different values of δ to show the impact of frequency offset. By choosing $\delta = 10Khz$ and $\delta = 100Khz$, it can be clearly observed in Fig. 5.4 (a)-(b) that changing frequency offset in MIMO-Log-FDA radar effect the width or sharpness of beampattern. In Fig. 5.4(a), beam pattern has become wider and showed a small spread in range. Since we are using a small δ, so it can be safely established that a smaller frequency offset will reduce the sharpness of beampattern. For next result, we have applied a bigger value of frequency offset. Fig. 5.4(b) has been clearly showing a beampattern which is a lot sharper than the beampattern in Fig. 5.4(a). Spread in range dimension is also much less compared to previous result. This changes in beampattern can be attributed to larger value of δ. Thus we can conclude that the variation in logarithmic frequency offset can control beampattern of MIMO-FDA in terms of its width, which can then contribute to enhanced localization. This conclusion has been investigated in the next section by using variable logarithmic frequency offset.

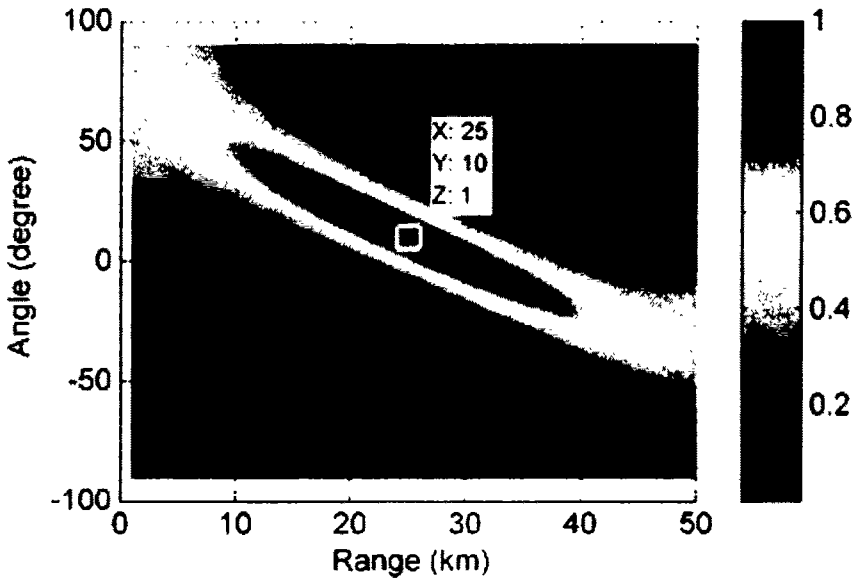

(a) MIMO-Log-FDA for $\delta = 10Khz$

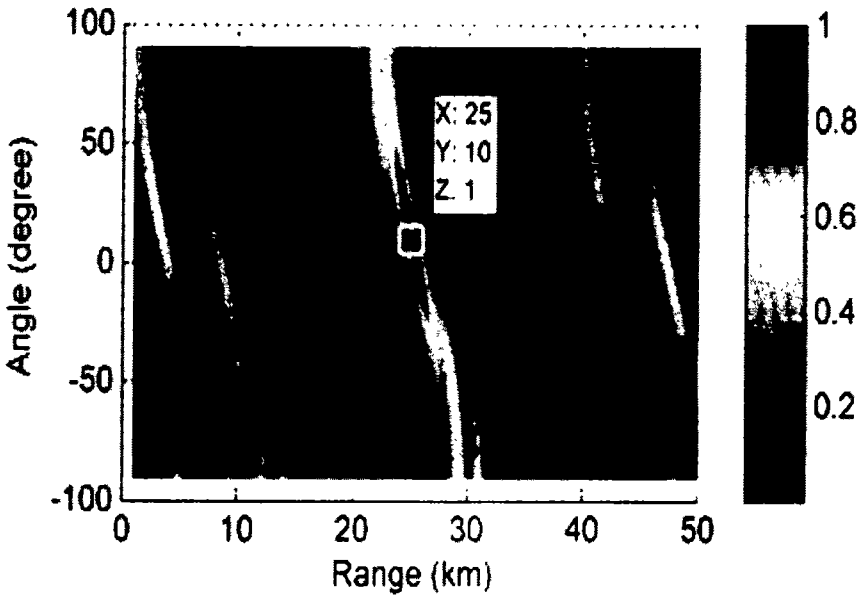

(b) MIMO-Log-FDA for $\delta = 100Khz$

Fig. 5.4 Normalized beampatterns of 1st subarray of MIMO-log-FDA for target a $(\theta_t, r_{t_1}) = (10^0, 25km)$, (a) $\delta = 10Khz$ (b) $\delta = 100Khz$

5.3 MIMO-Log-FDA with Variable Logarithmic Offset

This section provides a detailed analysis of using different logarithmic frequency offset in each subarray. It has been shown in simulation results of previous section that change in logarithmic frequency offset effect the sharpness of beampattern. Using this fact, we have proposed a new scheme in MIMO-Log-FDA, which apply variable logarithmic offset in each subarray to give single maxima as well as focus the target with multiple beams of variable width. As a result, we get a better estimation for target angle and range compared to existing frequency diverse radar systems.

In subsequent section, transmit side has been presented to show the impact of using different non-uniform offsets i.e. logarithmic offset. It has been observed that the variation

in logarithmic offsets adds an extra degree of freedom in terms of controlling the width of beampattern on the transmit side. This is followed by a detailed received signal model for MIMO-Log-FDA. Performance analysis has also been done in terms of Signal to interference plus noise ratio (SINR) and Cramer–Rao lower bound (CRLB). Comparison with existing FDA radar and MIMO-FDA radar clearly exhibit that the proposed MIMO-log-FDA radar has outperformed the existing radar systems.

5.3.1 Idea and formulation

The log-FDA radar uses only one value of configuration parameter δ to apply logarithmic offset throughout the transmit array. Likewise, existing MIMO-Log-FDA radar uses same configuration parameter in each subarray. However, in this work, we apply different configuration parameters in each subarray to produce multiple beampatterns of variable width. Proposed system uses the approach of overlapped subarrays to achieve maximum transmit gain.

In order to define subarrays in a transmit array of P elements, a $P\times 1$ vector P_n is defined which contains 0 and 1 as entries. For n^{th} subarray, a '1' in the vector at a particular index shows that antenna corresponding to that index belongs to n^{th} subarray and it can be assigned the configuring parameter associated with this subarray. Likewise, a zero in the vector means the corresponding antenna does not belong to n^{th} subarray and it will not be assigned the configuring parameter of n^{th} subarray. If each subarray has P_l elements, where $1 < P_l < P$, then number of 1's in P_n are P_l and number of 0's are $P - P_l$. Moreover a $P_l \times 1$ vector for a particular subarray can be obtained as $P_l = P_n \odot P$, where $\odot$ stands for Hadamard product. Since different configuration parameters are used in each subarray, the

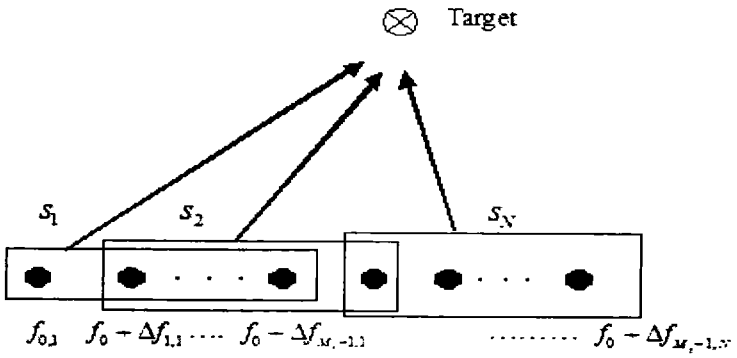

Fig. 5.5 MIMO-FDA with different logarithmic Offsets

offset selection will be slightly different from log-FDA. The frequency radiated by p^{th} element of n^{th} subarray will be

$$f_{p,n} = f_0 + \Delta f_{p,n} \tag{5.13}$$

where f_0 is the carrier frequency and $\Delta f_{p,n}$ is frequency offset given as

$$\Delta f_{p,n} = \log(p+1).\delta_n \quad , \quad 0 \le p \le P_l - 1, \quad 1 \le n \le N \tag{5.14}$$

Here P_l represent number of elements in each subarray while N represent number of subarrays formed in a transmit array of P antenna elements.

5.3.2 Signal Model

Consider a transmit array of P elements partitioned into N overlapping subarrays, as shown in Fig. 5.5. Since the transmit array is divided into equal subarray, so the number of elements in each subarray can be given by $P_l = P - N + 1$. The signal radiated by n^{th} subarray in the far field can be given as

$$X_{p,n}(t) = \rho s_n(t) w_{p,n} e^{j2\pi f_{p,n} t} \tag{5.15}$$

where $\rho = P / N$ is the energy transmitted by each subarray and $w_{p,n}$ is the weight given

to p^{th} element of n^{th} subarray. The n^{th} subarray contains P_l active weights and $P-P_l$ zeros weights corresponding to inactive elements. $s_n(t)$ is the waveform transmitted by n^{th} subarray. Overall signal observed in the far field can be written as

$$x(t;r_0,\theta)=\sum_{p=0}^{P-1}\sum_{n=1}^{N}X_{p,n}\left(t-\frac{r_p}{c}\right) \tag{5.16}$$

By using far field approximation i.e. $r_p=r_0+pdsin(\theta)$, the signal in (5.16) will be

$$x(t;r_0,\theta)\approx\sum_{p=0}^{P-1}\sum_{n=1}^{N}\rho s_n(t)w_{p,n}e^{-j2\pi f_{p,n}\left(t-\frac{r_0-pd\sin\theta}{c}\right)} \tag{5.17}$$

Using the value of $f_{p,n}$ from (5.13)

$$x(t;r_0,\theta)=e^{j2\pi f_0(t-r_0/c)}\times\sum_{p=0}^{P-1}\sum_{n=1}^{N}\rho s_n(t)w_{p,n}e^{j2\pi\left(f_0 md\sin\theta/c+\log(m+1)\delta_n(t-r_0/c)\right)} \tag{5.18}$$

Here the signal in (5.18) can be obtained by the assuming that $f_0>>\log(P)\delta_n$ .The term inside the summation can be taken as the array factor and its square is the transmit beampattern. Beam pattern transmitted by n^{th} subarray can be given as

$$B_n(t,r_0,\theta)\approx\left|AF_n(t,r_0,\theta)\right|^2\approx\left|\sum_{p=0}^{P-1}\sum_{n=1}^{N}\rho s_n(t)w_{p,n}e^{j2\pi\left(f_0 pd\sin\theta/c+\log(p+1)\delta_n(t-r_0/c)\right)}\right|^2 \tag{5.19}$$

It can be observed that beampattern depends upon the weights given to a particular subarray. Therefore, we can adjust these weight properly to get a single maxima which is one of the main attribute of logarithmic offset based radar systems.

5.3.3 Proposed Receiver side

Signal reflected from a far field target will contain each of the N waveform transmitted by transmit array. It is important to mention that we have used a ULA at the

receiver, where the waveforms will be matched filtered to get desired information. For a receiver array of R antenna elements, signal received on r^{th} element can be expressed as

$$m_r(t,\theta) = \rho \sum_{n=1}^{N} \sum_{p=1}^{P_t-1} \beta s_n\left(t-\tau_n-\tau_r\right) e^{j2\pi f_{p,n}(t-\tau_n-\tau_r)} \tag{5.20}$$

Here β is the complex valued reflection coefficient for a target in the far field. τ_n and τ_r are time delays on transmit and received side respectively. These time delays can be further written as

$$\tau_n = \frac{\tau_0}{2} - \frac{d_t \sin\theta}{c} = \frac{r - d_t \sin\theta}{c} \tag{5.21}$$

$$\tau_r = \frac{\tau_0}{2} - \frac{d_r \sin\theta}{c} = \frac{r - d_r \sin\theta}{c} \tag{5.22}$$

Where $\tau_0 = {}^{2r}/_{c}$, d_t and d_r are distance between elements of transmit array and received array. θ is the angle of target while r is range of target. By applying the narrow band assumption that $s_n(t-\tau) \approx s_n(t-\tau_0)$ and matched filtering the n^{th} waveform on r^{th} element, we will get the data

$$d_{n,r} \approx \rho\beta e^{-j4\pi \frac{f_n}{c} r} \times e^{j2\pi \frac{f_n}{c}[d_t \sin\theta + d_r \sin\theta]} \tag{5.23}$$

After applying value of f_n in (5.23) and using the approximation that frequency increment is negligible compared to fundamental frequency in second exponential term of (5.23), the signal can be further written as

$$d_{n,r} \approx \rho\beta e^{-j4\pi \frac{f_0}{c} r} e^{-j4\pi \frac{\Delta f_n}{c} r} e^{j2\pi \frac{f_0}{c}[d_t \sin\theta + d_r \sin\theta]} \tag{5.24}$$

Here Δf_n is the offset given to n^{th} subarray. Since r^{th} element will receive all the signal, so output of this element can be written as a vector

$$\mathbf{y} = \rho\tilde{\beta}\mathbf{u}(\theta, r)\mathrm{e}^{j2\pi\frac{f_0}{c}d_r\sin\theta} \tag{5.25}$$

Where $\tilde{\beta} = \beta.e^{-j4\pi\frac{f_0}{c}r}$ and $\mathbf{u}(\theta, r)$ is the transmit steering vector with extended length due to different logarithmic frequency offset in each subarray and given as

$$\mathbf{u}(\theta,r) = \left[1 \;\; e^{j\psi_1} \;\; e^{j2\psi_1} \ldots . e^{j(M_t-1)\psi_1} \;\; 1 \;\; e^{j\psi_2} \;\; e^{j2\psi_2} \ldots . e^{j(M_t-1)\psi_2} \ldots . . 1 \;\; e^{j\psi_N} \;\; e^{j2\psi_N} \ldots . . . e^{j(M_t-1)\psi_N}\right] \tag{5.26}$$

Where,

$$\psi_1 = \left(2\pi\frac{f_0}{c}d_t\sin\theta - 4\pi\frac{\Delta f_1}{c}r\right) \tag{5.26a}$$

$$\psi_2 = \left(2\pi\frac{f_0}{c}d_t\sin\theta - 4\pi\frac{\Delta f_2}{c}r\right) \tag{5.26b}$$

.

.

$$\psi_N = \left(2\pi\frac{f_0}{c}d_t\sin\theta - 4\pi\frac{\Delta f_N}{c}r\right) \tag{5.26c}$$

Likewise, the received steering vector can be written as

$$\mathbf{v}(\theta) = \left[1, \;\; \mathrm{e}^{j2\pi\frac{f_0}{c}d_r\sin\theta} \ldots . . . . . \mathrm{e}^{j2\pi\frac{f_0}{c}(r-1)d_r\sin\theta}\right] \tag{5.27}$$

Using (5.26) and (5.27), the virtual data vector for target signal can be written as

$$\mathbf{y}_s = \left[\mathbf{y}_1^T \mathbf{y}_2^T \mathbf{y}_3^T \ldots . . \mathbf{y}_N^T\right]^T = \rho\tilde{\beta}\mathbf{v}(\theta)\otimes\mathbf{u}(\theta,r) \tag{5.28}$$

where $\otimes$ stands for the kronecker product and $(.)^T$ represents transpose operator. Assuming Q interferences in the background of target and introducing the noise term, the final form can be written as

$$\mathbf{y} = \mathbf{y}_s + \mathbf{y}_t + \mathbf{y}_n$$

$$= \rho\tilde{\beta}\mathbf{v}(\theta_t)\otimes\mathbf{u}(\theta_t, r_t) + \sum_{q=1}^{Q}\tilde{\beta}_q\mathbf{v}(\theta_q)\otimes\mathbf{u}(\theta_q, r_q) + \mathbf{z}_n \qquad (5.29)$$

$\mathbf{n}_n$ is the noise vector which is assumed to be zero mean white circularly Gaussian noise with covariance $\sigma^2\mathbf{I}_{NR}$, where $\mathbf{I}_{NR}$ is the $N \times R$ identity matrix.

5.3.4 Beamforming for proposed radar

Using a non-adaptive conventional beamformer [21], the received weight vector can be given by $\mathbf{w}_R = \mathbf{v}(\theta_t)\otimes\mathbf{u}(\theta_t, r_t)$. Applying these weights, the normalized received beampattern can be written as

$$B_r(\theta, r) = \frac{\left|\mathbf{w}_r^H\left[\mathbf{v}(\theta)\otimes\mathbf{u}(\theta, r)\right]\right|^2}{\left|\mathbf{w}_r^H\left[\mathbf{v}(\theta_t)\otimes\mathbf{u}(\theta_t, r_t)\right]\right|^2} \qquad (5.30)$$

Where (θ_t, r_t) is the angle and range of target. Putting the value of weights, final beampattern will be

$$B_r(\theta, r) = \frac{\left|\left[\mathbf{v}(\theta_t)\otimes\mathbf{u}(\theta_t, r_t)\right]\left[\mathbf{v}(\theta)\otimes\mathbf{u}(\theta, r)\right]\right|^2}{\left\|\mathbf{v}(\theta_t)\otimes\mathbf{u}(\theta_t, r_t)\right\|^4} \qquad (5.31)$$

Next step is to estimate the angle and range of target. For non-adaptive Beamformer, angle can be estimated as

$$\hat{\theta} = \arg\left\{\max_{\theta_t}\left|\mathbf{w}_r^H\mathbf{v}(\theta_t)\otimes\mathbf{u}(\theta_t, r_t)\right|^2\right\} \qquad (5.32)$$

Likewise, range can be estimated as

$$\hat{r} = \arg\left\{\max_{r_t}\left|\mathbf{w}_r^H\mathbf{v}(\theta_t)\otimes\mathbf{u}(\theta_t, r_t)\right|^2\right\} \qquad (5.33)$$

After completing this step, we have the estimates of both angle and range. Therefore, we

can exactly locate the target in range-angle dimension i.e. (θ_t, r_t) . Estimation performance of proposed radar systems has been analyzed in subsequent section.

5.3.5 Performance analysis of MIMO-Log-FDA Radar

In this section, performance analysis of proposed radar has been done in terms of SINR and CRLB.

5.3.5.1 SINR of Proposed Radar

For SINR, modeling a covariance matrix is an important feature. This covariance matrix can be given as

$$\mathbf{C}_{i+n} = \rho^2 \sum_{i=1}^{Q} \sigma_i^2 \left[\mathbf{v}(\theta_i) \otimes \mathbf{u}(\theta_i, r_i)\right]\left[\mathbf{v}(\theta_i) \otimes \mathbf{u}(\theta_i, r_i)\right]^H + \sigma_n^2 \mathbf{I} \tag{5.34}$$

Where α_i and α_n are variances of reflection coefficient of interference and noise respectively. Since FDA beampattern is time dependent as well as angle and range dependent, therefore, to reduce its complexity, we can take one parameter as constant to show its dependence in terms of other two parameters. Here we will fix time to make it a range-angle dependent beampattern. It is important to mention that we take the snapshot of beampatterns at precise time given by $t = 1/\Delta_f$ .This assumption makes it easier to model the covariance matrix for this proposed system. SINR for MIMO-log-FDA radar can be given as

$$SINR = \frac{\rho^2 \sigma_t^2 \left|\mathbf{w}_r^H \mathbf{v}(\theta_t) \otimes \mathbf{u}(\theta_t, r_t)\right|^2}{\mathbf{w}_r^H \mathbf{C}_{i+n} \mathbf{w}_r} \tag{5.35}$$

By putting the values of received weight vector and covariance matrix, (5.35) can be further written as

$$SINR = \frac{\rho^2\sigma_t^2 \left\|\mathbf{v}(\theta_t)\right\|^2 \left\|\mathbf{u}(\theta_t,r_t)\right\|^2\Big|^2}{\mathbf{v}^H(\theta_t)\otimes\mathbf{u}^H(\theta_t,r_t)\left[\sum_{t=1}^{Q}\rho^2\sigma_t^2(\mathbf{v}(\theta_t)\otimes\mathbf{u}(\theta_t,r_t))(\mathbf{v}(\theta_t)\otimes\mathbf{u}(\theta_t,r_t))^H+\sigma_n^2\mathbf{I}\right]\mathbf{v}(\theta_t)\otimes\mathbf{u}(\theta_t,r_t)} \tag{5.36}$$

Using the fact that $\left\|\mathbf{u}(\theta_t,r_t)\right\|^2 = N$, $\left\|\mathbf{v}(\theta_t)\right\|^2 = R$ and simplifying further, SINR can be reduced to

$$SINR = \frac{\rho^2\sigma_t^2N^2R^2}{\rho^2\left[\sum_{t=1}^{Q}\sigma_t^2\left|\left(\mathbf{v}(\theta_t)\otimes\mathbf{u}(\theta_t,r_t)\right)^H\mathbf{v}(\theta_t)\otimes\mathbf{u}(\theta_t,r_t)\right|^2+\sigma_n^2NR\right]} \tag{5.37}$$

5.3.5.2 CRLB

CRLB is used to evaluate the estimation performance of an unbiased estimators. In this case, the objective is to analyze the range and angle estimation performance of MIMO-Log-FDA radar. The parameter vector to be estimated can be given $\boldsymbol{\gamma} = [\theta, r]^T$. Observed signal $\mathbf{d}$ has mean $\boldsymbol{\mu}$ and covariance matrix $\mathbf{R}$ given as

$$\boldsymbol{\mu} = \beta\mathbf{u}(\theta,r) \tag{5.38a}$$

$$\mathbf{R} = \sigma^2\mathbf{I}_{NR} \tag{5.38b}$$

Next, the fisher information matrix can be derived as

$$\mathbf{J} = 2\,\mathrm{Re}\left\{D_{\gamma_i}^H(\boldsymbol{\gamma})\left(\mathbf{R}_n^{-1}\right)D_{\gamma_j}(\boldsymbol{\gamma})\right\} \tag{5.39}$$

$$\mathbf{J} = \frac{2\beta^2}{\sigma_n^2}\begin{bmatrix} 2\omega_1^2C_1 & \omega_1\omega_2C_1 \\ \omega_1\omega_2C_1 & \omega_2^2C_1 \end{bmatrix} \tag{5.40}$$

Where,

$$\omega_1 = \left(\frac{2\pi f_0 d \cos\theta}{c} \right) \tag{5.41a}$$

$$\omega_2 = \left(\frac{4\pi \Delta f_1}{c} + \frac{4\pi \Delta f_2}{c} \ldots\ldots \frac{4\pi \Delta f_N}{c} \right) \tag{5.41b}$$

$$C_1 = \sum_{n=1}^{N} \sum_{p=0}^{P_l - 1} n.p^2 \tag{5.41c}$$

Since $\frac{2\beta^2}{\sigma_n^2}$ is the signal to noise ratio (SNR), the CRLB matrix can be obtained as

$$\mathbf{J}^{-1} = \frac{1}{2.SNR.C_2} \begin{bmatrix} \omega_2^2 C_1 & -\omega_1 \omega_2 C_1 \\ -\omega_1 \omega_2 C_1 & 2\omega_1^2 C_1 \end{bmatrix} \tag{5.42}$$

$$\text{Where } C_2 = 2\omega_1^2 C_1 . \omega_2^2 C_1 - \omega_1^2 \omega_2^2 C_1^2 \tag{5.43}$$

Finally, the CRLB for both estimates can be given as

$$CRLB_{\theta\theta} = \frac{1}{2.SNR.C_2} \omega_2^2 C_1 \tag{5.44}$$

$$CRLB_{rr} = \frac{1}{2.SNR.C_2} \omega_1^2 C_1 \tag{5.45}$$

It is important to mention that the extended data vector due to multiple waveforms and logarithmic frequency offset enable us to get better estimate compared to existing MIMO-FDA radar and Log-FDA radar.

5.3.6 Simulation Results

Consider an FDA array with 12 transmit antenna elements divided into 3 overlapped subarrays, where each subarray consists of 10 elements. The fundamental frequency is

$f_0 = 10GHz$ and configurable parameters for each subarray of MIMO-Log-FDA radar are $\delta_1 = 15Khz$ $\delta_2 = 30Khz$ and $\delta = 45Khz$ respectively. For MIMO-FDA radar [128] and Log-FDA radar [68], $\delta_1 = 15Khz$ will be used throughout the simulation. Distance between the antenna elements is taken as $\lambda/4$ to avoid the physical reallocation of the antennas elements in case of changing the configuring parameter δ . Target is assumed to be present at $\theta = 10^0$ and $r = 40km$. First part of simulation presents results for transmit side, while the second part presents the comparisons of beampattern on receiver side followed by performance analysis in last part of simulation.

In fig 5.6 (a)-(c), results for MIMO-FDA, Log-FDA radar and MIMO-Log-FDA radar are presented. It can be observed that MIMO-FDA exhibit multiple periodic maxima in the region of interest. These multiple maxima, other than the desired location, considerably degrades the SINR performance at receiver side. Fig 5.6 (b)-(c) shows that Log-FDA and MIMO-Log-FDA produces only a single maxima at the location of target, which can be attributed to non-uniform offset i.e. logarithmic offset, used instead of uniform offsets. Since MIMO-Log-FDA radar provides us with an extra degree of freedom by allowing different logarithmic offset in each subarray, so the beampattern of MIMO-Log-FDA radar is better than log-FDA in terms of spread in range dimension as well as side lobes. Less spread can be attributed to larger logarithmic frequency offset used in second and third subarray. This less spread in range dimension due to increase in logarithmic offset has already been shown in simulations of section 5.1, where sharpness in range dimension increases due to larger logarithmic offset and vice versa.

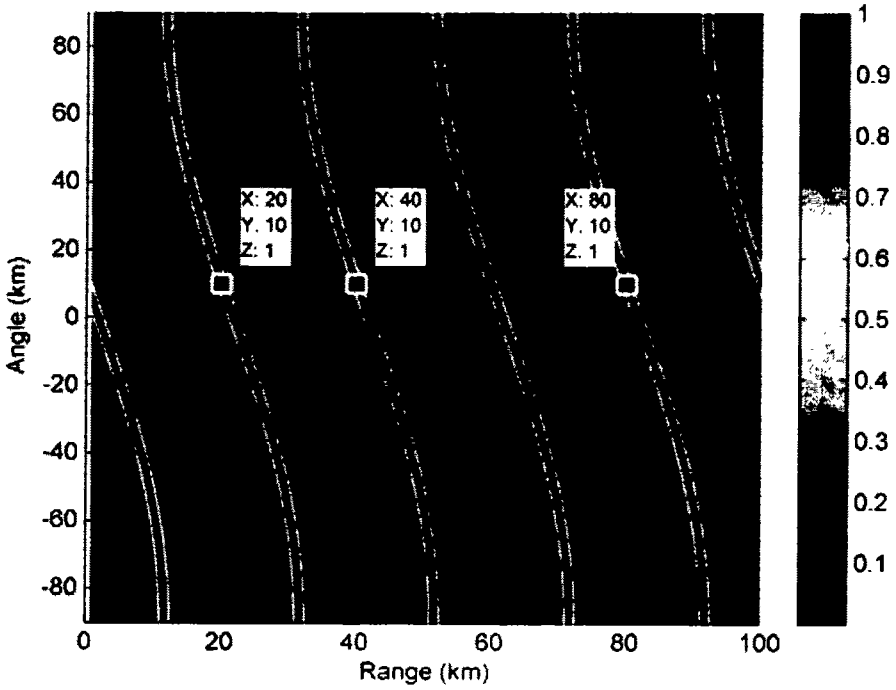

(a) MIMO-FDA beampattern

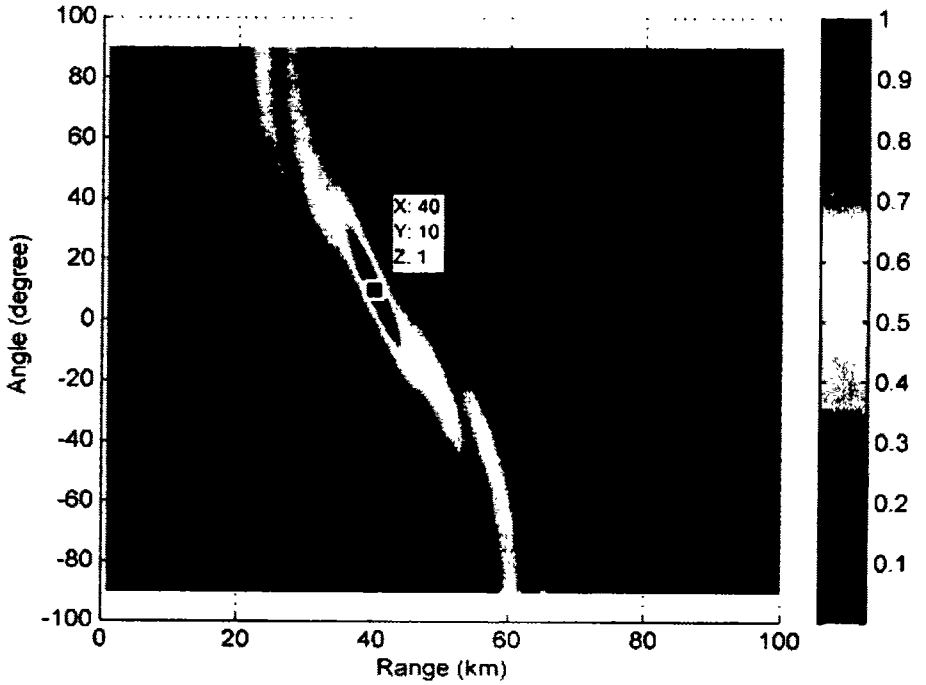

(b) Log-FDA beampattern

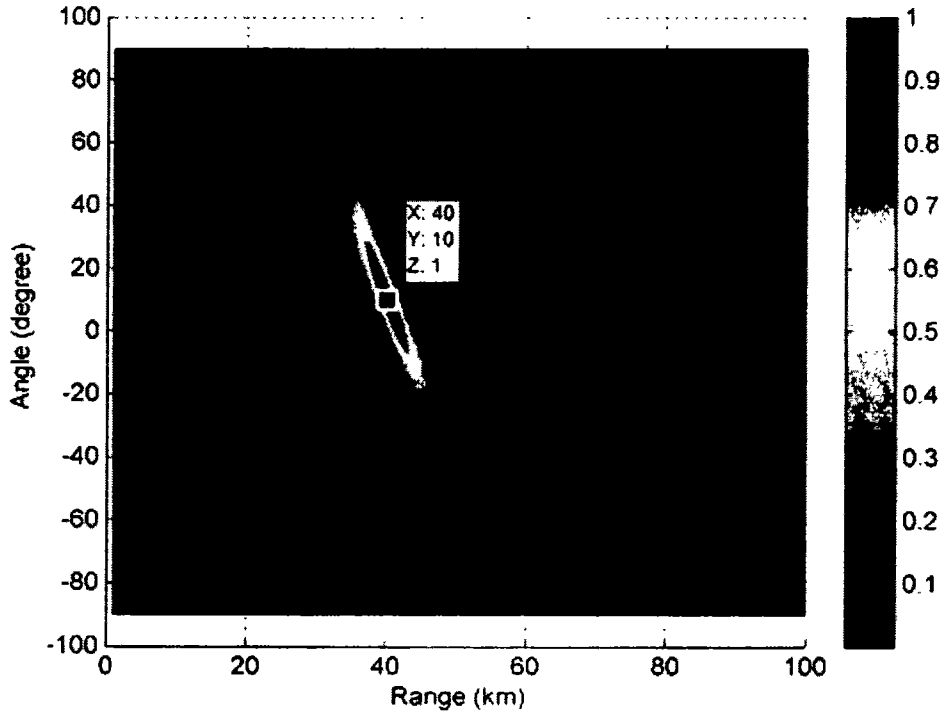

(c) MIMO-Log-FDA beampattern

Fig. 5.6 Normalized transmit beampatterns of (a) MIMO-FDA (b) Log-FDA (c) MIMO-Log-FDA

Side-lobes levels for Log-FDA and MIMO-LOG-FDA in terms of angle and range dimension are shown in Fig 5.7 and Fig 5.8 respectively by plotting only angle and range profile of both radar systems. Fig.5.7 (a) and 5.7 (b) shows the side lobes level of both radars in angle dimension. Clearly, side-lobes level of proposed radar are lower as compared to Log-FDA radar. In the same way, Fig 5.8(b) exhibit lower side lobes level in range dimension for proposed radar as compared to Log-FDA radar presented in Fig 5.8 (a). Thus by properly handling the non-uniform offset, an improvement in transmit beampattern can be achieved. MIMO-FDA is not compared due to its inability to produce single maxima in desired region.

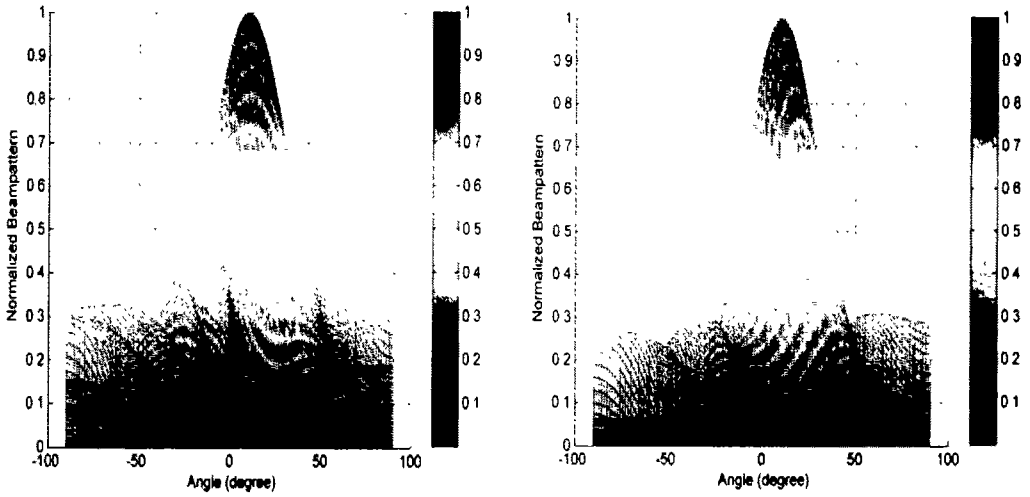

(a) (b)

Fig. 5. 7 Normalized transmit beampatterns in Angle dimension for (a) Log-FDA (b) MIMO-Log-FDA

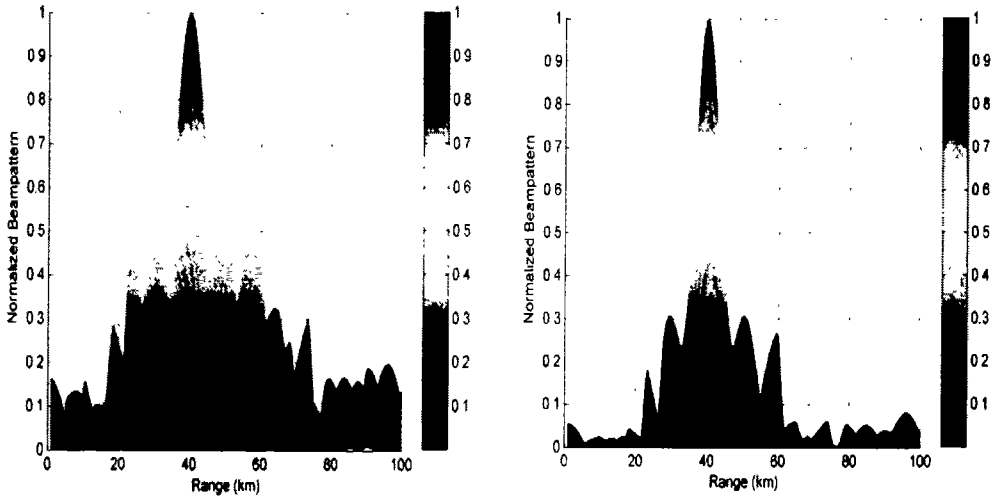

(a) (b)

Fig. 5. 8 Normalized transmit beampatterns in Range dimension for (a) Log-FDA (b) MIMO-Log-FDA

In the second part of simulation, receiver side has been presented. First of all received beampatterns for MIMO-FDA, Log-FDA radar and MIMO-Log-FDA radar systems have been shown in Fig. 5.9 (a)-(c). Due to more focused beams at transmit side, the received beampattern of MIMO-LOG-FDA outperform the rest of radar systems. Fig. 5.9 (a) show the performance of MIMO-FDA radar. It can be observed that MIMO-FDA has placed the maxima at right position, however, there are plenty of undesired interferences in the region of interest. This is due to multiple maxima at the transmit side. MIMO-Log-FDA and Log-FDA on the other hand have suppressed all the interferences in the region of interest. MIMO-Log-FDA has the best performance which can be attributed to extended data vector achieved at receiver side due multiple waveforms of MIMO used at transmitter and the non-uniform offset.

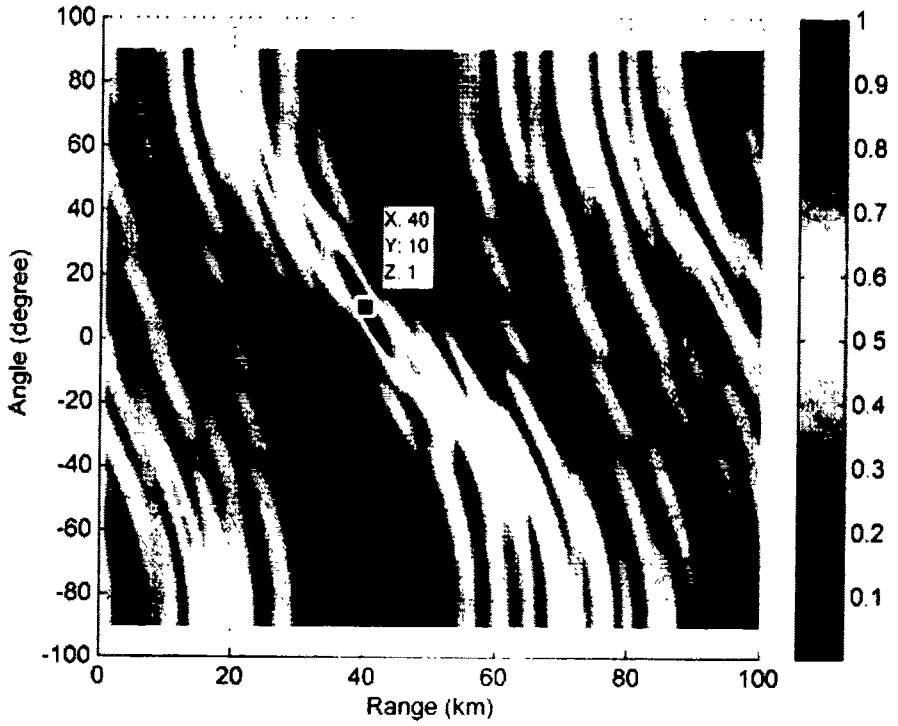

(a)

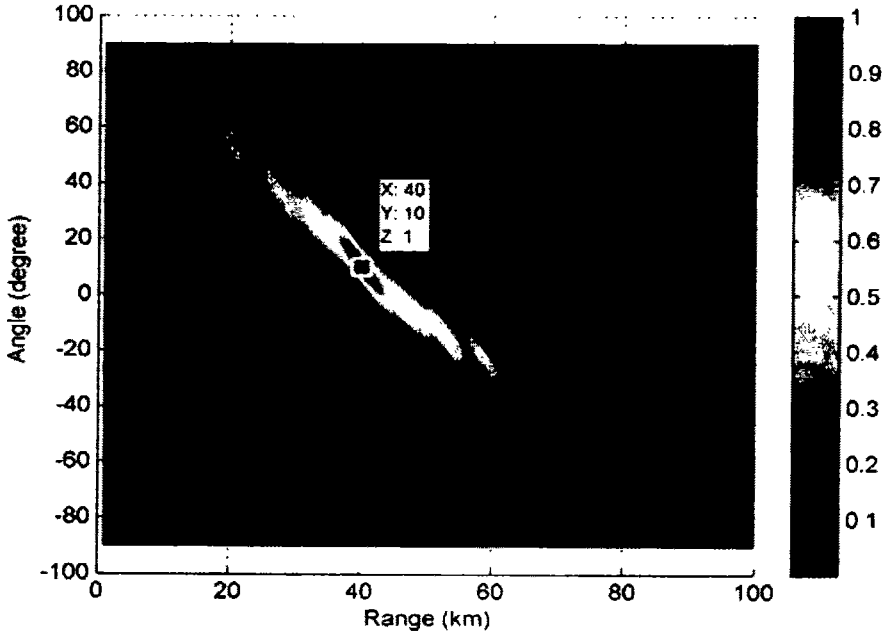

(b)

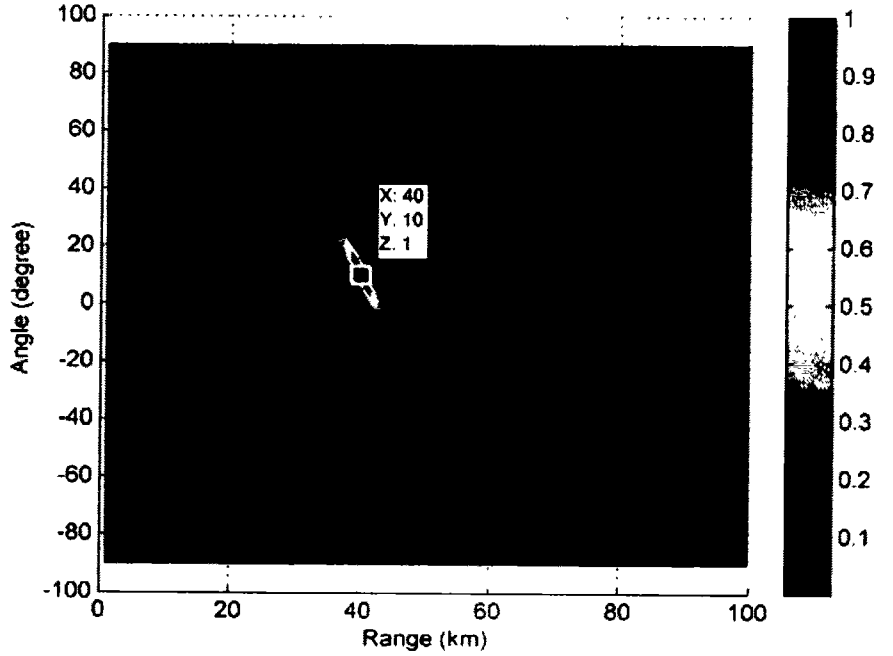

(c)

Fig. 5.9 Normalized Received beampatterns of (a) MIMO-FDA (b) Log-FDA (c) MIMO-Log-FDA

In the next plot, SINR versus SNR of all radar systems have been plotted. Fig. 5.10 clearly shows that Logarithmic offset based systems exhibit better performance compared to other radar systems due to single maxima for target at the transmit side. Moreover, performance of proposed system is better compared to Log-FDA in terms of suppression of undesired interferences due to variable logarithmic offset in each subarray.

Finally, Cramer Rao lower bound have been plotted for proposed radar system to show the performance of estimates in range and angle dimension. Fig. 5.11 gives angle CRLB of proposed as well as other radar systems. All the radars exhibit good estimation performance in angle dimension, however the proposed radar has better performance by attaining lower CRLB compared to Log-FDA and MIMO-FDA. Range dimension CRLB of all radar systems have been presented in Fig. 5.12. It can be seen that MIMO-LOG-FDA again

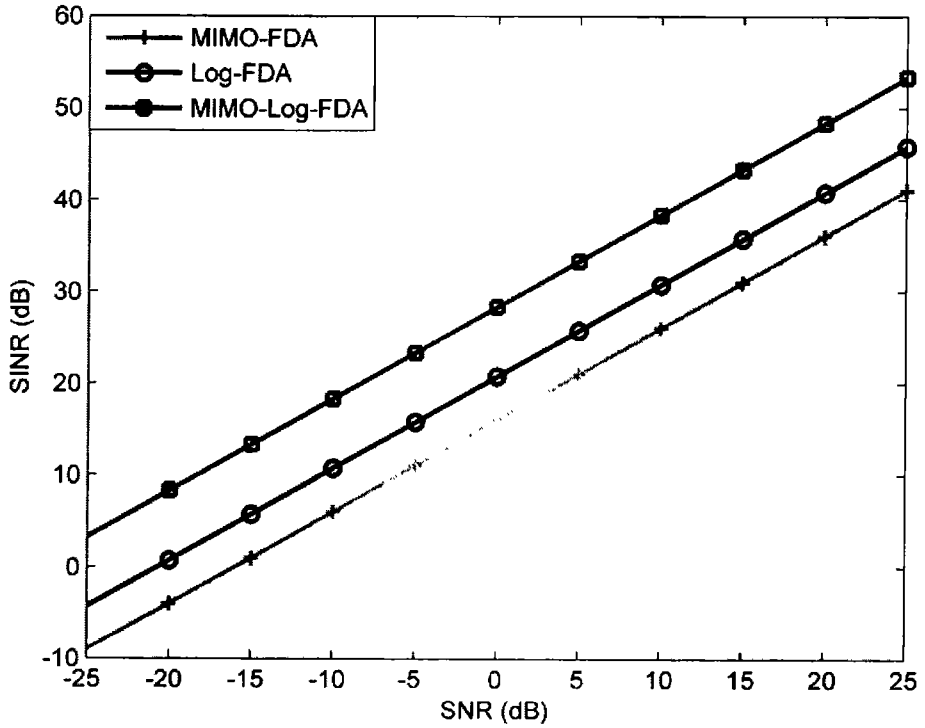

Fig. 5.10 Output SINR versus SNR performance comparison

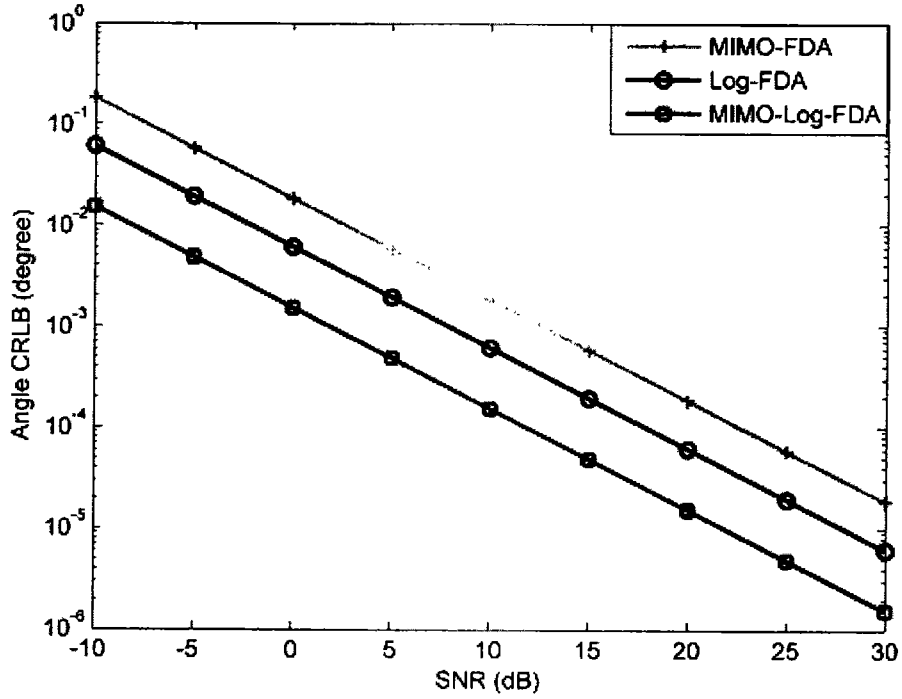

Fig. 5.11 CRLB versus SNR for angle estimation

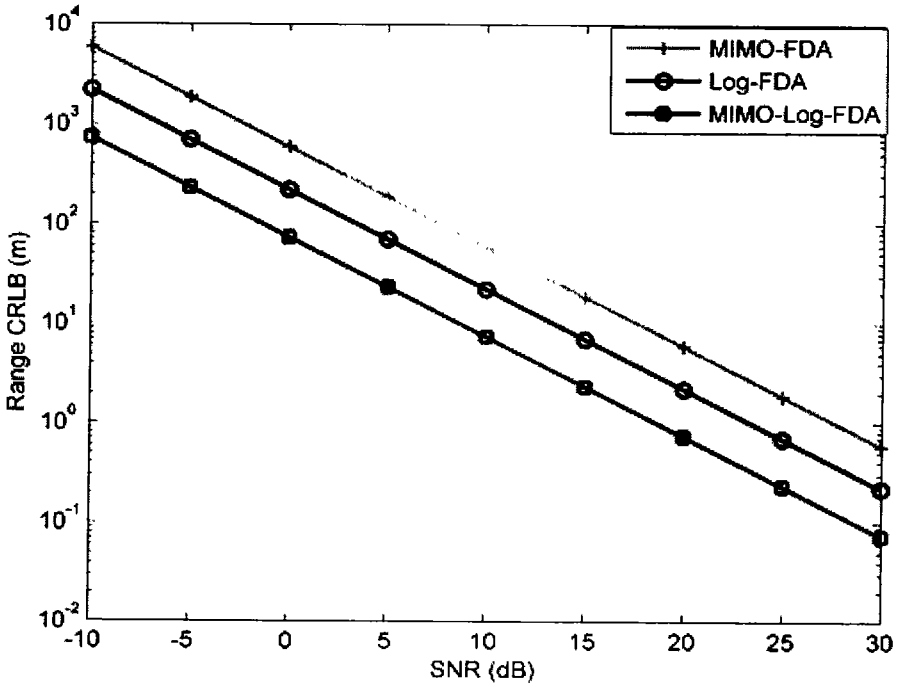

Fig. 5.12 CRLB versus SNR for range estimation

outperform the LOG-FDA and MIMO-FDA by producing better result. This improvement in estimation performance is the result of more focused transmission on transmit side. In other words the variable logarithmic offsets in each subarray contributes to performance improvement compared to MIMO-FDA and Log-FDA radar system.

5.4 Summary of Chapter

Hybrid MIMO-FDA radar with logarithmic offset has been proposed and explored in this chapter. Proposed MIMO-Log-FDA radar not only removes the periodicity issue in existing FDA and MIMO-FDA radar but also provide improved localization in range and angle through the subarray structure. First an idea of range bins has been presented to localize more than one targets present at different ranges and angle by using spacing of quarter of wavelength. Proposed system actually exploits the subarray structure to produce a more effective system compared to Log-FDA radar in terms of producing maximas for multiple targets at different ranges. Furthermore, a second proposed scheme investigates the possibility of variable logarithmic offset in each subarray to focus a single target in terms of range and angle. Simulations and results have established the effectiveness of proposed MIMO-Log-FDA with variable logarithmic offset.

Chapter 6

Conclusions and Future Work

6.1 Conclusions

In this dissertation, we have proposed various array partitioning schemes for Hybrid Phased MIMO radar and MIMO-FDA radar. The standalone Phased array radar and MIMO radar lacked very important features of waveform diversity and processing gain, respectively. In order to build a system having both capabilities, Hybrid Phased MIMO radar design was proposed. Furthermore, MIMO-FDA radar had added the range dependent features to the hybrid radar designs. However, it was felt that hybrid radar still needs a lot of research to meet the state of the art radar systems. In this regard the most preliminary problem is to propose efficient partitioning structures and effective offset selection.

In the work presented here, we have focused on direct partitioning of transmit array in both Phased MIMO radar and MIMO-FDA radar. In addition, for MIMO FDA, we have also worked on choosing effective frequency offset for improved performance. For Phased MIMO radars, we have proposed an unequal subarray based structure to focus same target with multiple beams of variable width. The scheme has resulted in improvement in side-lobes level, as well as, SINR. A slightly different type of partitioning has given maximum waveform diversity to give better interference cancellation than that of conventional MIMO radar, PAR and Phased MIMO radar.

In order to improve range angle localization in MIMO-FDA radar with uniform frequency offset, the idea of unequal subarrays and double pulse have been introduced to subarray structure. In particular, double pulse MIMO-FDA resulted in separating the peaks of coupled FDA pattern in terms of angle and range by treating each in a separate processing step. Both techniques have shown superiority compared to the existing FDA and double pulse FDA radar. Performance of these proposed systems have also been analyzed in terms of Probability of detection and CRLB.

In the last chapter, two structures of MIMO-FDA radar using a non-uniform i.e. logarithmic frequency offset has been proposed. First, a non-overlapped subarray structure with same logarithmic offset in each subarray has been presented to overcome the inability of Log-FDA radar in terms of producing multiple maxima in radar scene. Range bins have been introduced for each subarray to produce exactly one maxima for each of the target in different range bins. This is in contrast to MIMO-FDA which produces multiple maxima from each subarray resulting in serious degradation of SINR. Secondly, a MIMO-Log-FDA with variable logarithmic offset in each subarray has been proposed to analyze the effect of variation in non-uniform offset. The analysis and results have clearly shown improvements in terms of received beampattern, SINR and CRLB, as compared to MIMO-FDA radar and Log-FDA radar.

6.2 Future work

Future directions for extending the work in this dissertation are as follows

1. This dissertation has focused on linear arrays, however, this work can also be extended to planar and circular arrays. Planar arrays can localize the target in azimuth as well as elevation, whereas, circular array can scan horizontally for 360°.

We believe that working in planar and circular arrays will open some new research areas and can offer substantial improvements in hybrid radars.

2. Some recent research focuses on developing an intelligent radar called cognitive radar. A potential future work will be to add some cognition to the hybrid Phased MIMO and MIMO-FDA radar. Since cognition mainly depends on the feedback form the receiver, thus using a feedback in hybrid radar will indeed build a most powerful system, which can adapt according to the changes in surrounding environment.
3. Another important area of research is to design robust waveforms for hybrid radar systems. In this regard, waveform designs for MIMO radar can be used as basis to build new waveforms, which can be effectively applied to hybrid radars under different scenarios.
4. Finally, a non-uniform frequency offset based hybrid systems need more investigation in terms of developing an optimum system. In particular, a MIMO-Log-FDA can be mixed with non uniform antenna element spacing to open some new research opportunities in hybrid radar systems.

REFERENCES

[1] S. MI, "Introduction to RADAR systems." Mac-Graw Hill Book Company, New-York, 1980.

[2] M. A. Richards, *Fundamentals of radar signal processing*. Tata McGraw-Hill Education, 2005.

[3] R. W. Burns, "Radar development to 1945," 1988.

[4] L. N. Ridenour, *Radar system engineering*, vol. 1. Dover Publications, 1965.

[5] K. F. Molz, "Phased array radar systems," *Radio and Electronic Engineer*, vol. 28, no. 5. pp. 331–339, 1964.

[6] E. Brookner, "Phased-array radars," *Sci. Am.*, vol. 252, no. 2, pp. 94–102, 1985.

[7] A. J. Fenn, D. H. Temme, W. P. Delaney, and W. E. Courtney, "The Development of Phased-Array Radar Technology," *Physics (College. Park. Md).*, vol. 12, no. 2, pp. 321–340, 2000.

[8] M. Whorton, "Evaluating and managing Cold War era historic properties: the cultural significance of US Air Force defensive radar systems," *Matériel Cult. Archaeol. Twent. century Confl.*, pp. 216–226, 2002.

[9] P. Lacomme, *Air and spaceborne radar systems: An introduction*, no. 108. William Andrew, 2001.

[10] V. S. Chernyak, *Fundamentals of multisite radar systems: multistatic radars and multistatic radar systems*. CRC Press, 1998.

[11] S. A. Schelkunoff, "A mathematical theory of linear arrays," *Bell Syst. Tech. J.*, vol. 22, no. 1, pp. 80–107, 1943.

[12] D. R. Rhodes, "On a fundamental principle in the theory of planar antennas," *Proc. IEEE*, vol. 52, no. 9, pp. 1013–1021, 1964.

[13] H. P. Neff and J. D. Tillman, "An omnidirectional circular antenna array excited parasitically by a central driven element," *Am. Inst. Electr. Eng. Part I Commun. Electron. Trans.*, vol. 79, no. 2, pp. 190–192, 1960.

[14] M. I. Skolnik, "Introduction to radar," *Radar Handb.*, vol. 2, 1962.

[15] J. L. Allen, "The theory of array antennas (with emphasis on radar applications)," DTIC Document, 1963.

[16] A. A. Oliner and G. H. Knittel, *Phased array antennas*. Artech House Publishers, 1972.

[17] W. H. Von Aulock, "Properties of Phased Arrays," *Proceedings of the IRE*, vol. 48, no. 10. pp. 1715–1727, 1960.

[18] E. Brookner, "Phased array radars-past, present and future," *RADAR 2002*. pp. 104–113, 2002.

[19] D. D. King, R. F. Packard, and R. K. Thomas, "Unequally-spaced, broad-band antenna arrays," *Antennas Propagation, IRE Trans.*, vol. 8, no. 4, pp. 380–384, 1960.

[20] H. Unz, "Linear arrays with arbitrarily distributed elements," *IRE Trans. Antennas Propag.*, vol. 2, no. 8, pp. 222–223, 1960.

[21] R. C. Hansen, *Phased array antennas*, vol. 213. John Wiley & Sons, 2009.

[22] D. Parker and D. C. Zimmermann, "Phased arrays-Part I: Theory and architectures," *IEEE Trans. Microw. Theory Tech.*, vol. 50, no. 3, pp. 678–687, 2002.

[23] D. Parker and D. C. Zimmermann, "Phased arrays-part II: implementations, applications, and future trends," *IEEE Trans. Microw. Theory Tech.*, vol. 50, no. 3, pp. 688–698, 2002.

[24] F. T. Ulaby, E. Michielssen, U. Ravaioli, W. H. Hayt, and J. A. Buck, "Fundamentals of Applied Electromagnetics, ISBN: 978-0-13-213931-1," *Instructor*, 2013.

[25] R. J. Mailloux, "Phased array antenna handbook," *Boston, MA Artech House, 1994.*, 1994.

[26] B. Widrow and S. D. Stearns, "Adaptive signal processing," *Englewood Cliffs, NJ, Prentice-Hall, Inc., 1985, 491 p.*, vol. 1, 1985.

[27] H. L. Van Trees, "Optimum array processing: part IV of detection, estimation, and modulation." Wiley, New York, 2002.

[28] H. L. Van Trees, *Detection, estimation, and modulation theory, optimum array processing*. John Wiley & Sons, 2004.

[29] C. A. Balanis, *Antenna theory: analysis and design*, vol. 1. John Wiley & Sons, 2005.

[30] R. O. Schmidt, "Multiple emitter location and signal parameter estimation," *Antennas Propagation, IEEE Trans.*, vol. 34, no. 3, pp. 276–280, 1986.

[31] R. Roy and T. Kailath, "ESPRIT-estimation of signal parameters via rotational invariance techniques," *Acoust. Speech Signal Process. IEEE Trans.*, vol. 37, no. 7, pp. 984–995, 1989.

[32] R. D. Brown, R. Schneible, M. C. Wicks, H. Wang, and Y. Zhang, "STAP for clutter suppression with sum and difference beams," *Aerosp. Electron. Syst. IEEE Trans.*, vol. 36, no. 2, pp. 634–646, 2000.

[33] R. E. Kalman, "A new approach to linear filtering and prediction problems," *J. Fluids Eng.*, vol. 82, no. 1, pp. 35–45, 1960.

[34] S. J. Julier and J. K. Uhlmann, "New extension of the Kalman filter to nonlinear systems," in *AeroSense'97*, 1997, pp. 182–193.

[35] K. Chang, F. Beltran, and F. Steudel, "Wideband interference suppressor in a phased array radar." Google Patents, 07-Jan-1997.

[36] P. Rocca, R. L. Haupt, and A. Massa, "Interference suppression in uniform linear arrays through a dynamic thinning strategy," *Antennas Propagation, IEEE Trans.*, vol. 59, no. 12, pp. 4525–4533, 2011.

[37] H. H. M. Ghouz, F. I. A. Elghany, and M. M. Qutb, "Adaptive space-time processing for interference suppression in phased array radar systems. II. Tracking radar," *Radio Science Conference, 2000. 17th NRSC '2000. Seventeenth National.* pp. B9/1–B9/7, 2000.

[38] W. P. M. N. Keizer, "Low sidelobe phased array pattern synthesis with compensation for errors due to quantized tapering," *Antennas Propagation, IEEE Trans.*, vol. 59, no. 12, pp. 4520–4524, 2011.

[39] D. Thompson, M. Yeary, C. Fulton, and B. McGuire, "Optimized Beam Steering Approach for Improved Sidelobes in Phased Array Radars Using a Minimal Number of Control Bits," *Antennas Propagation, IEEE Trans.*, vol. 63, no. 1, pp. 106–112, 2015.

[40] P. Antonik, M. C. Wicks, H. D. Griffiths, and C. J. Baker, "Frequency diverse array radars," in *IEEE National Radar Conference - Proceedings*, 2006, pp. 215–217.

[41] P. Antonik, M. C. Wicks, H. D. Griffiths, and C. J. Baker, "Multi-mission multi-mode waveform diversity," in *Radar, 2006 IEEE Conference on*, 2006, p. 3–pp.

[42] M. C. Wicks and P. Antonik, "Method and apparatus for a frequency diverse array." Google Patents, Mar-2009.

[43] M. C. Wicks and P. Antonik, "Frequency diverse array with independent modulation of frequency, amplitude, and phase." Google Patents, Jan-2008.

[44] M. Secmen, S. Demir, A. Hizal, and T. Eker, "Frequency diverse array antenna with periodic time modulated pattern in range and angle," in *IEEE National Radar Conference - Proceedings*, 2007, pp. 427–430.

[45] J. Huang, K. F. Tong, and C. Baker, "Frequency diverse array: Simulation and design," in *Antennas & Propagation Conference, 2009. LAPC 2009. Loughborough*, 2009, pp. 253–256.

[46] P. Baizert, T. B. Hale, M. A. Temple, and M. C. Wicks, "Forward-looking radar GMTI benefits using a linear frequency diverse array," *Electron. Lett.*, vol. 42, no. 22, pp. 1311–1312, 2006.

[47] B. W. Jung, R. S. Adve, and J. Chun, "Frequency diversity in multistatic radars," in *Radar Conference, 2008. RADAR'08. IEEE*, 2008, pp. 1–6.

[48] T. Eker, S. Demir, and A. Hizal, "Exploitation of linear frequency modulated continuous waveform (LFMCW) for frequency diverse arrays," *Antennas Propagation, IEEE Trans.*, vol. 61, no. 7, pp. 3546–3553, 2013.

[49] J. Farooq, M. A. Temple, and M. A. Saville, "Application of frequency diverse arrays to synthetic aperture radar imaging," in *2007 International Conference on Electromagnetics in Advanced Applications, ICEAA'07*, 2007, pp. 447–449.

[50] J. Farooq, M. A. Temple, and M. A. Saville, "Exploiting frequency diverse array processing to improve SAR image resolution," in *2008 IEEE Radar Conference, RADAR 2008*, 2008.

[51] A. M. Jones and B. D. Rigling, "Planar frequency diverse array receiver architecture," in *Radar Conference (RADAR), 2012 IEEE*, 2012, pp. 145–150.

[52] S. Saeed, I. M. Qureshi, W. Khan, and A. Salman, "An investigation into uniform circular frequency diverse array (UCFDA) radars," *Remote Sens. Lett.*, vol. 6, no. 9, pp. 707–714, 2015.

[53] A. M. Jones, "Frequency diverse array receiver architectures." Wright State University, 2011.

[54] J. Shin, J.-H. Choi, J. Kim, J. Yang, W. Lee, J. So, and C. Cheon, "Full-wave simulation of frequency diverse array antenna using the FDTD method," in *Microwave Conference Proceedings , 2013 Asia-Pacific*, 2013, pp. 1070–1072.

[55] F. S. Johansson, L. G. Josefsson, and T. Lorentzon, "A novel frequency-scanned reflector antenna," *Antennas Propagation, IEEE Trans.*, vol. 37, no. 8, pp. 984–989, 1989.

[56] C. Vazquez, C. Garcia, Y. Alvarez, S. Ver-Hoeye, and F. Las-Heras, "Near field characterization of an imaging system based on a frequency scanning antenna array," *Antennas Propagation, IEEE Trans.*, vol. 61, no. 5, pp. 2874–2879, 2013.

[57] P. Antonik, M. C. Wicks, H. D. Griffiths, and C. J. Baker, "Range dependent beamforming using element level waveform diversity," in *Proceedings of the International Waveform Diversity and Design Conference*, 2006, pp. 1–4.

[58] P. F. Sammartino, C. J. Baker, and H. D. Griffiths, "Range-angle dependent waveform," *Radar Conference, 2010 IEEE*. pp. 511–515, 2010.

[59] W.-Q. Wang, H. Shao, and J. Cai, "Range-angle-dependent beamforming by frequency diverse array antenna," *Int. J. Antennas Propag.*, vol. 2012, 2012.

[60] A. Aytun, "Frequency diverse array radar." Monterey, California. Naval Postgraduate School, 2010.

[61] T. Higgins and S. D. Blunt, "Analysis of range-angle coupled beamforming with frequency-diverse chirps," in *Waveform Diversity and Design Conference, 2009 International*, 2009, pp. 140–144.

[62] W.-Q. Wang and H. Shao, "Range-angle localization of targets by a double-pulse frequency diverse array radar," *Sel. Top. Signal Process. IEEE J.*, vol. 8, no. 1, pp. 106–114, 2014.

[63] W.-Q. Wang, "Range-angle dependent transmit beampattern synthesis for linear frequency diverse arrays," *Antennas Propagation, IEEE Trans.*, vol. 61, no. 8, pp. 4073–4081, 2013.

[64] L. Zhuang, X. Liu, and W. Yu, "Precisely beam steering for frequency diverse arrays based on frequency offset selection," in *Radar Conference-Surveillance for a Safer World, 2009. RADAR. International*, 2009, pp. 1–4.

[65] H. Shao, J. Li, H. Chen, and W.-Q. Wang, "Adaptive Frequency Offset Selection in Frequency Diverse Array Radar," *Antennas Wirel. Propag. Lett. IEEE*, vol. 13, pp. 1405–1408, 2014.

[66] W. Khan and I. M. Qureshi, "Frequency Diverse Array Radar With Time-Dependent Frequency Offset," *Antennas Wirel. Propag. Lett. IEEE*, vol. 13, pp. 758–761, 2014.

[67] W.-Q. Wang, H. C. So, and H. Shao, "Nonuniform frequency diverse array for range-angle imaging of targets," *Sensors Journal, IEEE*, vol. 14, no. 8, pp. 2469–2476, 2014.

[68] W. Khan, I. M. Qureshi, and S. Saeed, "Frequency Diverse Array Radar With Logarithmically Increasing Frequency Offset," *Antennas Wirel. Propag. Lett. IEEE*, vol. 14, pp. 499–502, 2015.

[69] W.-Q. Wang, "Frequency Diverse Array Antenna: New Opportunities," 2015.

[70] J. Huang and K.-F. Tong, "Frequency diverse array with beam scanning feature," in *2008 IEEE Antennas and Propagation Society International Symposium*, 2008, pp. 1–4.

[71] P. F. Sammartino and C. J. Baker, "The frequency diverse bistatic system," in *2009 International Waveform Diversity and Design Conference*, 2009.

[72] B. H. Khalaj, A. Paulraj, and T. Kailath, "Antenna arrays for CDMA systems with multipath," in *Military Communications Conference, 1993. MILCOM'93. Conference record. Communications on the Move., IEEE*, 1993, vol. 2, pp. 624–628.

[73] D. Chizhik, G. J. Foschini, M. J. Gans, and R. A. Valenzuela, "Propagation and capacities of multi-element transmit and receive antennas," in *Antennas and Propagation Society International Symposium, 2001. IEEE*, 2001, vol. 1, pp. 438–441.

[74] G. J. Foschini and M. J. Gans, "On limits of wireless communications in a fading environment when using multiple antennas," *Wirel. Pers. Commun.*, vol. 6, no. 3, pp. 311–335, 1998.

[75] E. Fishler, A. Haimovich, R. Blum, D. Chizhik, L. Cimini, and R. Valenzuela, "MIMO radar: an idea whose time has come," in *Radar Conference, 2004. Proceedings of the IEEE*, 2004, pp. 71–78.

[76] R. Boyer, "Co-Located MIMO radar with orthogonal waveform coding: Cram{é}r-Rao lower bound," in *Computational Advances in Multi-Sensor Adaptive Processing (CAMSAP), 2009 3rd IEEE International Workshop on*, 2009, pp. 149–152.

[77] M. H. Rao, G. V. K. Sharma, and K. R. Rajeswari, "Orthogonal phase coded waveforms for MIMO radars," *Int. J. Comput. Appl.*, vol. 63, no. 6, pp. 31–35, 2013.

[78] D. R. Fuhrmann and G. S. Antonio, "Transmit beamforming for MIMO radar systems using partial signal correlation," in *Signals, Systems and Computers, 2004. Conference Record of the 38th Asilomar Conference on*, 2004, vol. 1, pp. 295–299.

[79] Y. Li, S. Vorobyov, and V. Koivunen, "Generalized ambiguity function for the MIMO radar with correlated waveforms," in *Acoustics, Speech and Signal Processing , 2014 IEEE International Conference on*, 2014, pp. 5302–5306.

[80] Q. He, R. S. Blum, H. Godrich, and A. M. Haimovich, "Target velocity estimation and antenna placement for MIMO radar with widely separated antennas," *Sel. Top. Signal Process. IEEE J.*, vol. 4, no. 1, pp. 79–100, 2010.

[81] C.-Y. Chen and P. P. Vaidyanathan, "MIMO radar ambiguity properties and optimization using frequency-hopping waveforms," *Signal Process. IEEE Trans.*, vol. 56, no. 12, pp. 5926–5936, 2008.

[82] B. Liu, Z. He, J. Zeng, and B. Liu, "Polyphase orthogonal code design for MIMO radar systems," in *2006 CIE international conference on radar*, 2006, pp. 1–4.

[83] H. Azami, M. Malekzadeh, S. Sanei, and A. Khosravi, "Optimization of orthogonal polyphase coding waveform for MIMO radar based on evolutionary algorithms," *J. Math. Comput. Sci*, vol. 6, no. 2, pp. 146–153, 2012.

[84] Y. Yang and R. S. Blum, "Minimax robust MIMO radar waveform design," *Sel. Top. Signal Process. IEEE J.*, vol. 1, no. 1, pp. 147–155, 2007.

[85] T. Naghibi, M. Namvar, and F. Behnia, "Optimal and robust waveform design for MIMO radars in the presence of clutter," *Signal Processing*, vol. 90, no. 4, pp. 1103–1117, 2010.

[86] H. Wang, G. Liao, J. Li, and H. Tao, "Robust waveform optimization for MIMO radar to improve the worst-case estimation performance," in *Signal Processing, Communications and Computing (ICSPCC), 2011 IEEE International Conference on*, 2011, pp. 1–4.

[87] E. Grossi, M. Lops, and L. Venturino, "Robust waveform design for MIMO radars," *Signal Process. IEEE Trans.*, vol. 59, no. 7, pp. 3262–3271, 2011.

[88] W. Zhu and J. Tang, "Robust Design of Transmit Waveform and Receive Filter For Colocated MIMO Radar," *Signal Process. Lett. IEEE*, vol. 22, no. 11, pp. 2112–2116, 2015.

[89] I. Bekkerman and J. Tabrikian, "Target detection and localization using MIMO radars and sonars," *Signal Process. IEEE Trans.*, vol. 54, no. 10, pp. 3873–3883, 2006.

[90] T. Ali, A. Z. Sadeque, M. Saquib, and M. Ali, "MIMO Radar for Target Detection and Localization in Sensor Networks," *Syst. Journal, IEEE*, vol. 8, no. 1, pp. 75–82, 2014.

[91] L. Xu, J. Li, and P. Stoica, "Target detection and parameter estimation for MIMO radar systems," *Aerosp. Electron. Syst. IEEE Trans.*, vol. 44, no. 3, pp. 927–939, 2008.

[92] J. Chen, P. Li, Y. Zhu, and J. Li, "Parameter Estimation Method for High-Speed Target Using Bistatic MIMO Radar with Dual-Frequency Transmitters," *Wirel. Pers. Commun.*, vol. 85, no. 4, pp. 2083–2098, 2015.

[93] A. M. Haimovich, R. S. Blum, and L. J. Cimini, "MIMO radar with widely separated antennas," *Signal Process. Mag. IEEE*, vol. 25, no. 1, pp. 116–129, 2008.

[94] N. Goodman and D. Bruyere, "Optimum and decentralized detection for multistatic airborne radar,"*Aerosp. Electron. Syst. IEEE Trans.*,vol.43, no.2, pp.806–813, 2007.

[95] E. Fishler, A. Haimovich, R. S. Blum, L. J. Cimini Jr, D. Chizhik, and R. Valenzuela, "Spatial diversity in radars-models and detection performance," *Signal Process. IEEE Trans.*, vol. 54, no. 3, pp. 823–838, 2006.

[96] N. H. Lehmann, E. Fishler, A. M. Haimovich, R. S. Blum, D. Chizhik, L. J. Cimini Jr, and R. Valenzuela, "Evaluation of transmit diversity in MIMO-radar direction finding," *Signal Process. IEEE Trans.*, vol. 55, no. 5, pp. 2215–2225, 2007.

[97] N. H. Lehmann, A. M. Haimovich, R. S. Blum, and L. Cimini, "High resolution capabilities of MIMO radar," in *Signals, Systems and Computers, 2006. ACSSC '06. Fortieth Asilomar Conference on*, 2006, pp. 25–30.

[98] F. C. Robey, S. Coutts, D. Weikle, J. C. McHarg, and K. Cuomo, "MIMO radar theory and experimental results," in *Signals, Systems and Computers, 2004. Conference Record of the 38th Asilomar Conference on*, 2004, vol. 1, pp. 300–304.

[99] E. Fishler, A. Haimovich, R. Blum, R. Cimini, D. Chizhik, and R. Valenzuela, "Performance of MIMO radar systems: advantages of angular diversity," in *Signals, Systems and Computers, 2004. Conference Record of the Thirty-Eighth Asilomar Conference on*, 2004, vol. 1, pp. 305–309.

[100] L. Xu, J. Li, and P. Stoica, "Adaptive techniques for MIMO radar," in *Sensor Array and Multichannel Processing, 2006. Fourth IEEE Workshop on*, 2006, pp. 258–262.

[101] J. Li and P. Stoica, "MIMO radar with colocated antennas," *Signal Process. Mag. IEEE*, vol. 24, no. 5, pp. 106–114, 2007.

[102] P. Stoica, J. Li, and Y. Xie, "On probing signal design for MIMO radar," *Signal Process. IEEE Trans.*, vol. 55, no. 8, pp. 4151–4161, 2007.

[103] J. Li, L. Xu, P. Stoica, K. W. Forsythe, and D. W. Bliss, "Range compression and waveform optimization for MIMO radar: a Cramer–Rao bound based study," *Signal Process. IEEE Trans.*, vol. 56, no. 1, pp. 218–232, 2008.

[104] D. R. Fuhrmann and G. S. Antonio, "Transmit beamforming for MIMO radar systems using signal cross-correlation," *Aerosp. Electron. Syst. IEEE Trans.*, vol. 44, no. 1, pp. 171–186, 2008.

[105] C.-Y. Chen and P. P. Vaidyanathan, "A subspace method for MIMO radar space-time adaptive processing," in *Acoustics, Speech and Signal Processing, 2007. ICASSP 2007. IEEE International Conference on*, 2007, vol. 2, pp. II–925.

[106] M. Akçakaya and A. Nehorai, "MIMO radar sensitivity analysis for target detection," *Signal Process. IEEE Trans.*, vol. 59, no. 7, pp. 3241–3250, 2011.

[107] A. Hassanien and S. Vorobyov, "Transmit energy focusing for DOA estimation in MIMO radar with colocated antennas," *Signal Process. IEEE Trans.*, vol. 59, no. 6, pp. 2669–2682, 2011.

[108] J. Wu, T. Wang, L. Zhang, and Z. Bao, "Range-dependent clutter suppression for airborne sidelooking radar using MIMO technique," *Aerosp. Electron. Syst. IEEE Trans.*, vol. 48, no. 4, pp. 3647–3654, 2012.

[109] S. Sun, A. P. Petropulu, and W. U. Bajwa, "Target estimation in colocated MIMO radar via matrix completion," in *Acoustics, Speech and Signal Processing (ICASSP), 2013 IEEE International Conference on*, 2013, pp. 4144–4148.

[110] M. T. Frankford, K. B. Stewart, N. Majurec, and J. T. Johnson, "Numerical and experimental studies of target detection with MIMO radar," *Aerospace and Electronic Systems, IEEE Transactions on*, vol. 50, no. 2. pp. 1569–1577, 2014.

[111] A. Khabbazibasmenj, A. Hassanien, S. Vorobyov, and M. W. Morency, "Efficient transmit beamspace design for search-free based DOA estimation in MIMO radar," *Signal Process. IEEE Trans.*, vol. 62, no. 6, pp. 1490–1500, 2014.

[112] J. Li, P. Stoica, L. Xu, and W. Roberts, "On parameter identifiability of MIMO radar," *Signal Process. Lett. IEEE*, vol. 14, no. 12, pp. 968–971, 2007.

[113] N. Lehmann, A. M. Haimovich, R. S. Blum, and L. Cimini, "MIMO-radar application to moving target detection in homogenous clutter," in *Proc. Adaptive Sensor Array Processing Workshop, Lexington, USA*, 2006.

[114] Y. Qu, G. Liao, S.-Q. Zhu, X.-Y. Liu, and H. Jiang, "Performance analysis of beamforming for MIMO radar," *Prog. Electromagn. Res.*, vol. 84, pp. 123–134, 2008.

[115] J. Bergin, S. McNeil, L. Fomundam, and P. Zulch, "MIMO phased-array for SMTI radar," in *Aerospace Conference, 2008 IEEE*, 2008, pp. 1–7.

[116] A. Hassanien and S. A. Vorobyov, "Phased-MIMO Radar: A Tradeoff Between Phased-Array and MIMO Radars," *Signal Processing, IEEE Transactions on*, vol. 58, no. 6. pp. 3137–3151, 2010.

[117] A. Hassanien and S. A. Vorobyov, "Why the phased-MIMO radar outperforms the phased-array and MIMO radars," *Signal Processing Conference, 2010 18th European*. pp. 1234–1238, 2010.

[118] H. Li and B. Himed, "Transmit subaperturing for MIMO radars with co-located antennas," *Sel. Top. Signal Process. IEEE J.*, vol. 4, no. 1, pp. 55–65, 2010.

[119] J. Bergin, P. Techau, M. Greenspan, and J. Guerci, "MIMO phased-array for airborne radar," in *2008 IEEE Antennas and Propagation Society International Symposium*, 2008.

[120] D. Wilcox and M. Sellathurai, "Beampattern optimisation for sub-arrayed MIMO radar for large arrays," in *Phased Array Systems and Technology (ARRAY), 2010 IEEE International Symposium on*, 2010, pp. 567–572.

[121] D. Wilcox and M. Sellathurai, "On MIMO radar subarrayed transmit beamforming," *Signal Process. IEEE Trans.*, vol. 60, no. 4, pp. 2076–2081, 2012.

[122] T. D. Backes and L. D. Smith, "Array design in a linear phased-subarray MIMO radar," in *Aerospace Conference, 2012 IEEE*, 2012, pp. 1–6.

[123] J. P. Browning, D. R. Fuhrmann, and M. Rangaswamy, "A hybrid MIMO phased-array concept for arbitrary spatial beampattern synthesis," in *Digital Signal Processing Workshop and 5th IEEE Signal Processing Education Workshop, 2009. DSP/SPE 2009. IEEE 13th*, 2009, pp. 446–450.

[124] D. R. Fuhrmann, J. P. Browning, and M. Rangaswamy, "Signaling strategies for the hybrid MIMO phased-array radar," *Sel. Top. Signal Process. IEEE J.*, vol. 4, no. 1, pp. 66–78, 2010.

[125] D. R. Fuhrmann, J. P. Browning, and M. Rangaswamy, "Adapting a MIMO/phased-array radar transmit beampattern to target location," in *Cognitive Information Processing (CIP), 2010 2nd International Workshop on*, 2010, pp. 354–359.

[126] N. E.-D. Ismail, S. H. Mahmoud, A. S. Hafez, and T. Reda, "A new phased MIMO radar partitioning schemes," in *Aerospace Conference, 2014 IEEE*, 2014, pp. 1–7.

[127] W.-Q. Wang and H. Shao, "Phased-MIMO radar with frequency diversity for increased system flexibility," *Signal Processing, Communication and Computing (ICSPCC), 2012 IEEE International Conference on*. pp. 16–19, 2012.

[128] P. F. Sammartino, C. J. Baker, and H. D. Griffiths, "Frequency diverse MIMO techniques for radar," *IEEE Trans. Aerosp. Electron. Syst.*, vol. 49, no. 1, pp. 201–222, 2013.

[129] J. Xu, G. Liao, S. Zhu, and H. C. So, "Deceptive jamming suppression with frequency diverse MIMO radar," *Signal Processing*, vol. 113, pp. 9–17, 2015.

[130] J. Xu, G. Liao, S. Zhu, L. Huang, and H. C. So, "Joint Range and Angle Estimation using MIMO Radar with Frequency Diverse Array," 2015.

[131] K. Gao, H. Shao, J. Cai, and H. Chen, "Frequency Diverse Array MIMO Radar Adaptive Beamforming with Range-Dependent Interference Suppression in Target Localization."

[132] W.-Q. Wang and H. Shao, "A flexible phased-MIMO array antenna with transmit beamforming," *Int. J. Antennas Propag.*, vol. 2012, 2012.

[133] W. Q. Wang, "Phased-MIMO radar with frequency diversity for range-dependent beamforming," *IEEE Sens. J.*, vol. 13, no. 4, pp. 1320–1328, 2013.

[134] W. Q. Wang and H. C. So, "Transmit subaperturing for range and angle estimation in frequency diverse array radar," *IEEE Trans. Signal Process.*, vol. 62, no. 8, pp. 2000–2011, 2014.

[135] W.-Q. Wang, "Subarray-based frequency diverse array radar for target range-angle estimation," *Aerospace and Electronic Systems, IEEE Transactions on*, vol. 50, no. 4. pp. 3057–3067, 2014.

[136] P. Stoica and R. L. Moses, *Spectral analysis of signals*. Pearson/Prentice Hall Upper Saddle River, NJ, 2005.

[137] D. Chazan, M. Zakai, and J. Ziv, "Improved lower bounds on signal parameter estimation," *Inf. Theory, IEEE Trans.*, vol. 21, no. 1, pp. 90–93, 1975.

[138] A. Van den Bos, "A Cramér-Rao lower bound for complex parameters," *IEEE Trans. Signal Process. [see also Acoust. Speech, Signal Process. IEEE Trans. on]*, *42*, 1994.

[139] R. Boyer, "Co-Located MIMO radar with orthogonal waveform coding: Cramér-Rao lower bound," in *Computational Advances in Multi-Sensor Adaptive Processing (CAMSAP), 2009 3rd IEEE International Workshop on*, 2009, pp. 149–152.

[140] Q. He, J. Hu, R. Blum, and Y. Wu, "Generalized Cramer-Rao Bound for Joint Estimation of Target Position and Velocity for Active and Passive Radar Networks," 2015.